THE UNIVERSITY OF HULL
FACULTY OF SCIENCES AND ENGINEERING
SCHOOL OF ENGINEERING

PhD Thesis

Eni Oko

STUDY OF POWER PLANT, CARBON CAPTURE AND TRANSPORT NETWORK THROUGH DYNAMIC MODELLING AND SIMULATION

Supervisors: Prof Meihong Wang and Prof Ron Patton

January, 2015

This thesis is submitted in fulfilment of the requirements for a Doctor of Philosophy (PhD) degree in Engineering

Abstract

The unfavourable role of CO_2 in stimulating climate change has generated concerns as CO_2 levels in the atmosphere continue to increase. As a result, it has been recommended that coal-fired power plants which are major CO_2 emitters should be operated with a carbon capture and storage (CCS) system to reduce CO_2 emission levels from the plant. Studies on CCS chain have been limited except a few high profile projects. Majority of previous studies focused on individual components of the CCS chain which are insufficient to understand how the components of the CCS chain interact dynamically during operation. In this thesis, model-based study of the CCS chain including coal-fired subcritical power plant, post-combustion CO_2 capture (PCC) and pipeline transport components is presented. The component models of the CCS chain are dynamic and were derived from first principles. A separate model involving only the drum-boiler of a typical coal-fired subcritical power plant was also developed using neural networks.

The power plant model was validated at steady state conditions for different load levels (70-100%). Analysis with the power plant model show that load change by ramping cause less disturbance than step changes. Rate-based PCC model obtained from Lawal *et al*. (2010) was used in this thesis. The PCC model was subsequently simplified to reduce the CPU time requirement. The CPU time was reduced by about 60% after simplification and the predictions compared to the detailed model had less than 5% relative difference. The results show that the numerous non-linear algebraic equations and external property calls in the detailed model are the reason for the high CPU time requirement of the detailed PCC model. The pipeline model is distributed and includes elevation profile and heat transfer with the environment. The pipeline model was used to assess the planned Yorkshire and Humber CO_2 pipeline network.

Analysis with the CCS chain model indicates that actual changes in CO_2 flowrate entering the pipeline transport system in response to small load changes (about 10%) is very small (<5%). It is therefore concluded that small changes in load will have minimal impact on the transport component of the CCS chain when the capture plant is PCC.

Keywords: Process Modelling, Process Simulation, System Identification, Coal-fired Subcritical Power Plant, Post-combustion CO_2 Capture, Pipeline Transport System

Acknowledgements

The past three years on this research was so far the most difficult period in my life. I was able to come through due to the support I received from numerous people. Words are not enough to articulate the depth of gratitude that I owe them. Due to lack of space, only a few of these people are mentioned here.

Secondly, I am thankful to Prof Meihong Wang for guiding me through this project. During this time, he provided every necessary support for me to succeed. He has been more than a supervisor to me and I am eternally grateful to him. I am also grateful for the support of Prof Ron Patton who co-supervised the project and Dr Jim Gilbert who chaired all the Thesis Advisory Panel (TAP) meetings. Useful discussions with Prof Chuanglong Xu and Prof Jianhong Lyu both of South East University, China are also appreciated. Dr Adekola Lawal whose work provided a starting point for this work cannot be appreciated enough. I made calls to him at very odd periods and he always managed to hear me regardless of his own tight schedules.

Admin support provided by members of staff at Cranfield University, University of Hull and South East University China are all appreciated. Things could have been more difficult without you guys.

My friends around town have made life so easy for me studying at Hull. The get-together events often arranged by you guys used to provide an excellent opportunity for me to freshen up and so was our usual football meet on Saturday mornings at Clough road. I cannot thank you guys enough.

I am indebted to my parents (Mr/Mrs Emma Abagha) who have been a strong inspiration for me and my siblings who have given me every moral and spiritual support to succeed. I am blessed with the best wife (Uzoma EniOko) any man can ask for. She made every sacrifice to keep me sane during this time. I am a lucky man! Finally, I am grateful to God who gave me life, desire and good health to complete this study.

Table of Contents

List of Figures

List of Tables

Nomenclature

A	Cross sectional area (m^2)
a	Total specific surface area of packing (m^2/m^3)
a_w	Effective interfacial area of packing (m^2/m^3)
C_p	Specific heat capacity at constant pressure (J/kg K)
C_V	Specific heat capacity at constant volume (J/kg K)
$C_{p,ash}$	Specific heat capacity of ash (J/kg K)
$C_{p,coal}$	Specific heat capacity of coal (Btu/lb ^oF)
D	Diffusivity coefficient (m^2/s), Pipe diameter
D_i, D_o	Inside and outside pipe diameter (m)
d_p	Diameter of packing pore (m)
f	Darcy friction factor
g	Acceleration due to gravity (m/s^2)
GP	Compressor power (W)
h	Specific enthalpy (J/kg)
hi, ho	Inside and outside convective heat transfer coefficient (W/m^2 K)
H_D	Burial depth of pipeline (m)
H_{poly}	Compressor polytropic head (m)
k	Attenuation coefficient, Adiabatic index for compressors
k_f	Dimensionless friction coefficient
k_G	Gas phase mass transfer coefficient (kmol/m2 s Pa)
k_L	Liquid phase mass transfer coefficient (kmol/m2 s Pa)
K	Empirical constant
L	Level (m)
L_w	Liquid phase superficial mass velocity (kg/m^2s)
$\dot{m}$	Mass flowrate (kg/s)
M	Mass of metal (kg)
MW	Molecular weight (kg/kmol)
n	Polytropic index
N	Pump speed (rev/s)
Nu	Nusselt number
P	Pressure (Pa)
P_Q	Power (W)
Pr	Prandtl number
q	Heat flux per unit length (m)
Q	Heat flow (W)
Q_C	Convective heat input into *water-steam in riser*
Q_{IR}	Total radiant heat absorbed by riser tubes
r	Pressure ratio
R	Ideal gas constant (Pa m3/kmol K)
Re	Reynolds number
r_i, r_o	Inside and outside pipe radius (m)
s	Specific entropic (J/kg K)
T	Temperature (K)
T_F, T_A	Fluid and ambient temperature (K)
Torq	Torque (J)
u	Internal energy (J/kg)
U	Admittance (W/K)

U_{OHTC}	Overall heat transfer coefficient (W/m K)
v	Fluid velocity (m/s)
V	Volume (m^3)
v_f	Valve coefficient
V_w	Gas phase superficial mass velocity (kg/m^{2}s)
Z	Deaerator altitude (m)
Z_a	Average compressibility factor

Greek Letters

α	Steam quality
$\bar{\alpha}_v$	Average steam volume fraction in riser
σ	Stefan-Boltzmann constant (W/m^{2}K^4)
σ_c	Critical surface tension (N/m)
σ_L	Liquid phase surface tension (N/m)
β	Empirical factor
ε	Pipe roughness factor
κ	Thermal conductivity
κ_{pipe}	Pipe conductivity (W/m K)
κ_{soil}	Soil conductivity (W/m K)
τ_r	Heat transfer parameter for riser
η_p	Polytropic efficiency
θ	Pipe elevation angle
ρ	Mass density (kg/m^3)
μ	Dynamic viscosity (kg/m s)
π	Pie

Subscript

bfp	Boiler feedwater pump
c	Condensation
dis	Discharge
D	Drum
dc	Downcomer
Dtorout	Deaerator outlet
F	Furnace
fw	Feed*water*
g	Flue gas
g,ad	Flue gas (Adiabatic condition)
g,avg	Flue gas (Average)
in	Inlet
L	Liquid phase
M	Metal
out	Outlet
r	Riser, rated
R	Radiant
rsuc	Rated suction condition
s	Steam in drum-downcomer-riser loop
sD	Steam below water level in drum
son	Sound
suc	Suction
s,avg	Steam (Average)

t	Sum of water and steam in drum-downcomer-riser loop
trb	BFP turbine
ν	Specific volume (m^3/kg)
v	Vapour phase
W	Wall
wD	Water in drum
wt	Water in drum-downcomer-riser loop

Abbreviations

ARMAX	AutoRegressive Moving Average model with eXogenous input
BFP	Boiler Feedwater Pump
BRICS	Brazil, Russia, India, China and South Africa
CAPEX	CAPital Expenditure
CAPE-OPEN	Computer-Aided Process Engineering-Open
CCS	Carbon Capture and Storage
COBRA	Common Object Request Architecture
COM	Common Object Model
CO2CRC	Cooperative Research Centre for Greenhouse Gas Technologies
CO-LaN	CAPE-OPEN Laboratories Network
DAE	Differential and Algebraic Equations
DEA	Diethanolamine
ElecNRTL	Electrolyte Non-Random Two-Liquid
EOS	Equation of State
GA	Genetic Algorithm
GERG	Groupe Européen de Recherches Gazières: European Group of Gas Research
GHG	Greenhouse Gas
gPROMS	General PROcess Modelling and Simulation
HP	High Pressure
ID	Inside Diameter
IEA	International Energy Agency
IP	Intermediate Pressure
IPCC	Intergovernmental Panel on Climate Change
LP	Low Pressure
MDEA	Methyldiethanolamine
MEA	Monoethanolamine
MOL	Method of Lines
MSE	Mean Squared Error
MTC	Mass Transfer Coefficients
NCV	Net Calorific Value
NARX	Nonlinear AutoRegressive with eXogenous inputs
NIST	National Institute of Standard and Technology
NN	Neural Networks
OD	Outside Diameter
ODE	Ordinary Differential Equation
Ofgem	Office of Gas and Electricity Markets
OPEX	OPerating EXpenditure
PCC	Post-combustion CO_2 Capture
PDE	Partial Differential Equation
PSE	Process Systems Enterprise
PRBS	Pseudo Random Binary Sequence
ROAD	Rotterdam Capture and Storage Demonstration
SE	Stodola Ellipse
TAME	Tert-amyl methyl ether
TBWES	Thermax Babcock & Wilcox Energy Solutions

Chapter 1: Introduction

This chapter sets the context of the research. The background of the study is presented in Section 1.1. Section 1.2 provides the technological concerns that motivated the study. The aim, objectives and novel contributions of the PhD research are presented in Section 1.3. The scope of the research is presented in Section 1.4. Tools used in the study are described briefly in Section 1.5 and the structure of the entire PhD Thesis outlined in Section 1.6.

1.1 Background

For many years, coal-based power generation has been a major source of global electricity and currently accounts for about 40.8% of global electricity generation (IEA, 2010). With expected economic growth, mostly coming from emerging economies such as the BRICS nations, and increasing concern about security, sustainability and economy of energy supply, it is predicted that coal will remain a key component in the energy mix for many years. Coal-based power generation is however accompanied by unacceptable levels of CO_2 emissions. The release of about 8000 tons CO_2/day from a 500 MWe supercritical power plant when operated at 46% efficiency-LHV basis (BERR, 2006) puts this in perspective. Fig.1.1 and 1.2 indicate that coal-based power and heat generation are the main culprits in CO_2 emissions among other stationary sources. Continued reliance on coal for electricity generation without reduction of the accompanying CO_2 emission levels has disastrous consequences (IPCC, 2005).

1.1.1 The problem with CO_2

CO_2 remains the major anthropogenic GHG with 76% of total GHG emissions in 2010 (IPCC, 2014a) and rising levels of CO_2 in the atmosphere has continued to draw more attention due to the associated adverse implication, namely global warming. According to IPCC (2014b), global warming has been unequivocal and the consequences, namely acidification of the oceans, the melting of Arctic ice and poorer crop yields among others are already visible around the world.
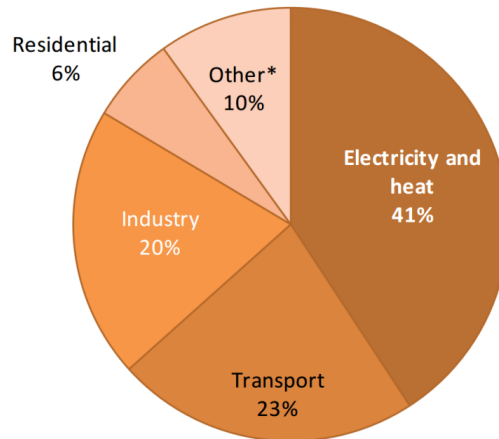
Fig.1.1 World CO$_2$ emissions by sector in 2009 (IEA 2011)
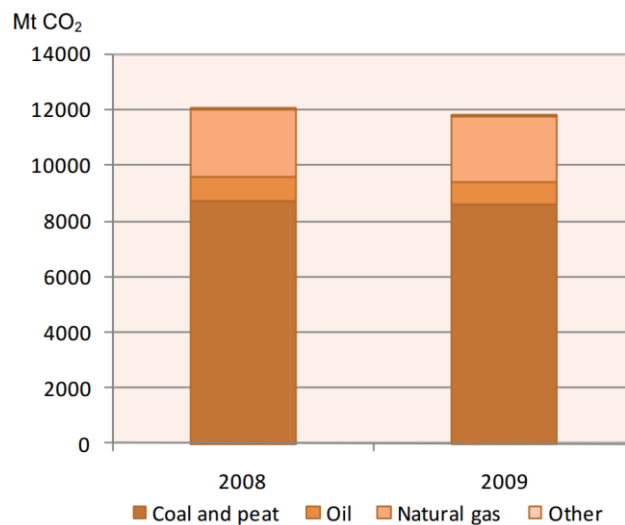
Fig.1.2 CO$_2$ emission from electricity and heat generation by fuel (IEA 2011)

Recently, the World Meteorological Organisation (WMO) in its GHG Bulletin (Sept., 2014) called for a global climate treaty with reports which show that the concentrations of CO$_2$ in the atmosphere between 2012 and 2013 grew at their fastest rate since 1984 (WMO GAW, 2014). In the same report, WMO stated that CO$_2$ concentration in the atmosphere reached 396ppm in 2013 an increase of about 3ppm over the previous year which represents about 142% of the levels in 1750, before the start of the industrial revolution. On the basis of the baseline scenario (business-as-usual scenario) where the future is viewed as a continuation of past and present, IEA (2010) predicts that energy consumption will double by 2050 and CO$_2$ emissions will rise to two-and-a-half times the current level regardless of possible energy efficiency gains and technological progress. These can only be avoided by realising significant cuts in CO$_2$ emission.

1.1.2 Cutting down CO_2 emissions

In the UK, a GHG emission reduction target of 80% (from the 1990 baseline) is set to be achieved in 2050 through implementation of relevant policies (Ofgem e-serve, 2013). In the BLUE MAP scenario (Fig.1.3), IEA outlined a portfolio of technologies for decarbonizing the power industry. The power industry is targeted because it is the biggest stationary source of anthropogenic CO_2 emission into the atmosphere as evidenced in Fig.1.1 and the IPCC report (IPCC, 2014a). Decarbonizing the industry is therefore a significant step to reach CO_2 emission reduction expectations. The portfolio of technologies for decarbonizing the power industry includes (IEA, 2010):

- Switching to carbon free sources such as nuclear and renewable energy
- Improving generation and end-use efficiency
- Switching to less carbon-intensive fuels
- Carbon capture and storage (CCS).

The reputation of the nuclear industry has been affected by the Fukushima meltdown in Japan leading to cancellation of nuclear power projects and closure of some existing nuclear power plants across the world (TCE, 2013). On the other hand, renewable energy provides 22% of global electricity (IEA, 2014). This has been possible because of extensive government subsidies which amounted to £150bn for 2013 alone. Higher costs of subsidies due to falling prices of oil and gas will mean that government may not be able to support renewable energy for too long. There is a risk of security, sustainability and economy of energy supply with a switch to less carbon-intensive fuel (e.g. natural gas) from coal. Due to these circumstances, operation of existing/yet-to-be built coal-fired power plants with CCS looks like the most realistic option for sustainably, economically and safely reaching CO_2 emission reduction target particularly in the short run. IPCC has recently suggested that fossil fuel-fired power stations without CCS should be phased out "almost entirely" by 2100 (IPCC, 2014b).

1.1.3 CCS

CCS technology involves capturing CO_2 from large stationary sources (e.g. coal-fired power plants) and other carbon-intensive industries (e.g. refineries), and transporting the CO_2 to underground storage sites, namely saline aquifer and depleted oil and gas reserves, where they are stored permanently and prevented from entering the

atmosphere. In some cases, the captured CO_2 could be utilized in enhanced oil recovery (EOR) or in manufacturing products like urea fertilizers etc. An illustrative diagram of a typical CCS network showing CO_2 capture from a power plant and pipeline transport to underground storage sites is shown in Fig. 1.4. From the definition, typical CCS chain includes CO_2 emitter, capture plant, transport system and storage/sequestration components. Examples of each of the components will be discussed in the following subsections.
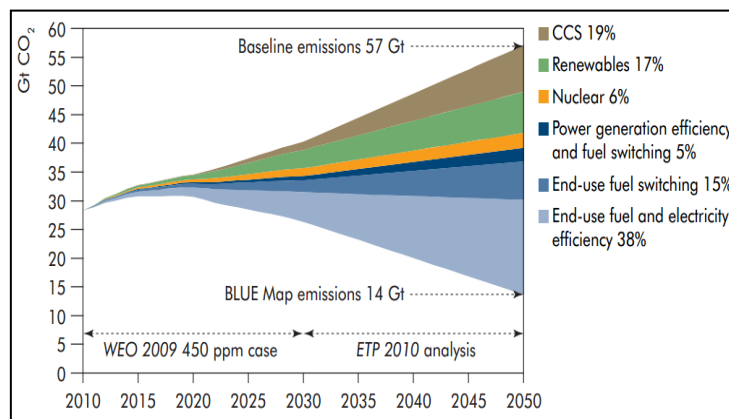
Fig.1.3 IEA's BLUE MAP scenario (IEA, 2010)
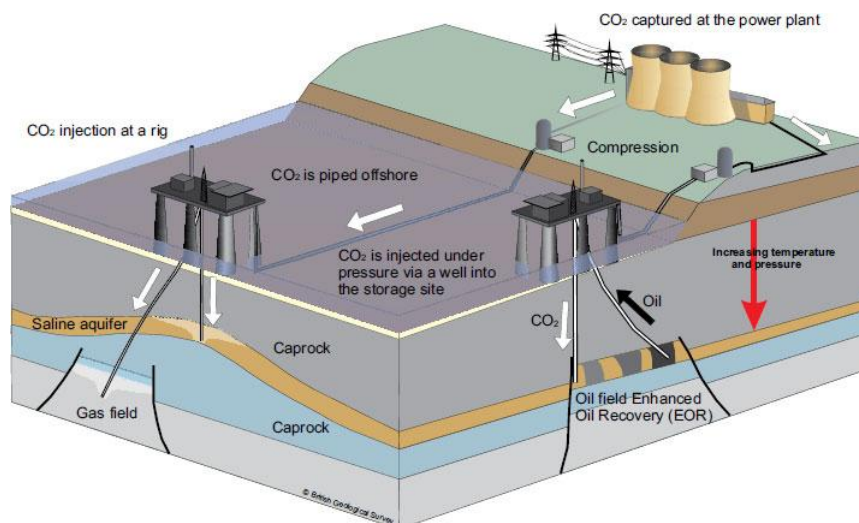
Fig.1.4 Typical CCS network (NERC, 2014)

1.1.3.1 Coal-fired power plants

In a typical coal-fired power plant (Fig.1.5), heat energy from coal combustion is used to generate steam in the boiler. The steam goes through steam turbines at high pressure and consequently generates torque which is converted to electricity in the generator. Low pressure steam leaving the low pressure steam turbine is condensed

and pumped back to the boiler. The process follows a Rankine thermodynamic cycle with regeneration. Regeneration is accomplished by feedwater heating using steam extracted from the steam turbine stages. In addition, combustion air is preheated by flue gases and steam reheating is done between HP and IP turbine stages. The resulting flue gases which have up to 25 wt% CO_2 (Lawal *et al.*, 2010) ends up in the atmosphere without CCS.
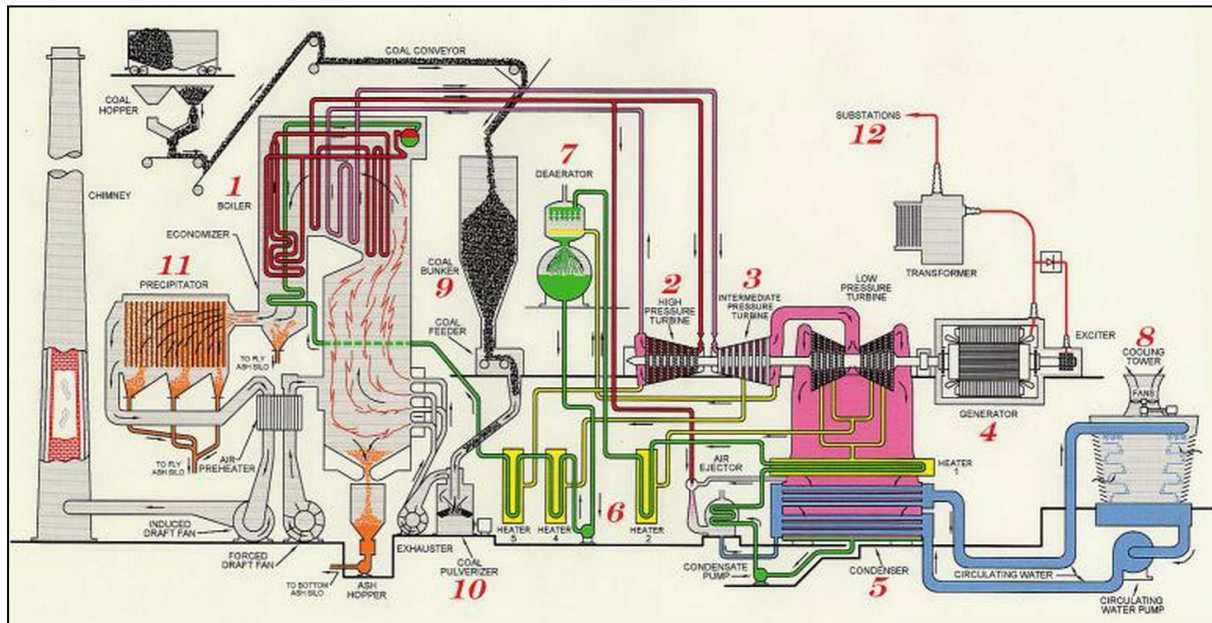
Fig.1.5 Coal-fired subcritical power plant (TSA, 2014)

1.1.3.2 CO_2 capture

There are generally three major technology options for CO_2 capture in CCS, namely post-combustion, pre-combustion and oxyfuel combustion CO_2 capture (Wang *et al.,* 2011). Post-combustion CO_2 capture (PCC) with chemical absorption (Fig.1.6) is regarded as having the highest potential for commercialization particularly for capture from coal-fired power plant flue gases (IEA GHG, 2006). This is due to its maturity level, high CO_2 selectivity and retrofit-ability to existing power plants.

In the PCC with chemical absorption process, CO_2-rich flue gas from a power plant (or industrial process) enters the bottom of the absorber. At the same time, a CO_2 lean solvent enters the top of the absorber. The solvent captures CO_2 from the flue gas by reacting with them to form a weakly bonded intermediate compound (Wang *et al.* 2011). The CO_2 lean gas exits the absorber from the top side while the CO_2 rich solvent leaves through the bottom. The rich solvent is pumped to a stripper column

where the solvent is regenerated through application of heat. Before entering the stripper, the rich solvent goes through a cross heat exchanger where it is preheated by oncoming hot lean solvent. Heat for regeneration is often supplied from the power cycle (Lucquiaud and Gibbins, 2011a) although solar collectors have also been suggested (Parkinson, 2012). Regenerated solvent is pumped back to the absorber while the recovered CO_2 (up to 99% pure) exits the stripper from the top side.
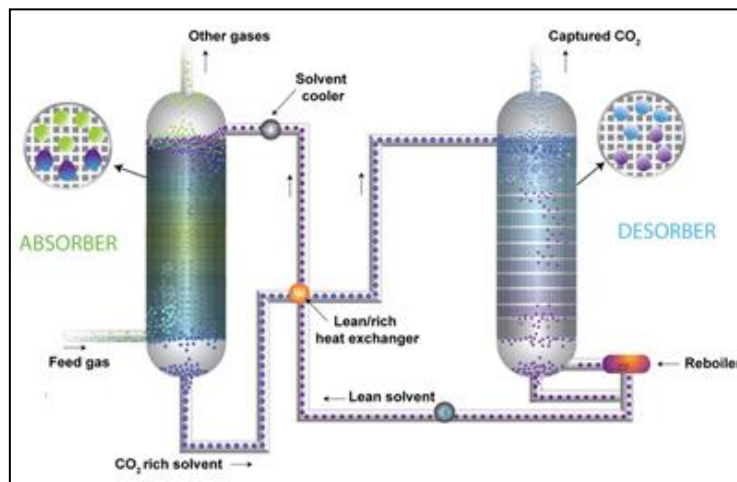
Fig.1.6 PCC process with chemical absorption (CO2CRC, 2011)

The solvent used in this process is commonly monoethanolamine (MEA) solution with 30 wt% concentration. This solution can absorb about 80-95% of CO_2 in the flue gas (Biliyok *et al.*, 2012). Higher concentration of the MEA solution will accelerate corrosion of the equipments. On the other hand, there will be considerable decrease in CO_2 capture efficiency with less concentrated MEA solution. Other solvents also used include diethanolamine (DEA), methyldiethanolamine (MDEA), ammonia, piperazine (PZ), solvents blends (e.g. MEA/MDEA) and sterically hindered amine such as KS-1, KS-2 and KS-3 developed by Kansai Electric Power Co (Wang *et al.*, 2011). MEA is more commonly used due to its high reactivity with CO_2. However, it has higher tendency of causing equipment corrosion and requires more energy for regeneration.

Solvents used in PCC process are generally susceptible to degradation by oxygen, SOx and NO_x usually present in the flue gas (Eswaran *at al.,* 2010). High temperature of the flue gas can also cause solvent loss by evaporation. To maintain the integrity of the solvent, the flue gas is therefore conditioned to meet the entry requirements of the PCC plant (<10ppm SOX and about 45^OC-50^OC temperature

etc.). Flue gas cleaning units for removing SO_x, NO_x, and particulates in the flue gas, and a cooler are therefore needed upstream the PCC unit so as to satisfy the entry requirements (Rao *et al.,* 2004, Ramezan *et al.,* 2007).

1.1.3.3 CO_2 transport and storage

In IPCC (2005), a number of options are outlined for CO_2 transport, namely marine tankers (shipping), rail and road tankers and pipeline. In CCS, huge volumes of CO_2 are expected to be transported over long distances. For example in the planned White Rose CCS project in the UK, about 2 million tonnes of CO_2 per year (Capture Power, 2014) captured from planned 450 MWe oxyfuel power plant at Drax in the UK will be transported over 167 km distance to offshore storage location (Luo *et al.,* 2014). As a result, pipeline transport is considered the most reliable and economical of all the transport options in CCS applications (Lazic *et al.,* 2013). However, under some circumstances such as deep offshore, shipping transport is more economical compared to pipeline transport (IPCC, 2005).

CO_2 pipelines have been in operation in North America since 1970s and globally there about 5800km of high pressure CO_2 pipelines transporting about 50 Mt/year of CO_2 mostly for EOR projects (IPCC, 2005). Pipelines have also been used for decades for transporting hydrocarbons. However, CO_2 pipelines in CCS applications differ from hydrocarbon pipelines and CO_2 pipelines in EOR applications in a number of ways:

- CO_2 transported in EOR applications come from naturally occurring sources (Cortez, Sheep Mt, Bravo, Central Basin pipelines) and gasification plants (Canyon Reef, Weyburn, Val Verde, Bairoil pipelines) and are relatively pure as a result. In CCS applications, transported CO_2 contain impurities since they are from anthropogenic sources (IPCC, 2005). Thermodynamic analyses show that impurities alter CO_2 properties significantly (Li and Yan, 2006). As a result, pipeline transport of impure CO_2 in CCS will require a different design and operation compared to pipeline transport of pure CO_2 in EOR projects.
- More amounts of CO_2 are expected to be transported in CCS applications through areas that are likely densely populated. In comparison, EOR CO_2 pipelines are often routed through sparsely populated areas. Therefore, more

precise evaluation of the pipelines in CCS applications is necessary to reduce the chances of associated hazards.

- Compared to hydrocarbon pipelines, design and operation of CO_2 pipelines in CCS application is more complex due to the highly non-linear thermodynamic properties of CO_2, complexities introduced by impurities and the requirement to transport CO_2 above critical point conditions (*i.e.* dense/supercritical phase) (Paul *et al.,* 2010).

Captured CO_2 will be stored either in geological formations (e.g. depleted oil and gas reservoir, saline aquifers), underwater (ocean storage) or through mineralization (IPCC, 2005). Among these options, geological storage is the most matured since it relies on well established technologies already developed for the oil and gas industry. Utilization of captured CO_2 for EOR purposes or manufacturing is also possible. CO_2 utilization can help balance the economics of the CCS technology.

1.2   Motivations

Commercialization of CCS has become more likely in recent years with some of the world's largest CCS projects expected to become operational soon (MIT, 2014a):

- Boundary Dam CCS project, Canada 2014
- Kemper County CCS Project, USA 2015
- ROAD CCS project, Netherland 2017

In the past, most studies on CCS had focused on individual components of the CCS chain, namely CO_2 emitter (Oko and Wang, 2014), CO_2 capture process (Lawal *et al.*, 2010), CO_2 transport (Chaczykowski and Osiadacz, 2012) and storage (Werner *et al.*, 2014). These studies do not uncover the implications of integrating these components and operating them as a single unit as expected. The components are dynamically coupled to each other and understanding how they interact with each other during operation can be useful for designing and operating the CCS chain. Studies involving integrated CO_2 emitter (coal-fired subcritical power plant) and PCC process have been reported (Lawal *et al.*, 2012). Lawal *et al.* (2012) showed that PCC has slower dynamics compared to the power plant. This understanding will be useful for designing controls for the process and determining a reliable operation strategy. This shows the usefulness of studying integrated components of the CCS

chain. Similar view probably inspired the development of gCCS modelling tool-kit[®] which was launched recently by PSE Ltd (PSE, 2014a). The gCCS modelling tool-kit[®] provides a platform for modelling and simulation of the CCS chain to support design and operating decisions across the CCS chain.

In addition, the Mountaineer CCS project which is a pilot-based study of the CCS chain has also been reported. The project comprised of a 30 MWe side slip from the 1300 MWe Mountaineer coal-fired power station in West Virginia, USA (MIT, 2014b). The project was launched in Oct., 2009 and operated for about 4,400 hours during which 15,000 metric tons for CO_2 was captured, transported by pipeline and stored underground. The second phase of the project (demonstration phase) planned to start in 2015 where the capacity was to be scaled up to 235 MWe capacity was cancelled due to unknown climate policy. The pilot scale is insufficient to properly understand the dynamic behaviour for a large scale CCS chain. Also, in Oct. 2014, the Boundary Dam CCS Project in Saskatchewan, Canada was commissioned (MIT, 2014c). The project involves CO_2 capture from a 160 MWe (gross) coal-fired power plant (rebuilt unit #3 of Boundary Dam Power Station) using PCC with chemical absorption. About 1 million tonnes per year of captured CO_2 is transported via a 66km pipeline to Weyburn fields where it is used for EOR purposes. This makes the Boundary Dam CCS the biggest operational CCS project in the world. The CCS chain studies described above are all confidential and their details are unavailable in open literature. More studies are therefore required on CCS chain to properly understand how the components will interact during operation.

1.3 Aim, objectives and novel contributions

The aim of the research is to develop dynamic models of a CCS chain from first principle. The CCS chain will include CO_2 emitter (coal-fired subcritical power plant), CO_2 capture plant (PCC with chemical absorption), CO_2 compression and pipeline transport network. As explained in the previous section, a dynamic model of the CCS chain is useful for studying the dynamic behaviour of the process. Modelling and simulation provide a safe, reliable and economic option for studying the behaviour of any process. The importance of modelling and simulation is further highlighted by the absence of establish CCS chain in operation except Boundary Dam CCS. To accomplish this aim, the following objectives were set out.

- Comprehensive and detailed review of existing literature on modelling and simulation of CCS chain. This is necessary to determine the level of existing work in the area so as to clearly spell out which existing knowledge gaps that could be filled with the outputs of this research.

- Dynamic modelling of the individual components of the CCS chain. The PCC model developed in Lawal *et al.* (2010) will be used. The model is very detailed and has been validated at steady state and dynamic conditions (Biliyok *et al.* 2012). The detailed PCC model is very complex and takes lots of time for simulating different case studies. The CCS integrated model is expected to be used for studying different process scenario within a short time. As a result, the detailed PCC model was considered unsuitable for use in the CCS integrated model. Consequently, the detailed PCC model will be simplified. The simplified PCC model will be validated against the detailed PCC model.

- Dynamic modelling and simulation of the CCS chain. The model of the CCS chain derived from a combination of the component models will be used to investigate the impact of load change on the network.

In addition, a blackbox model of the drum boiler in a coal-fired subcritical power plant will also be developed.

This study represents a significant contribution to knowledge as there are yet to be a dynamic model of an integrated CCS network available in open literature to the best of my knowledge. There are existing/planned pilot/demonstration integrated CCS networks mentioned in the previous sections. However, the details of those studies remain confidential and unavailable in open literature. Other novel contributions of this research include:

- Detailed model of coal-fired subcritical power plant which captures key behaviour over wide operating range (70-100% load). The model included detailed model of the drum and feedwater heater train. The drum involved a good description of steam volume below water level in the drum. This is essential for capturing the drum level and pressure dynamics accurately. Steam drum and feedwater heater train models are often very simple in majority of existing coal-fired subcritical power plant models.

- Simplification of detailed rate-based dynamic model of PCC with chemical absorption. In this study, the strategy used by Peng *et al.* (2003) for simplifying

model of packed reactive distillation column for the production of tert-amyl methyl ether (TAME) was used. The simplification strategy was improved successfully for the rate-based model of PCC with chemical absorption.

- Dynamic modelling and simulation of a multi-source CO_2 pipeline transport network based on the planned Yorkshire and Humber pipeline transport network (Luo *et al.*, 2014). Existing dynamic models of CO_2 pipeline transport network are based on single sources. Expected compositions of the captured CO_2-rich stream and elevation changes have been included in modelling the CO_2 pipeline transport network.

- Dynamic modelling and simulation of the drum boiler in a coal-fired subcritical power plant using NARX neural networks. Existing neural network models of the drum boiler have been derived using static feedforward networks. Static feedforward network models cannot be used for dynamic studies of plant behaviour. Dynamic neural network models are developed using recurrent networks such as NARX neural networks (Connor *et al.*, 1994; Beale *et al.*, 2014).

1.4   Scope of the thesis

In this thesis, model-based investigation of a CCS chain is presented. The CCS chain includes CO_2 emitter, capture, and compression and transport systems. The storage/sequestration component was not considered. The storage/sequestration sites are geological formations which require specialist applications (e.g. Schlumberger's ECLIPSE® (Schlumberger, 2014)) and lots of parameters for accurate or at least near accurate modelling of its behaviour. Also, CO_2 storage models developed with the specialist applications cannot be incorporated into process simulators such as gPROMS ModelBuilder® for the purpose of modelling the CCS chain. The problem with combining geological models of CO_2 storage and process models of CO_2 emitters, capture, compression and pipeline transport to obtain a model of a CCS chain has been solved in gCCS modelling tool-kit®. The tool-kit® contains simple geological model for CO_2 storage and relatively simple models of other components of the CCS chain. Model of the CCS chain starting from the CO_2 emitter to storage can therefore be developed using the tool-kit®. The problem with using specialist applications in modelling CO_2 storage and the limitation

of relying on simple models in gCCS modelling tool-kit[®] are the reasons why modelling of CO_2 storage was excluded in this thesis.

The CO_2 emitter used in this study is a coal-fired subcritical power plant. This choice has been made because about 50% or more of existing coal-fired power plants around the world are subcritical power plants (Oko and Wang, 2014). PCC with MEA solvent was selected as the capture method. As noted earlier, PCC with MEA solvent is the most matured CO_2 capture method and has the highest potential for commercialization. A detailed model of the process developed in Lawal *et al.* (2010) will be used. Finally, the CO_2 compression and pipeline transport network is based on the planned Yorkshire and Humber CO_2 pipeline project (Luo *et al.*, 2014). The Yorkshire and Humber CO_2 pipeline is planned to cater for the transport of CO_2 captured from the future IGCC plant at Don Valley in South Yorkshire and Oxy-coal power plants near Selby in North Yorkshire to saline aquifers beneath the North Sea off the coast of Bridlington in UK for storage.

1.5   Tools to be used

The Process Systems Enterprise's gPROMS ModelBuilder[®] was used in this thesis for modelling the CCS chain. The gPROMS ModelBuilder[®] supports development of custom process models and flowsheeting from first principle in steady state and dynamic conditions (PSE, 2014b). The platform has in-built solvers for differential and algebraic equations (DAE). Partial differential equations (PDEs) are solved using method of lines (MOLs) (PSE, 2012b). The MOLs is a solution method that converts a PDE into a set of ODEs involving only time-dependent functions and time-derivatives. The resulting set of ODEs is then solved efficiently using the in-built DAE solvers. With MOLs, PDEs are therefore solved efficiently using advanced DAE solvers. In addition, gPROMS ModelBuilder[®] is CAPE-OPEN compliant. CAPE-OPEN standards are the uniform standards based on universally recognized software technologies such as COM and CORBA for interfacing process modelling software components developed specifically for the design and operation of chemical processes (CO-LaN, 2014). It is therefore possible to interface gPROMS ModelBuilder[®] with other external packages.

Aspen HYSYS[®] was used to obtain a benchmark model for providing some form of validation for the CO_2 pipeline transport model. Most CO_2 pipeline projects are still in

planning phase and as such there are no operating/design data for validating the CO_2 pipeline transport models. Aspen HYSYS® comprise of models of different process components and is used widely for process simulations in the industry.

MATLAB® was used for developing the blackbox model of the drum boiler. MATLAB® is a general purpose modelling and simulation platform.

Thermodynamic and transport properties were calculated using robust platforms, namely Aspen Properties® and Infochem's Multiflash®. These platforms rely on well established equations of state (EOS) such as the ElecNRTL, GERG 2008, and Peng-Robinson among others and are well validated. Aspen Properties® is CAPE-OPEN compliant and can easily be interfaced with gPROMS ModelBuilder®. Infochem's Multiflash® is directly accessible within gPROMS ModelBuilder®. It is presently not possible to call thermodynamic property derivatives (*i.e.* $\frac{\partial \rho}{\partial P}, \frac{\partial h}{\partial P}, \frac{\partial T_{sat}}{\partial P}$) across the interface from gPROMS ModelBuilder®. As a result, the property derivatives in this thesis were obtained using polynomial approximation of steam table calculations from NIST REFPROP® V9.1. NIST REFPROP® is widely used in the industry especially for water/steam property calculations. Aspen HYSYS® have in-built fluid packages, namely Peng-Robinson, Soave-Redlich-Kwong, among others for calculating properties.

1.6 Thesis organisation

The thesis is organised into eight chapters. The rest of the chapters are organised as follows:

In **Chapter 2**, review of existing study on modelling of coal-fired subcritical power plant, PCC plant and CO_2 compression and pipeline transport is presented. Conclusions arising from the review are also presented.

Dynamic modelling of the reference coal-fired subcritical power plant is presented in **Chapter 3**. This includes a description of the reference plant and model equations of the plant components. Results of steady state validation of the model in addition to analyses performed using the model is also presented.

In **Chapter 4**, simplification of the detailed rate-based model of the PCC process with chemical absorption is presented. The detailed rate-based model of the PCC was developed in Lawal *et al.* (2010). Some high level information will be given

about the model to help the readers. Results of validation of the simplified model will also be presented.

In **Chapter 5,** models for the compressor and pipeline network alongside general information on issues considered in CO_2 pipeline transport are presented. Results of a multi-source dynamic model of the Yorkshire and Humber CO_2 pipeline network are also presented. The model considers CO_2 transport from different capture sites using a common trunk pipeline.

In **Chapter 6**, the model of the CCS chain is presented. Results and discussions from analysis of different operating scenario performed with the CCS chain are also presented.

In **Chapter 7**, modelling of drum-boiler dynamics using NARX neural networks is presented. Brief description of neural networks is given alongside procedure for model development. Dynamic validations of the NARX neural networks model are also presented.

Finally, conclusions and recommendations for future direction drawn from the thesis are presented in **Chapter 8**.

Chapter 2: Literature review

In this chapter, review of existing studies will focus on specific examples of the various components of the CCS chain, namely coal-fired subcritical power plant presented in Section 2.1 CO_2 emitters, post-combustion CO_2 capture presented in Section 2.2 and CO_2 pipeline transport presented in Section 2.3. As noted in Chapter 1, CO_2 storage is not included in this thesis. Review of studies on integrated CCS components is presented in Section 2.4. Finally, concluding remarks on all the studies reviewed is presented in Section 2.5.

2.1 Modelling of coal-fired subcritical power plants

There has been extensive study on modelling and simulation of coal-fired subcritical power plants (Fig.2.1) based on different approaches, namely blackbox (data-based), first principle and a combination of both. Majority of the studies have however focused on individual components of the power plant particularly the boiler. As a result, in carrying out the review of existing coal-fired power plant models, reported models of the plant components (*i.e.* boilers and steam turbines) are also reviewed. The feedwater heating train are rarely studied as stand-alone since they are generally heat exchangers of which sufficient studies already exist.

2.1.1 Boiler

Boilers are generally classified into supercritical boilers when they operate above the critical point of water and subcritical boilers when they operate below the critical point of water. In this thesis, interest is on subcritical boilers since majority of operational coal-fired power plants across the world uses subcritical boilers (Finkenrath *et al.*, 2012). Subcritical boilers comprise of a steam drum-downcomer-riser loop and heat exchangers, namely superheaters, reheaters, and the economiser. The steam drum is an accumulating tank. It receives feed water from the economizer at sub-cooled condition, distributes the water to the furnace walls (waterwall) through the downcomers. In the waterwall, the water receives radiant heat from the furnace and transforms into a water-steam mixture. The water-steam mixture returns to the drum through the risers where they become separated. Water is re-circulated while the saturated steam exits the loop and goes through a series of

superheaters before entering the steam turbine. In literature, different approaches, namely first principle and data-driven methods (blackbox) have been used in modelling the boiler.
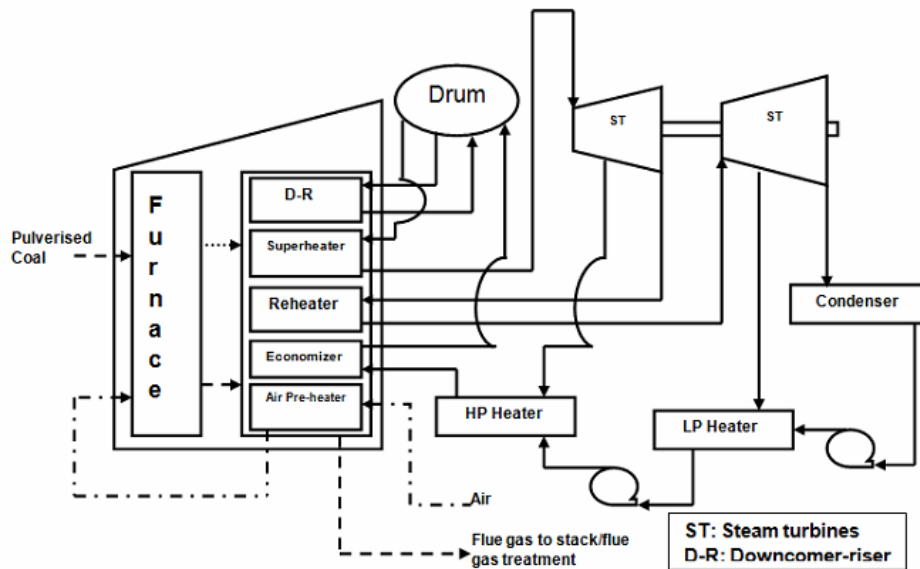
Fig. 2.1 Descriptive block flow diagram of coal-fired subcritical power plant

2.1.1.1 First principle models

The foremost subcritical boiler model was reported in Chien *et al.* (1958). In this model, only the drum-downcomer-riser loop, superheater and furnace components were represented. The model is a linear model obtained by small perturbations around operating point. Similarly, a dynamic model of a 200MWe coal-fired subcritical boiler was presented in Thompson (1967). The economiser was modelled in addition to the components modelled by Chien *et al.* (1958). Circulation in the drum-downcomer-riser loop of the boiler modelled in Thompson (1967) was by forced circulation in contrast to the boiler modelled in Chien *et al.* (1958) which was by natural circulation. In Chien *et al.* (1958), water/steam properties were assumed constant in the water walls and superheater. However, in Thompson (1967) a unique iterative method was to compute accurate steady-state profiles of the superheater and water wall section thereby obtaining more accurate prediction of the properties across the length of the superheaters and waterwalls. Finally, burner tilt parameter was included in the furnace model in Thompson (1967). More simplistic representation was used in Chien *et al.* (1958). The model in Thompson (1967) is more robust and detailed than Chien *et al.* (1958) but more complicated.

Eklund (1968) developed a linear dynamic model from first principle for a natural circulation drum-boiler. In this model, only the drum-downcomer-riser loop was considered and extensive validation was provided. Tyssø (1981) developed a linear dynamic model of a drum-downcomer-riser loop using natural circulation. The author used extended Kalmar filter method with real plant measurements to determine the process parameters. Steam bubble distribution below the drum level was ignored and as a result the model may not predict drum level accurately. In De Mello (1991), a model of drum-downcomer-riser loop with forced circulation plus superheater is reported. The drum-downcomer-riser loop was modelled together and better description was given for the drum level.

Flynn and Malley (1999) presented more comprehensive first principle dynamic model of a 305MWe subcritical boiler. The components modelled included the furnace, drum, downcomer-riser loop, superheater, reheater and throttle valve. The model was used to investigate the effect of long term disturbances (>30sec) such as sharp rise in frequency due to load loss etc. Investigation of long term disturbances using a model of a subcritical boiler have also been reported in Chang and Yu (2008) and Roytelman and Shahidehpour (1994). Flynn and Malley (1999) however used distributed models for the superheater, reheater and economiser and lumped model for the furnace. Chang and Yu (2008) and Roytelman and Shahidehpour (1994) used lumped model for all the components.

Åström and Bell (2000) presented a first principle non-linear dynamic model for natural circulation drum-boiler with extensive dynamic validation. Extensive validation for drum-boiler model is also given in Leva *et al.* (1999). Åström and Bell (2000) model considered only the drum-downcomer-riser loop. The model gave a good description of shrink and swell behaviour by accounting for steam-water distribution in the drum. As a result, the model gave good predictions of the drum level and pressure behaviour. Good representation of the shrink and swell behaviour was also reported in Liu *et al.* (2001) and Kim and Choi (2005). In contrast to the model in Åström and Bell (2000), condensation in the drum was neglected in Liu *et al.* (2001). Condensation in the drum has strong implication for describing the shrink and swell mechanism in the drum. Kim and Choi (2005), on the other hand, provided more detailed description of steam distribution below water level in the drum by taken phase slip into account in the riser.

In Adam and Marchetti (1999), separate non-linear dynamic models for evaporation in the vertical tubes (risers) and phase separation in the steam drum using first principle for a 30MWe subcritical thermo-electric power plant was presented. The models were combined to represent a drum type natural circulation boiler. The shrink and swell behaviour in the drum was described in detail in the model. Diaz (2001) presented a boiler model with the following components: furnace, superheaters, attemperators, economiser, water pre-heater, steam drum, and tube banks (water walls) with detailed description of the shrink and swell behaviour in the drum. In Bhambare *et al.* (2007), a boiler model with drum-downcomer-riser loop, superheater, reheater, attemperators and the furnace is presented. The furnace model included parameters for number of burners in service and burner tilt.

2.1.1.2 Data-driven (blackbox) models

Majority of existing boiler models are derived from a first principles approach. Few models have however been derived using data-driven methods. Data-driven models are simpler to develop and have less computational requirement compared to first principle models. Rusinowski and Stanek (2007) presented a boiler model based on feedforward neural network (NN) which is able to predict energy losses in the boiler furnace. The training data was obtained from a combination of physical measurements and a first principle model of the boiler studied. In another study, same authors, Rusinowski and Stanek (2010), showed that combination of empirical and first principle approach are simpler than using wholly first principle approach and more robust than empirical models only. Smrekar *et al.* (2009) presented a neural network model of a coal-fired boiler capable of predicting steam temperature, pressure and mass flowrate. The training data was obtained from real plant and was subject to filtering to remove outliers and hence reduce erroneous measurements.

2.1.1.3 Summary

In summary, assumptions of no slip between vapour and liquid phases in the riser loop are common in reported models. Reported results show this to be reasonable at normal operating conditions (Åström and Bell, 2000). Secondly, good representation of drum level is only possible if steam-water distribution is adequately described in the drum (shrink and swell effect). Finally, incorporation of empirical methods within

first principle models simplifies first principle models without compromising satisfactory results (Rusinowski and Stanek, 2010). Existing blackbox boiler models are mostly used for steady state predictions and not fit for studying operating behaviour.

2.1.2 Modelling of steam turbine

Steam turbines comprise of a bank of turbine stages (*i.e.* HP, IP and LP turbine stages) arranged either on a single end-to-end axle tandem arrangement) (Fig.2.2) or on separate axles (cross compound arrangement) (Fig.2.3). The HP turbine steam outlet is either reheated before entering the IP turbine or goes straight to the LP turbine depending on the arrangement. Steam is also extracted at different stages of the turbine for feedwater heating. This enhances the efficiency of the thermodynamic cycle by reducing the amount of heat rejected in the condenser. Existing models of steam turbine have been developed using first principle and/or blackbox methods.
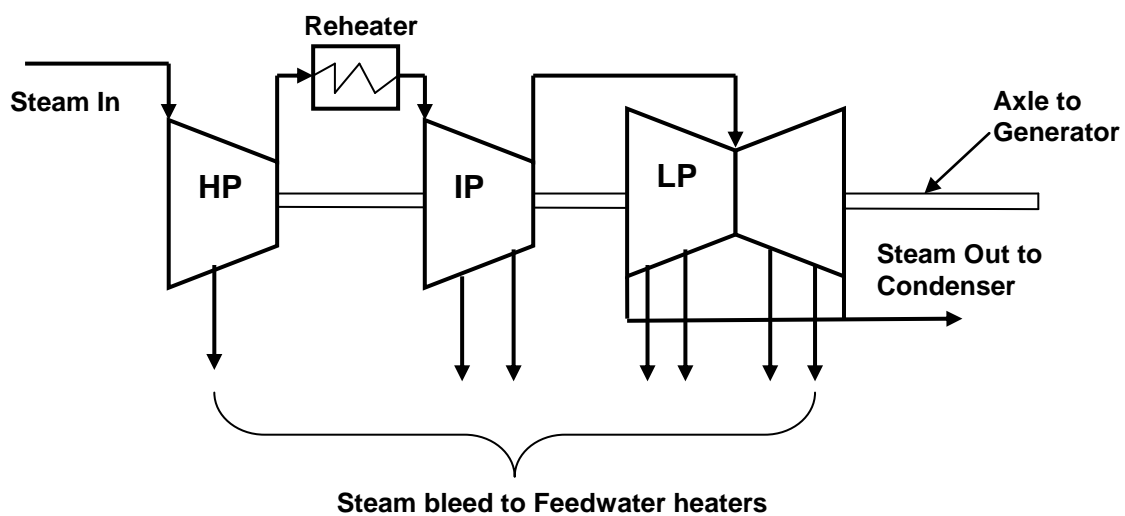
Fig. 2.2 Steam turbine in tandem arrangement

2.1.2.1 First principle models

First principle steam turbine models are generally developed based on the Stodola ellipse (Cooke, 1983; Lo and Song, 1990). Basic transfer function model of a steam turbine is presented in IEEE Committee Report (1973). The components modelled include the HP, IP and LP turbine, reheater, steam chest, crossover piping and the speed-governing system. Different turbine arrangements (tandem and cross compound) for different cases, namely non-reheat, single reheat and double reheat

were investigated. Also, Ray (1980) presented a nonlinear dynamic model of a steam turbine with sufficient simplicity and accuracy for controller design. Zimmer (2008) presented steam turbine models with different complexities levels. In the model with the least complexity, energy and mass storage potentials were neglected and vice versa for the model with the highest complexity.

Fig. 2.3 Steam turbine in cross compound arrangement

2.1.2.2 Data-driven (blackbox) models

Empirical approach using single-layered perceptron (neural networks) has also been exploited for steam turbine modelling (Sobanska and Szczepaniak, 2006). The model components included a 10.5MWe back-pressure steam turbine, 6MWe condensing steam turbine, heat exchanger and valve. The training data as obtained from an experimental facility and the model showed acceptable response within the conditions considered. Combination of empirical and first principle approach for steam turbine modelling was demonstrated by Chaibakhsh and Ghaffari (2008). The non-linear dynamic model comprised of the HP turbine, IP turbine, LP turbine, reheater, and generator components. The model parameters were determined by empirical relations obtained from experimental data and adjusted to optimal values using GA. Steam properties between IP and LP were represented by correlations

20

that accounted for non-ideal behaviour. Steam properties deviate from ideal behaviour at this region and assuming ideal condition limits the model performance.

2.1.2.3 Summary

In summary, the Stodola ellipse expressed in terms of temperature has been used in majority of the first principle models reviewed in this thesis. The Stodola ellipse in this form gives satisfactory results at conditions that the perfect gas law is valid (Lo and Song, 1990). The Stodola ellipse expressed in terms of specific volume give satisfactory results at all conditions (Lo and Song, 1990). Steam turbine models intended to capture the dynamics over wide operating condition should therefore be based on this form of the of the Stodola ellipse. Finally, considering energy and mass storage characteristics in the turbine results to better dynamic performance over wide operating conditions (Zimmer, 2008).

2.1.3 Modelling of coal-fired subcritical power plant (Whole plant)

The boiler and steam turbine models alone do not provide holistic insights about the dynamic behaviour of the whole plant (*i.e.* boiler, steam turbine, condenser and feedwater heater). Studying the overall behaviour of the whole plant therefore requires a model of the whole plant. In literature, different methods have been used to model the whole plant as follows.

2.1.3.1 First principle models

One of the earliest whole plant models was reported in Kwan and Anderson (1970). The authors obtained a linear whole plant model (boiler and turbines) using the same approach as Chien *et al.* (1958). The condenser and feedwater heater train was not included in the model. In Åström and Eklund (1972), a simple non-linear model of a 160MW drum boiler-turbine unit is presented. The model was obtained by a combination of empirical and first principle approach. The model was extended with improved performance in Bell and Åström (1987). In De Mello *et al.* (1991), a simplified boiler-turbine model unique in simulating extended period of disturbances such as load loss among others (long term simulation) was presented. The feedwater heater train components was however not included in the model.

Lu (1999) presented boiler-turbine models for a 677MW coal-fired subcritical power plant. The model included a fairly detailed description of the water/steam two-phase flow with heat transfer in the water walls. Liu *et al.* (2004) and Colonna and VanPutten (2007) presented a whole plant model of a coal-fired subcritical power plant that included the condenser component. Colonna and VanPutten (2007) however did not model the furnace component. More detailed whole plant model is presented in Lu and Hogg (2000). The model is based on a 200MWe coal-fired subcritical power plant and the components modelled include the boiler, steam turbine, feedwater heater train, valves, piping and the generator. In Li *et al.* (2005), a computer program reportedly capable of simulating start-up behaviour of forced and natural circulation subcritical power plant is presented. The model benchmark was a 600MW subcritical coal-fired power plant. Distributed parameter approach was adopted for heat transfer in the water walls, superheaters, reheater and economiser while lumped parameter approach was adopted for drum, downcomer and risers. Finally, Lin and Yiping (2011) presented a simple linear dynamic boiler-turbine model derived from transfer functions.

2.1.3.2 Data-based (blackbox) models

Chawdhry and Hogg (1989) identified the model for a 200 MWe unit at Ballylumford Power Station (Northern Ireland) using two-stage recursive least squares (RLS). The data used to derive the model were obtained by applying PRBS inputs to the plant. Irwin *et al.* (1995) developed feedforward NN model of the same plant in Chawdhry and Hogg (1989). The model predictions were comparable to results obtained from linear multivariable ARMAX model of the plant. In Lu and Hogg (2000), NN model of a 200MWe coal-fired subcritical power plant was developed and the predictions were in agreement with a first principle model of the same plant. NN modelling approach is also reported in De *et al.* (2007) for the steam process of a coal-biomass co-fired combined heat and power plant. Validation results showed good prediction of the power output.

Habbi *et al.* (2003) developed a non-linear model of a natural circulation boiler-turbine using Takagi–Sugeno–Kang fuzzy technique. The model reportedly captured the key dynamic behaviour over wide operating conditions. Also the model gave similar predictions as complex first principle models such as Bell and Åström (1987).

Boiler-turbine models derived using the Takagi-Sugeno (T-S) fuzzy technique have also been reported in Lin and Shen (2011) and Jinxing and Jiong (2011). T-S is based on fuzzy clustering, least square and GA. Self-organizing fuzzy model generation strategy based on GA was used to choose optimal fuzzy model with a good trade-off between fitting the training data and model simplicity.

2.1.3.3 Summary

In summary, most whole plant dynamic models studied only consider the boiler-turbine (forward loop) without the condenser and feedwater heaters (backward loop). While this may be enough to predict output trajectories, it do not give good picture of reality as it cannot be relied on for studying how changes propagate around the power cycle. Also, most of the models are very simple especially in representing the furnace and drum boiler dynamics. Finally, blackbox methods show good credibility for modelling the whole plant. The only difficulty however is in obtaining the right sets of plant operation data that can be used to develop the model.

2.2 PCC process with chemical absorption

2.2.1 Experimental studies

PCC process has been studied extensively through experimental investigation (Wang *et al.*, 2011). These studies have been useful for validating model-based results and for developing correlations used in modelling. For instance, CO_2 reaction kinetics information which are very useful in PCC modelling have been derived from experimental studies and reported in Aboudheir *et al.*, (2003) and Edali *et al.* (2009) among others. Aboudheir *et al.* (2003) developed a termolecular-kinetics model for CO_2 reaction with MEA solutions which reportedly bettered other published kinetic models. Edali *et al.* (2009) developed kinetic models for CO_2 reaction in a mixed solution of MDEA and MEA. Information about thermodynamic and solubility of CO_2 in different solvents (MEA, MDEA etc) obtained through experimental study are reported in Bishnoi and Rochelle (2002) and Inoue *et al.* (2013). Goff and Rochelle (2004) examined the rate of oxidative degradation of MEA under typical operating conditions for PCC.

Some other experimental studies have focused on screening different solvents to determine the solvents that gives best performance in terms of regeneration energy requirement and degradability (Idem *et al*., 2006; Notz *et al*., 2007; Knudsen *et al*., 2009; Mangalapally and Hasse, 2011a; Moser *et al*., 2011). Characteristics of different packing material have equally been assessed to determine their impact on capture performance (Park *et al.*, 2004; Mangalapally and Hasse, 2011b). Comparison of different packings and impact of packing height and column was investigated extensively in Dugas (2006).

Finally, Faber *et al.* (2011) investigated the transient behaviour of the PCC process through step response test. The test was performed at a 1 ton CO_2/hour pilot plant for the amine-based PCC within the EU project CESAR. It was found that the overall system acts like a buffer and tends to accommodate perturbations at the inlet with minor fluctuations downstream. This behaviour is desirable considering the future downstream compression unit.

2.2.2 Model-based studies

CO_2 absorption/stripping in PCC process with chemical absorption involves complicated gas-liquid mass transfer and chemical reactions. When modelling the process from first principle, gas-liquid mass transfer can be described based on the assumption of gas-liquid equilibrium (*i.e.* equilibrium-based approach). In reality, gas-liquid equilibrium is hardly achieved and the approach is therefore not very accurate (Kenig *et al.,* 2001; Peng *et al.*, 2002). More accurate representation of the mass transfer process is obtained using two-film theory (Lawal *et al.,* 2010) or penetration theory (Tobiesen *et al.*, 2007) (*i.e.* rate-based or non-equilibrium approach). Details of two-film and penetration theories are available in literature.

On the other hand, CO_2 reaction kinetics can be approximated by assuming that the reactions reach equilibrium (Lawal *et al.*, 2010). When the reactions progresses very rapidly as it is the case with fast reacting solvents like MEA solvent, then this assumption is sufficient (Kenig *et al.,* 2001; Lawal *et al.*, 2010). With less reactive solvents such as DEA, MDEA etc, this assumption is less accurate. More accurate description of the CO_2 reaction kinetics can be obtained using actual kinetics model (Zhang *et al.,* 2009). This can be simplified by assuming pseudo first order reaction

and introducing an enhancement factor which accounts for the kinetics (Kucka *et al.,* 2003; Kvamsdal *et al.*, 2009).

From a combination of the methods for describing mass transfer and reaction kinetics, models of PCC processes with chemical reactions can be classified into different levels of complexities. In literature, five levels of complexity shown in Fig.2.4 was identified (Kenig *et al.,* 2001) with Level 5 considered to be the most accurate because it adopts a rate-based approach for describing mass transfer process and actual kinetic model for the chemical reactions. There have been varied PCC models in literature with different level of complexities.

Dynamic models involving only the absorber (Kvamsdal and Rochelle, 2008; Lawal *et al.*, 2009a; Kvamsdal *et al.,* 2009; Khan *et al.*, 2011; Posch and Haider, 2013) and only the stripper (Lawal *et al.*, 2009b; Ziaii *et al.*, 2009) are available in literature. In these models, rate-based approach has been used to describe gas-liquid mass transfer process except in Posch and Haider, (2013) where gas-liquid equilibrium conditions were assumed.

In Lawal *et al.* (2009a), Lawal *et al.* (2009b) and Ziaii *et al.* (2009), the reaction kinetics is approximated by the assumption that the reactions reach equilibrium. This is an example of level 3 complexity model. As noted earlier, for fast reacting solvents such as MEA, this assumption can be considered fairly reasonable.

On the other hand, in Kvamsdal and Rochelle (2008) and Kvamsdal *et al.* (2009) the reaction kinetics was approximated by an enhancement factor with the reactions assumed to be pseudo first order. In Khan *et al.* (2011), fast second-order kinetics for the CO_2–MEA reactions alongside an enhancement factor was used. These models have higher computational requirement and will give better results since the reaction kinetics is represented more accurately (Gáspár and Cormoş, 2011). This is an example of level 4 complexity model. In Posch and Haider (2013), reaction kinetics was obtained using the termolecular reaction scheme presented in Aboudheir *et al.* (2003). The model is as a result a 2 complexity model.

Dynamic model of the complete PCC process with chemical absorption including the absorber and stripper is also available (Lawal *et al.*, 2010; Harun *et al.*, 2011; Gáspár and Cormoş, 2011; MacDowell *et al.*, 2013). Mass transfer process in the models was described using rate-based approach. The reaction kinetics was approximated with equilibrium reactions in Lawal *et al.* (2010) and MacDowell *et al.*

(2013) as per level 3 complexity and enhancement factors in Harun *et al.* (2011) and Gáspár and Cormoş (2011) as per level 4 complexity.

Lawal *et al.* (2010) used ElecNRTL for determining thermophysical properties and found that the absorber is more sensitive to L/G ratio than actual solvent flowrate (L) and flue gas flowrate (G). Dynamic validation of the model developed by Lawal *et al.* (2010) is reported by Biliyok *et al.* (2012). Harun *et al.* (2011) showed that performance of the PCC process is affected by load reduction at the absorber inlet significantly affects the performance of absorber and stripper.
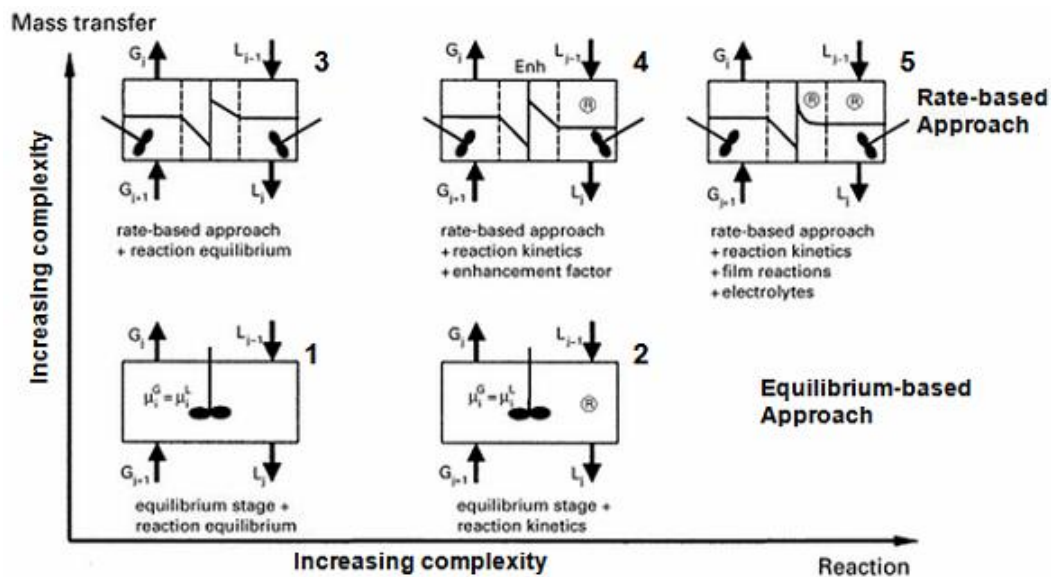
Fig.2.4 Complexity levels of PCC models (Kenig *et al.,* 2001)

MacDowell *et al.* (2013) used SAFT-VR EOS for property calculations. The EOS accounts for all of the inter-species interactions in the fluid, including the reactions and therefore avoids the need for enhancement factors. They found that the position and extent of the mass transfer zone is a function of competing interphase fluxes of H_2O and CO_2. Gáspár and Cormoş (2011) used a combination of methods for estimating different thermophysical properties, namely Antoine equation, Lee Kesler, and Wilson-NRF. They conclude from their analysis that reduction of the solvent temperature at the stripper inlet has strong influence on the behaviour of the whole process.

2.2.3 Summary

In the models reviewed, insufficiency of plant data for detailed validations has been a recurring difficulty. This challenge was highlighted in a review by Chikukwa *et al.* (2012). As a result, some of the conclusions arising from the models are yet to be validated against actual plant data. However, the results of the models are reasonably in agreement with each other. Secondly, it is also found that there is yet to be a level 5 dynamic model of the PCC process which is based on rate-based mass transfer and actual CO_2 reaction kinetics. With detailed reaction kinetic modelling, the model is more complex and the amount of accuracy such complexity can bring into the model have been questioned a times with MacDowell *et al.* (2013) suggesting that it is enough to assume the reactions reach equilibrium as commonly adopted in many existing models. Finally, existing data such as the one in Dugas (2006) are obtained from pilot plants with capacities in the order of one-hundredth of typical large scale PCC. It is therefore difficult to extrapolate the findings from pilot plant to predict the behaviour of large scale plants.

2.3 CO_2 pipeline transport

2.3.1 Existing studies

There have been a lot of studies on feasibility and viability of CO_2 pipeline transport (IEA GHG, 2002; Svensson *et al.*, 2004; McCoy and Rubin, 2008; Seevam et al, 2008; Lazic *et al.*, 2013). Most of the studies agree that that transport of CO_2 in the dense phase is the most efficient. More information will be given on this in Chapter 5. Also, levelized cost estimates of CO_2 pipelines in different studies have been similar (IPCC, 2005; Lazic *et al.*, 2013). More detailed techno-economic analysis by Luo *et al.* (2014) show higher levelized cost. The study by Luo *et al.* (2014) involved steady state simulation of a typical CO_2 transport network with compression stations unlike previous techno-economic studies which were solely based on correlations.

More detailed studies which focuses on operation and design have also been carried out (Nimtz *et al*, 2010; Liljemark *et al.*, 2011; Chaczykowski and Osiadacz, 2012; Witkowski *et al*, 2013; Raimondi, 2014). Aursand *et al.* (2013) highlighted some of the challenges with CO_2 mixture pipeline modelling. Some of these challenges are summarised in Chapter 5. Nimtz *et al.* (2010) investigated the temperature, pressure, density and velocity profile along transport and injection pipeline under different operating scenario using a steady state pipeline transport model. They suggest that

two-phase flow condition could result under some scenario based on the profile. Liljemark *et al.* (2011) assessed start-up, shutdown, normal operation and emergency shutdown scenario for a CO_2 pipeline network using a dynamic model of the network. They found that load change and shutdown situation could result to two-phase flow scenario. It must be noted that this finding is subject to the CO_2 mixture composition (98 %CO_2 and 2% N_2) used in the study. Due to the influence of impurities on CO_2 properties (Refer to Chapter 5), different behaviour is possible with different compositions.

More detailed dynamic model of a CO_2 pipeline is given in Chaczykowski and Osiadacz (2012). In this study, they found that the amount of impurities have a significant influence on the hydraulics of the pipeline transport system. Witkowski *et al.* (2013) provided a thermodynamic assessment of different compressor options for CO_2 compression including conventional multistage centrifugal compressor, integrally geared centrifugal compressor, supersonic shock wave compressor and pump machines. They found that compressor duty is correlated strongly with the thermodynamic properties of CO_2. In addition, they investigated safe transport distance before boosting can be required based on inlet and environmental conditions. Raimondi (2014) compared the performance of different EOS using a CO_2 pipeline model and concluded that GERG-2004 EOS was the best EOS particularly with possibilities of two-phase flow. The conclusion was not validated against experimental data and is arguable as a result. Other studies investigated CO_2 depressurization to understand what happens in the event of leakage of high pressure CO_2 (Clausen and Munkejord, 2012; Clausen *et al.*, 2012).

2.3.2 Summary

From the review, most of the CO_2 pipeline transport models studied have been very simple, neglecting pipeline profile changes, presence of impurities, distributed nature of pipeline, and assumption of average physical properties among others. These simplifications have significant impact on the model capability. The fact the models are not validated for obvious reasons raises more concern about the abilities of the models. Also, there are no reported models for offshore CO_2 pipeline. Reported models are onshore CO_2 pipelines. In the UK for instance where most of the storage sites are beneath the sea, offshore pipelines are expected to be linking the capture

sites to the storage sites. Heat transfer with the environment and consequently the temperature profile in offshore and onshore pipelines is expected to differ. As a result, offshore CO_2 pipeline deserves separate assessment.

2.4 Studies on integrated CCS network components

There has been considerable research involving individual components of the CCS chain as described before. However, there have been studies also involving integrated components of the CCS chain. Some of these studies are reviewed below according to research direction. Only the ones that involve PCC process are considered in this review.

2.4.1 Design studies

Lucquiaud and Gibbins (2011a & 2011b) assessed different power cycle configurations for steam withdrawal for PCC solvent regeneration using a power plant with PCC reboiler model. This included replacing the LP turbine cylinder, installing pass-out back-pressure turbine from reheater, a separate ancillary boiler and an optional back-pressure turbine for the capture unit, using throttle valve at LP inlet among others. Earlier study by Cifre *et al.* (2009) showed that the lower the steam pressure extracted for solvent regeneration, the less the energy penalty incurred in the power cycle. Very low steam pressure will however be insufficient to drive the regeneration process. Aroonwilas and Veawab (2007), Romeo *et al.* (2008), and Yang and Zhai (2010) showed that the optimal location for steam extraction for solvent regeneration is from LP turbine not IP-LP crossover. However, existing LP turbines do not have extraction point within the pressure range. Based on their studies, optimal integration of PCC and the power plant is potentially possible for new builds only.

2.4.2 Heat integration studies

Harkin *et al.* (2009, 2010, and 2012) and Ho *et al.* (2009) performed steady state model-based PCC integration with a 200MWe subcritical coal-fired power plant for heat integration purposes. Using different heat integration approaches, the authors showed that energy penalty associated with PCC was potentially less than reported figures. On another study, Leng *et al.* (2010) modelled an integrated coal-fired power

plant and PCC (30 wt% MEA) for heat integration study using pinch analysis. Leng *et al.* (2010) reported significant reduction in PCC energy penalty and cooling water requirement (up to 55%). However, Leng *et al.* (2010) modelled the PCC process using an ASPEN HYSYS® stoichiometric reactor. Such simplification makes the reported results debatable. Also, Khalilpour and Abba (2011) undertook similar investigation using heat exchanger network optimization technique instead of pinch analysis. Khalilpour and Abba (2011) showed 3.5% reduction in energy penalty. Finally, Romeo *et al.* (2008) from a steady state simulation of MEA-based PCC integration with a 350MWe coal-fired power plant proposed injection of part of returning condensate from the reboiler into the extracted steam for regeneration. This will limit the amount of steam extracted for solvent regeneration and consequently reduce energy penalty.

2.4.3 Operation studies

Alie *et al.* (2006) presented a steady state model of an integrated 500MWe subcritical coal-fired power unit and PCC unit simulated at full load. They found that CO_2 loading in the lean solvent increases as stripper heat duty decrease till a certain minimum is reached beyond which CO_2 loading of the solvent increases with regenerator heat duty. Aroonwilas and Veawab (2007) using a power plant with PCC model showed that a blend of MEA and MDEA and split flow PCC configuration potentially lowers energy penalty relative to conventional PCC configuration with MEA solvent only. In Yang and Zhai (2010), dependence of capture performance on stripper pressure, solvent flowrate and loading was demonstrated using integrated power plant and PCC model. Generation efficiency was correlated with heating and cooling duties of the PCC process in Liebenthal *et al.* (2011) a model of 1100MWe supercritical coal-fired power plant integrated with a PCC plant.

Lawal *et al.* (2012) and more recently, MacDowell and Shah (2014) presented dynamic models of integrated power plant and PCC plant. Based on 500MWe coal-fired subcritical power plant, Lawal *et al.* (2012) found that PCC plant have slower dynamics than the power plant. MacDowell and Shah (2014) on the other hand showed that about 2.8% in power generation efficiency can be achieved using split flow PCC configuration when the power plant is operated under base load condition.

Study of integrated power plant and capture plant for investigating operability was extended in Cifre *et al.* (2009) and Sanpasertparnich *et al.* (2010) with the inclusion of CO_2 compression. Cifre *et al.* (2009) investigated integration with different types of power plant, namely 600MW hard coal and 1000MW lignite power stations and concludes that stripper pressure has a strong influence on power cycle efficiency. Sanpasertparnich *et al.* (2010) on the other hand assessed impacts of different coal ranks and capture level using an 800MWe supercritical coal-fired power plant. The authors found that lower capture level at partial load incurs higher energy penalty and the energy penalty vary from one coal rank to another.

2.4.4 Control studies

Control studies involving the integrated coal-fired power plant and PCC plant is limited in literature with Lin *et al.* (2012) the only of such study at the time of preparing this thesis to the best of my knowledge. Other PCC related control studies, namely Panahi *et al.* (2010), Panahi and Skogestad (2011), Lin *et al.* (2011) and Panahi and Skogestad (2012), did not consider integration with the power plant. Lin *et al.* (2011a) showed that by regulating solvent loading while maintaining gas flow in the stripper by recycling some portions of captured CO_2 to the stripper that considerable flexible operation can be achieved without disrupting the hydraulic conditions in the absorber and stripper.

2.4.5 Economic studies

Zhang *et al.* (2011) presented an integrated model of a 500MW supercritical coal-fired power plant and PCC plant to investigate scenarios of cost per tonne of CO_2 avoided versus capture levels. Xu *et al.* (2010) similarly developed a comprehensive techno-economic model of power generation systems with PCC to investigate the correlative relationship between the efficiency penalty, investment increment, and CO_2 avoidance cost. Their investigations showed that for the power generation systems with CO_2 capture, the efficiency penalty not only affect the costs on fuel, but the incremental investment cost for CO_2 capture (US $ kW^{-1}) as well. Romeo *et al.* (2008) showed reduction of capture cost from €55/ton of CO_2 to €25.3/ton CO_2 at a capture level of 60-65% from a steady state simulation of integrated 350MWe coal-fired power plant and PCC plant.

2.4.6 Summary

The studies reviewed highlight the need for integrated modelling of components of the CCS chain. The majority of existing studies involve integration of CO_2 emitter and the capture plant. In addition only a few of these studies are based on dynamic models (Lawal *et al.,* 2012; MacDowell and Shah, 2014). Apart from sensitivity analysis, steady state models are not adequate for investigating operating behaviour under load changing scenario. As a result, more studies involving dynamic models of integrated components of the CCS chain is needed to carry out more dynamic studies of the CCS chain.

2.5 Concluding remarks

Most reported models of coal-fired power plants are steady state models which cannot be used for investigating process behaviour during operation. Existing dynamic models of the whole plant are simple and do not represent some key dynamic features such as the drum-boiler dynamics. The drum-boiler dynamics is very important for determining the overall dynamics of the power plant due to its relatively slower dynamics. In choosing a power plant model for studying CCS chain, it is important that the model include these details so that comprehensive assessment of the impacts of the downstream CCS components on the power plant can be carried out using the model.

Secondly, there are lots of experiment-based and model-based studies on PCC. There is a limit to the process manipulation that can be done during experiments. This highlights the importance of modelling and simulation for studying scenario that cannot be mimicked in experiments. Existing PCC models have been done to different extent of complexities which reflects the abilities of the models. The most complex PCC model and in theory the most accurate will involve rate-based mass transfer and detailed CO_2 reaction kinetic modelling. We find that no existing PCC model have been represented to this level of complexity. Existing models are mostly rate-based with CO_2 reaction kinetics approximated with enhancement factors or assumption that CO_2 reactions reach equilibrium. Results from the studies show that the approximations are reasonable and the PCC model is relatively simpler. As a result, existing models such as Lawal *et al*., (2010) can be used as a component of the CCS chain model.

Thirdly, CO_2 pipeline transport models have been mostly onshore pipeline network and pipeline elevation profile is not included in most of them. Elevation profile has a major impact on fluid pressure profile in the pipeline. Therefore, dynamic models of CO_2 pipeline transport system for both offshore and onshore that include pipeline elevation are necessary. Also, within the context of CCS clusters, common pipeline trunk is expected to be used for transporting CO_2 captured from different capture sites. CO_2 coming from different sources come with different amounts of impurities and impurities have significant impact on CO_2 thermodynamic and transport properties (See Chapter 5). CO_2 behaviour in such pipeline trunk will therefore differ from pipelines conveying CO_2 from a single source with specific composition. So far, there has been no case where pipeline trunks conveying CO_2 from multiple sources have been investigated dynamically.

Finally, there have been reported models of integrated components of CCS chain involving mainly CO_2 emitter with capture. Most of those are steady state model and cannot be used for studying process behaviour during operation. However, they highlight the benefit of studying integrated components of the CCS chain.

Chapter 3: Dynamic modelling of coal-fired subcritical power plant

Existing studies on coal-fired subcritical power plant modelling have been reviewed in Chapter 2. Information from some existing studies on power plant modelling such as Masada (1979), Lo and Song (1990), Åström and Bell (2000) and Lawal *et al.* (2012) have been combined in this chapter to obtain a more realistic model of the power plant.

Brief description of the reference power plant is given in Section 3.1 followed by general modelling assumptions in Section 3.2. Model equations for the power plant components are presented in Section 3.3 and the model of the complete plant in Section 3.4. Steady state validation of the complete plant model is presented in Section 3.5. The results of the dynamic tests and discussion of the results are given in Section 3.6 followed by a concluding remark in Section 3.1.

3.1 Description of the reference plant

The reference plant is a unit of the 2000 MWe Didcot A power station in Oxfordshire, UK owned by RWE npower which was closed recently (Oke, 2008). Didcot A power plant comprises of four generating units, each of which have a capacity of 500 MWe. For each unit, the boiler comprises of a single drum (subcritical) and single furnace dry bottom type with walls of tubes forming box-like compartments. The radiant primary and secondary platen superheaters are situated in the top space of the furnace and the inlet and outlet banks of the secondary convection superheater are situated above the furnace nose. The primary superheater and the reheater occupy the upper space of the rear enclosure and the economiser occupies the lower space of the rear enclosure. A boiler configuration similar to that of the reference power plant is shown in Fig. 3.1. The steam turbine on the other hand is a three-stage tandem-compound steam turbine with single-reheat. The feedwater heaters comprises of a four-stage low pressure heater and three-stage high pressure heater plus a deaerator. The power plant also includes a coal mill and electrostatic precipitators (ESP) for cleaning the combustion gases. The coal mill and ESP are however not included in the model presented in this thesis since the interest is

mainly on the power cycle. At 100% load, the main plant variables are shown in Table 3.1.
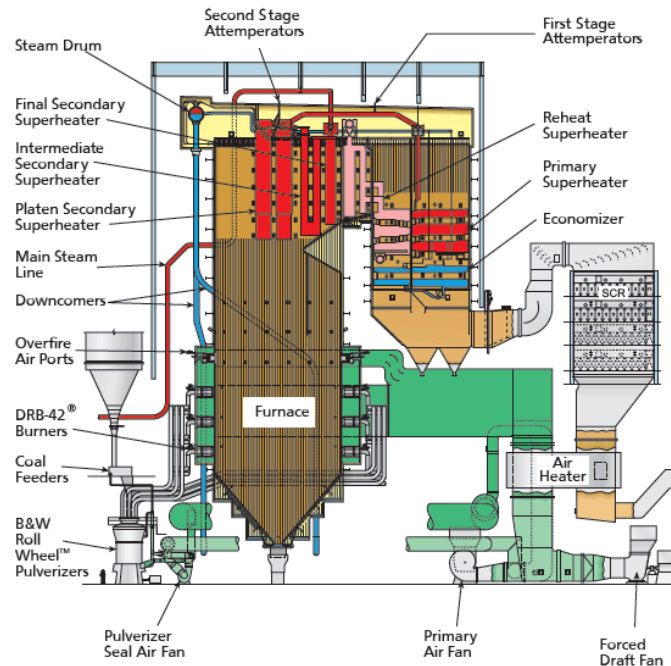
Fig. 3.1 Typical boiler set-up for the reference power plant (TBWES, 2014)

3.2 General modelling assumptions

Coal-fired power plant is highly complex with non-linear and multi-dimensional interactions of many operating variables. As a result, in this thesis, the model of the power plant will be classified into sub-systems for ease of handling. This includes: furnace, drum-downcomer-riser loop, heat exchangers, steam turbines, condenser, pumps, deaerator and governor valve. The sub-unit models are then linked together to obtain the model of the complete plant.

In addition, some simplifying assumptions are used to ensure balance between simplicity and fidelity. Evidences in literature show that these assumptions are reasonable (Oke, 2008; Lawal *et al.*, 2012). Assumptions specific to individual sub-systems are stated under the sections where they are discussed. General assumptions adopted are as follows.

- Lumped parameter modelling approach for the various components.
- The various model constants have been derived from plant construction and operating data at full load conditions (Oke, 2008; Lawal *et al.*, 2012).

- Energy losses and leakages of steam/water have not been taken into account.
- Bituminous coal is selected as the feed fuel (Table 3.2). The composition and its properties are assumed constant. Air is assumed to be composed of 0.7811 mol% nitrogen, 0.2096 mol% oxygen and 0.0093 mol% argon.
- The four-stage LP feedwater heaters and the three-stage HP feedwater heaters ere lumped into single stage models respectively.

Table 3.1 Plant data at 100% load (Oke, 2008)

Data	Value
Net Power (MWe)	500
Fuel flow (kg/s)	52.2
Excess air (%vol)	20
Drum pressure (Bar)	180
Steam flow at superheater outlet (kg/s)	422.1
Superheater exit temperature (^{o}C)	568
Superheater exit pressure (bar)	165.5
Steam flow at reheater inlet (kg/s)	330
Reheater inlet temperature (^{o}C)	365
Reheater exit temperature (^{o}C)	568
Reheater exit pressure (bar)	40.35
Condenser CW inlet mass flow (kg/s)	17000
Condenser CW inlet temperature (^{o}C)	20
Mass flow of condensing steam(kg/s)	290

3.3 Model Components

3.3.1 Furnace

Heat flux distribution along the heights of the waterwall/riser has been neglected and only the total heat flow rate was considered (Maffezzoni, 1992). This is due to unavailability of temperature profile data in the furnace. This assumption implies uniform surface temperature for the waterwall/riser. Studies by Coelho and Carvalho (1992) showed that this assumption is reasonable when dealing with complete plant model as is the case in this thesis. Heat transfer between the furnace gases/flame

and waterwall/riser is mostly by radiation, the convective heat transfer component is negligible (Blokh, 1987; Yun-tao, *et al.,* 2008). This is because of low velocity of gases and small temperature differences at the boundary between the flame and the surfaces of waterwall/riser. Radiant heat transfer in the furnace depends on a number of conditions, namely dimension and shape of furnace, burner arrangement, type of fuel burnt, and operational conditions of the furnace. Thermal efficiency of the furnace waterwall may deteriorate over time with accumulation of slag. These characteristics are not taken into account in this model.

Again, the total radiant heat released during combustion is usually distributed between the water walls and the platen superheater. According to Bhambare *et al.,* (2007), the fractions of the radiant heat that is absorbed by the waterwall and platen superheaters depend on the number of burners in service and the burner tilt. The number of burners in service and the burner tilt determine the position of the fireball relative to a base position. As a result, the amount of radiant heat absorbed by the superheater can differ. Due to lack of data, number of burners in service and burner tilt is not taken into account explicitly in the model presented in this thesis. Instead, an attenuation factor determined from operating data was used to account for radiant heat distribution between the waterwall and the platen superheaters (Lawal *et al.*, 2012).

Table 3.2 Coal Specifications (Lawal *et al.*, 2012).

Composition	wt% as received basis
Moisture	8.00
Ash	20.00
C	59.11
H	3.99
N	1.00
S	2.00
O	5.90
CV*	MJ/kg, as received basis
GCV *	24.51
NCV *	23.33

Dynamics of flue gas temperature is captured using global energy balance equation (Eq.3.1). Mass accumulation is however ignored (Eq.3.2) since the gas flow adjusts quickly enough to changes in inlet conditions (Lawal *et al.,* 2012). The symbols used in the equations are annotated in the schematic diagram of the furnace in Fig.3.2 for clarity. This implies that re-circulating flue gas in the furnace is neglected. Similar

assumption was made in Flynn and Malley (1999) and their results show that the assumption is reasonable.

$$\dot{m}_{coal}(NCV_{coal} + h_{coal}) + \dot{m}_{air}h_{air} - \dot{m}_g h_g - \dot{m}_{ash}h_{ash} - Q_R = V_F\rho_g \frac{dh_g}{dt} \tag{3.1}$$

$$\dot{m}_{gas} = \dot{m}_{coal} + \dot{m}_{air} - \dot{m}_{ash} \tag{3.2}$$
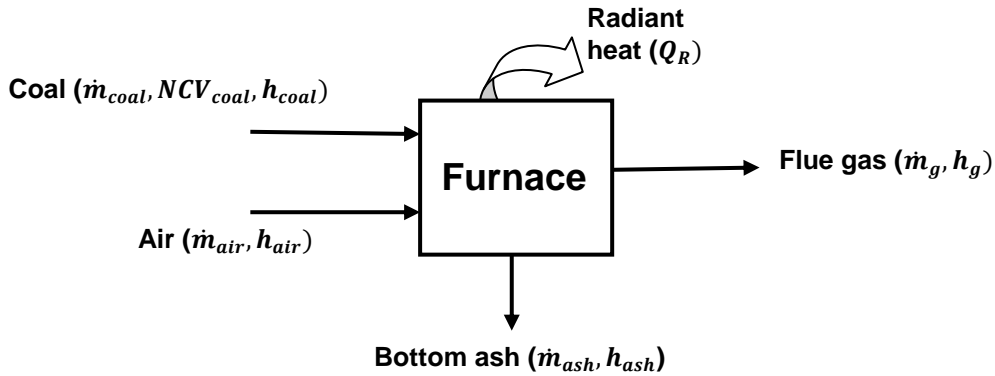
Fig.3.2. Schematic diagram of the furnace with annotations

Flue gas composition is obtained on the basis of 20 vol% excess air (at 100% load) and stoichiometric reactions involving carbon, hydrogen and sulphur (R3.1, R3.2 and R3.3). Other components of coal such as nitrogen among others are assumed inert. NO_X formation is consequently disregarded. SO_X formation is obtained as SO_2. Complete combustion is also assumed leaving only negligible amounts of unreacted components or partial combustion products such as carbon monoxide.

$$C + O_2 \rightarrow CO_2 \tag{R3.1}$$
$$S + O_2 \rightarrow SO_2 \tag{R3.2}$$
$$2H_2 + O_2 \rightarrow 2H_2O \tag{R3.3}$$

Total radiant heat energy released in the furnace (Q_R) is obtained using Stefan-Boltzmann law of radiation expressed as Eq.3.3 (Ordys *et al.*, 1994).

$$Q_R = k\sigma V_F T_g{}^4 \cdot \frac{1}{\rho_g} \tag{3.3}$$

The effective gas temperature inside the furnace (T_F) at flame conditions is obtained using Eq.3.4 (Lawal *et al.,* 2012; Bhambare *et al.,* 2007).

$$T_F = \beta T_{g,ad} + (1 - \beta)T_g \tag{3.4}$$

The parameter β accounts for the effect of soot blowing on heat transfer and heat loss to the atmosphere (Lu, 1999). The flue gas temperature at furnace exit (T_g) is obtained from the global energy balance equation (Eq. 3.1). The adiabatic flame temperature ($T_{g,ad}$) is obtained from energy balance under adiabatic conditions (*i.e.* no heat loss). Under such circumstance, the global energy balance is as follows:

$$\dot{m}_{coal}(NCV_{coal} + h_{coal}) + \dot{m}_{air}h_{air} = \dot{m}_g h_{g,ad} + \dot{m}_{ash}h_{ash,ad} \qquad (3.5)$$

3.3.2 Drum-downcomer-riser loop

In this thesis, the riser and waterwalls are assumed to be lumped together and as a result represented by a single model similar to Åström and Bell (2000). Circulation in the downcomer-riser loop is by natural circulation (*i.e.* flow is driven by density differences between the downcomer and riser). Slip between the liquid and vapour phase in the riser is neglected. In other words, both phases move at the same velocity. This assumption is reasonable at normal operating pressure (Blokh, 1987) and it simplifies the model by eliminating the need for determining slip ratios and local void fractions. It is also assumed that there is no temperature gradient in the drum. The assumption is reasonable given that there is sufficient turbulence in the drum and the water-steam phases are well mixed as a result. Finally, the water-steam mixture in the drum and riser are at saturated conditions. A schematic diagram of the drum-downcomer-riser loop is given in Fig.3.3.

The dynamic model of the loop is based on global mass and energy balances around the entire loop as follows (Åström and Bell, 2000):

Global mass balance:

$$\frac{d}{dt}[\rho_s \cdot V_s + \rho_{wt} \cdot V_{wt}] = \dot{m}_{fw} - \dot{m}_s \qquad (3.6)$$

Global energy balance:

$$\frac{d}{dt}[\rho_s \cdot V_s \cdot h_s + \rho_{wt} \cdot V_{wt} \cdot h_{wt}] = Q_C + \dot{m}_{fw}h_{fw} - \dot{m}_s h_s \qquad (3.7)$$

The total volume of the loop (V_t) is then obtained as follows from the steam volume (V_s) and water volume (V_{wt}) in the loop.

$$V_t = V_s + V_{wt} \qquad (3.8)$$

To describe the riser dynamics, linear distribution of steam quality in the riser is assumed (Åström and Bell, 2000). On this basis, the average steam volume fraction ($\overline{\alpha_v}$) is obtained as follows:

$$\overline{\alpha_v} = \frac{\rho_{wt}}{(\rho_{wt}-\rho_s)}\left(1 - \frac{\rho_s}{(\rho_{wt}-\rho_s)\alpha_r}\ln\left(1 + \frac{(\rho_{wt}-\rho_s)\alpha_r}{\rho_s}\right)\right) \tag{3.9}$$

The riser dynamics is captured using mass and energy balances around the riser are as follows:

Mass balance:

$$\frac{d}{dt}[\rho_s\overline{\alpha_v}V_r + \rho_{wt}(1-\overline{\alpha_v})V_r] = \dot{m}_{dc} - \dot{m}_r \tag{3.10}$$

Energy balance:

$$\frac{d}{dt}[\rho_s\overline{\alpha_v}V_rh_s + \rho_{wt}(1-\overline{\alpha_v})V_rh_{wt}] = Q_c + \dot{m}_{dc}h_{wt} - (\alpha_rh_c + h_{wt})\dot{m}_r \tag{3.11}$$
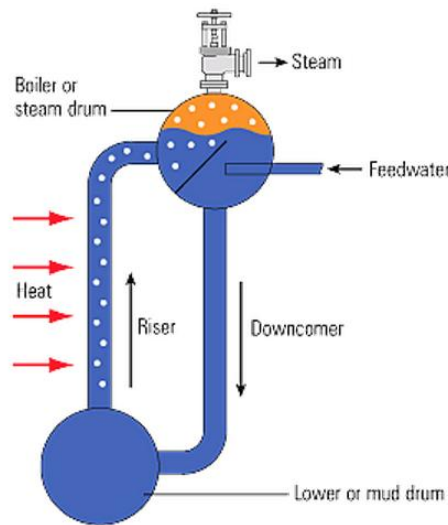
Fig.3.3 Subcritical boiler - drum-downcomer-riser loop (Spirax Sarco, 2015)

In this thesis, the metal energy storage component was not been lumped into the energy balance equations (Eq. 3.7and Eq.3.11) as it is in Åström and Bell (2000). Earlier study by Flynn (1999) showed that this exclusion does not have significant impact on the model capability.

The heat input into the loop (Q_c) is essentially convective heat transfer from the riser tube to the water-steam mixture. This quantity is obtained as follows (Lawal *et al.*, 2012):

$$Q_C = \tau_r (T_M - T_{sat})^3 \tag{3.12}$$

The term τ_r is a heat transfer parameter obtained based on physical data. The heat of condensation term (h_c) in Eq.3.11 is given as follows:

$$h_c = h_s - h_{wt} \tag{3.13}$$

Circulation flowrate ($\dot{m}_{dc}$) is obtained using steady state momentum conservation equation as follows (Åström and Bell, 2000) :

$$\frac{1}{2} k_f (\dot{m}_{dc})^2 = \rho_{wt}\ A_{dc}(\rho_{wt} - \rho_s)gV_r\overline{\alpha_v} \tag{3.14}$$

Transient of riser metal is obtained as follows:

$$M_r \cdot C_p \cdot \frac{d}{dt} T_M =\ Q_{IR} - Q_C \tag{3.15}$$

The term Q_{IR} is the radiant heat quantity absorbed by the riser from the furnace and platen superheaters.

Finally, provision is made to account for *shrink and swell behaviour* (non-minimum phase behaviour of drum level dynamics) in predicting drum level (Åström and Bell, 2000). *Shrink and swell* behaviour is attributed to the existence of steam bubbles below the drum level. When drum pressure decreases, as it is the case when the steam valve is opened (during an increase in load), the bubbles tend to swell leading to a momentary rise in drum level (*swell behaviour*) and vice versa for *shrink behaviour*. To model drum level accurately, the volume of steam bubbles below the drum level must be taken into account. This is accomplished as follows following the procedure outlined in Åström and Bell (2000).

First, drum level L is obtained thus:

$$L = \frac{V_{wD} + V_{sD}}{A_D} \tag{3.16}$$

The cross sectional area of the drum (A_D) is measured at design condition. This is necessitated by the complicated nature of the drum geometry. Volume of water in the drum (V_{wD}) is obtained from:

$$V_{wD} = V_{wt} - V_{dc} - (1 - \overline{\alpha_v})V_r \tag{3.17}$$

Steam volume below drum level (V_{SD}) is obtained from mass balance as follows:

$$\frac{d}{dt}\rho_s V_{SD} = \alpha_r \dot{m}_r - \dot{m}_{sd} - \dot{m}_c \qquad (3.18)$$

In Eq.3.18, the term $\dot{m}_{sd}$ is the flowrate of steam escaping from the water surface in the drum. It is obtained using the following correlation (Åström and Bell, 2000):

$$\dot{m}_{sd} = \frac{\rho_s}{t_D}\left(V_{SD} - V_{SD}{}^0\right) + \alpha_r \dot{m}_{dc} + \alpha_r \beta(\dot{m}_{dc} - \dot{m}_r) \qquad (3.19)$$

On the other hand, the condensation flowrate in the drum ($\dot{m}_c$) is obtained thus:

$$\dot{m}_c = \dot{m}_{fw}\frac{h_{wt} - h_{fw}}{h_c} + \frac{1}{h_c}\left(\rho_s V_{SD}\frac{dh_s}{dt} + \rho_{wt}V_{wD}\frac{dh_{wt}}{dt}\right) \qquad (3.20)$$

In Eq.3.19), the term t_D is the residence time of the steam in the drum. The physical parameter β is equal to 0.3 (Åström and Bell, 2000) and $V_{SD}{}^0$ is the volume of steam in the drum in the hypothetical situation when there is no condensation of steam in the drum. The residence time parameter t_D obtained from Åström and Bell (2000) was adjusted to fit data of the boiler in this thesis.

3.3.3 Heat exchangers
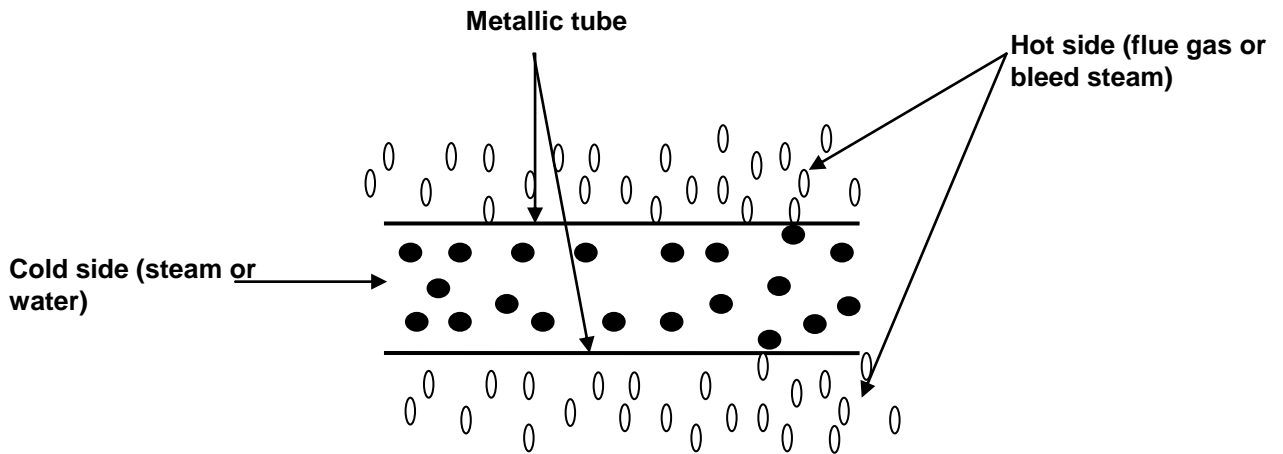
Fig.3.4 Schematic diagram of a segment of the heat exchanger

In this thesis, the following are classified as heat exchangers: superheaters, reheaters, economiser and feedwater heaters. Dynamic equations on both steam and gas side have been used to model convective heat transfer in the superheater and reheater. Dynamic equations were only used on the water side in the feedwater heaters. The platen and secondary superheaters also included the radiative heat

transfer. This was estimated using Stefan-Boltzmann Law (Eq.3.3). Schematic diagram of a segment of the heat exchangers showing important parts is given in Fig.3.4.

The general equations for the steam sides (or water side for the feedwater heaters) and flue gas sides (or bleed steam side for the feedwater heaters) are expressed as follows:

Mass balance:

$$\dot{m}_{in} - \dot{m}_{out} = V\frac{d\rho}{dt} \qquad (3.21)$$

Energy balance:

$$\dot{m}_{in}h_{in} - \dot{m}_{out}h_{out} + Q = \rho V\frac{dh_{out}}{dt} \qquad (3.22)$$

Empirical relations obtained from Ordys *et al.* (1994) were used to estimate the convective heat Q_c. These relations are as follows:

Steam (or water) side: $Q_S = U_s(\dot{m}_s)^{0.6}(T_w - T_{s,avg})$ $\qquad$ (3.23)

Gas (or bleed steam) side: $Q_g = -U_g(\dot{m}_g)^{0.8}(T_{g,avg} - T_w)$ $\qquad$ (3.24)

The Q term in Eq.3.22 is replaced by either Q_S or Q_g for steam (or water) and gas (or bleed steam) side respectively. Also, the $\dot{m}_s$ and $\dot{m}_g$ in Eq.3.23 and 3.24 are average flowrate of inlet and outlet flows for the steam (or water) and gas (or bleed steam) side respectively. Finally, the temperature transients of the metallic tubes separating the steam and gas side were obtained as follows:

$$MC_P\frac{dT_w}{dt} = Q_g - Q_S \qquad (3.25)$$

3.3.4 Steam turbines

The steam turbine model was obtained using the Stodola ellipse law expressed in terms of specific volume as shown in Eq.3.26 (Lo and Song, 1990). This form of Stodola ellipse law is valid for all cases of compressible fluid compared to the form expressed in terms of temperature which is only valid when the perfect gas law ($Pv = RT$) is valid (Lo and Song., 1990). A schematic diagram of the steam turbine is shown in Fig.3.5.
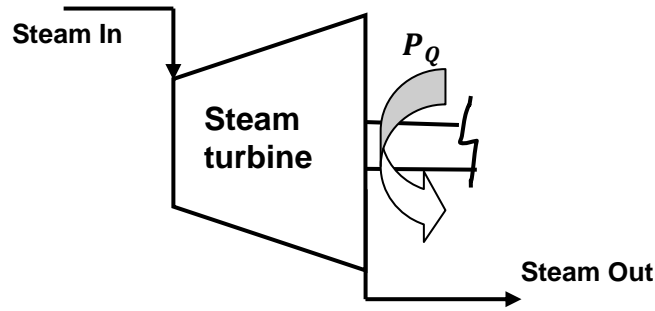
Fig.3.5 Schematic diagram of the steam turbine

Considering the rapid response capability of the steam turbine compared to the boiler, steady state models are used for the steam turbine. Main governing equations are as follows:

$$\dot{m}_{in} = \frac{K_{SE}}{\sqrt{v_{in}}} \sqrt{\frac{P_{in}^2 - P_{out}^2}{P_{in}}} \tag{3.26}$$

$$\frac{T_{out}}{T_{in}} = \left(\frac{P_{out}}{P_{in}}\right)^{\left(\frac{\gamma-1}{\gamma}\right)} \tag{3.27}$$

$$P_Q = \dot{m}_{in}\left(h_{in} - h_{out}\right) \tag{3.28}$$

3.3.5 Condenser

In the condenser, only latent heat exchange between the cooling water and the condensing steam is considered. Sub-cooling in the condenser is therefore ignored. Steady state conditions were assumed on the steam side. Dynamic conservation equations were applied in the cooling water side. Huge volumes of cooling water compared to condensing steam makes this decision reasonable.

The condenser sump (hotwell) was considered separately. It was modelled as a holding tank as follows.

Mass balance:

$$\rho A \frac{d\mathrm{L}}{dt} = \dot{m}_{in} - \dot{m}_{out} \tag{3.29}$$

Energy Balance:

$$\rho A L \frac{dh_{out}}{dt} = \dot{m}_{in}h_{in} - \dot{m}_{out}h_{out} \tag{3.30}$$

3.3.6 Deaerator

The deaerator is used for removing dissolved gases from the boiler feedwater. It comprises of two parts, namely deaeration head and feedwater holding tank. In this thesis, the chemical reactions involved in the deaeration process have not been considered. As a result, the deaerator model is represented as a simple holding tank similar to the condenser sump described earlier for steam and water mixing.

3.3.7 Pumps

The boiler feed pump is turbine-driven. The turbine is operated using steam extracted from the IP turbine outlet. This was modelled as follows.

$$0.1047K_{fptrb}\frac{dN_{bfp}}{dt} = Torq_{trb} - Torq_{bfp} \tag{3.31}$$

$$P_{bfp} - (P_{Dtorout} + g\rho Z) = K_0\rho(0.1047N_{bfp})^2 + K_1\dot{m}_{bfp}(0.1047N_{bfp}) + \frac{K_2\dot{m}_{bfp}^2}{\rho} \tag{3.32}$$

The constants K_0, K_1 and K_2 are derived from the pump characteristic equation (Masada, 1979). In this thesis, the original values of the parameters obtained from Masada (1979) were adjusted to fit actual data.

3.3.8 Governor valve

The turbine governing method is assumed to be throttle governing and it involves only one governor valve. The valve regulates steam flow to the turbine and consequently the turbine load changes. The key equation in the governor valve model is as follows:

$$m_{in}^2 = K_{vf}^2 v_{in}(P_{in} - P_{out}) \tag{3.33}$$

3.4 Whole plant model

3.4.1 Physical properties

Model equations for the sub-systems of the coal-fired subcritical power plant described above were implemented in gPROMS ModelBuilder® and thereafter linked to obtain the whole plant model (Fig. 3.6). Thermodynamic properties of water/steam, air and flue gas, namely density and specific enthalpy were obtained using Peng-

Robinson equation of state in Infochem's Multiflash® which is accessed directly from gPROMS ModelBuilder®. Derivatives of thermodynamic properties $(\frac{\partial \rho_s}{\partial P}, \frac{\partial \rho_w}{\partial P}, \frac{\partial h_s}{\partial P}, \frac{\partial h_w}{\partial P}, \frac{\partial T_s}{\partial P})$ used in the drum-downcomer-riser loop model were obtained using polynomial approximations of steam table obtained from NIST REFPROP V9.1. The specific enthalpies of coal and coal ash were obtained using specific heat capacity correlations by Lee (1967) for specific heat capacity of coal ($C_{p,coal}$) and Richardson (1993) for specific capacity of ash ($C_{p,ash}$) (Eq.3.34 and 3.35 respectively).

$$C_{p,coal}(\text{Btu/lb } °F) = 0.03464 + 2.261 \times 10^{-5} \cdot T \tag{3.34}$$

$$C_{p,ash}(\text{J/kg K}) = 191.2 + 2.238T - 1.464 \times 10^{-3}T^2 \tag{3.35}$$

The correlation for specific heat capacity of coal was developed for different classes of coal depending on the volatile matter (VM) content in Lee (1967). On the basis of 20% VM content for the bituminous coal used in this thesis, the correlation for specific heat capacity of coal in Lee (1967) was therefore adjusted to obtain Eq.3.34. On the other hand, the correlation for specific heat capacity of ash was obtained as an average fit of ash samples from ten different coals in Richardson (1993).

3.4.2 Control loops

Basic control loops, namely main steam temperature, reheat steam temperature and power output, have been included in the model. These loops are necessary for load change analysis to be carried out using the model. In this thesis, the interest was not necessarily to replicate actual control loops in a typical coal-fired plant or to provide detailed design of the controllers. Default PI controllers in gPROMS ModelBuilder® were therefore used with their settings manually adjusted to suit the model. More accurate controller settings can be obtained using Ziegler Nichols tuning method which can be obtained from good process control textbooks.

3.4.2.1 Main steam temperature

The main steam temperature is controlled using spray water attemperators. This involves mixing the steam in-between the superheater banks with controlled flow of spray water taken from the boiler feedpump discharge to achieve desired

temperature. Due to small storage volume of the attemperators, the dynamics are neglected and steady state flow equations are used (Flynn, 1999):

$$\dot{m}_{s,in} + \dot{m}_{att} = \dot{m}_{s,out} \tag{3.34}$$

$$\dot{m}_{s,in} h_{s,in} + \dot{m}_{att} h_{att} = \dot{m}_{s,out} h_{s,out} \tag{3.35}$$

3.4.2.2 Reheat steam temperature

The reheat steam temperature is controlled using rear gas pass biasing damper. This involves controlling the flow of flue gas along the divided rear pass between the superheater and the reheater. The dynamics of the rear pass divide are similarly neglected. Consequently, the following steady state flow equations were used:

$$\dot{m}_{gas} = \dot{m}_{spter,gas} + \dot{m}_{rhter,gas} \tag{3.36}$$

$$\dot{m}_{gas} h_{gas} = \dot{m}_{spter,gas} h_{spter,gas} + \dot{m}_{rhter,gas} h_{rhter,gas} \tag{3.37}$$

3.4.2.3 Power output

Control of the power output is needed to simulate changes in load in a manner similar to load changes in real plant. The target power output is controlled through manipulation of fuel burn rate and governor valve. The target power plant output is directly controlled by the governor valve; this target also sets the drum pressure which is controlled by the fuel burn rate.
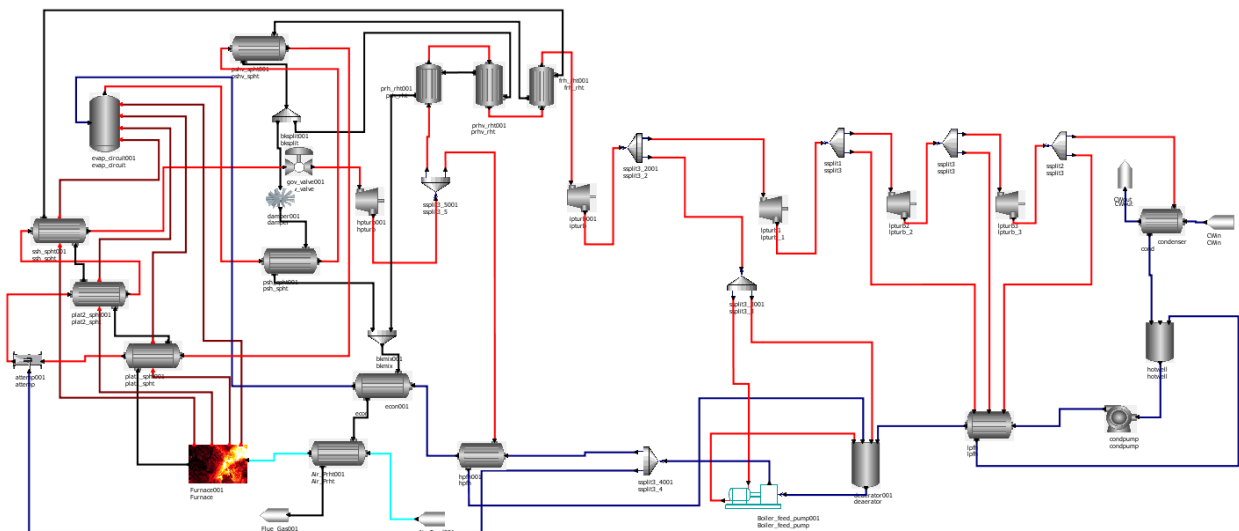
Fig. 3.6 Flowsheet of the power plant model in gPROMS ModelBuilder®

3.5 Steady state model validation

3.5.1 Justification of steady state validation

Model validation is important to establish a basis for the capability of the model. For a model to be considered fit-for-purpose, it should be able to reasonably predict steady state values of different variables at different operating levels (or load). In addition, it should be able to demonstrate capability for predicting plant behaviour over time especially during periods when changes in load are implemented.

In this thesis, only steady state validation is performed. Dynamic validation was not performed due to unavailability of good dynamic data for coal-fired subcritical power plant in literature. Also, air/ flue gas side measurements for the reference plant are unavailable. As a result, the validations are limited to the water/steam side where measurement/design data are available.

3.5.2 Inputs to the model

The inputs to the model include fuel burn rate, the governor valve stem position, cooling water flowrate, percentage excess air in furnace, attemperator setting, condenser pressure, feedwater valve setting, and back pass damper setting.

3.5.3 Results

During the validation exercise, the model was first simulated at full load with the governor valve fully opened and the fuel burn rate at 52.2 kg/s. Key variables were then compared with plant measurements taken at a similar condition (Table 3.3). In addition, the predictions of different process variables at different load levels were compared to plant measurements taken at similar conditions. This comparison is necessary to determine the model capability away from full load condition. The model parameters remained unchanged for the different load levels tested. Main steam temperature and pressure are controlled and remained the same for the different load levels $i.e.$ 568.69^{O}C and 170.92 bar respectively. The model was simulated at 100%, 94.4%, 80% and 70% load levels corresponding to 500, 472, 400 and 350 MWe. The values of selected process variables at these conditions were compared against plant measurements at similar conditions (Fig.3.7 and Fig.3.8). The results of the steady state validation show the model predicts the plant

measurements with less than 5% relative error. Considering the inherent errors in plant measurements, the model predictions can therefore be considered to be within acceptable range.

Table 3.3 Steady state validation at 100% load (500 MWe)

	Plant	Model	Relative Error (%)
Main steam flow (kg/s)	422	423.51	0.36
Superheater steam out temp (^{O}C)	568	568.69	0.12
Superheater steam out pressure (bar)	165.5	170.92	3.27
Feedwater temp at economizer inlet (^{O}C)	256	251.66	1.70
Reheater steam inlet temp (^{O}C)	365	351.03	3.83
Reheater steam outlet temp (^{O}C)	568	566.21	0.32
Reheater steam flow (kg/s)	330	328.38	0.49
Reheater outlet pressure (bar)	40.3	40.6	0.74
Absolute pressure turbine exhaust (mbar)	50.8	50	1.57
Condenser outlet temperature (^{O}C)	33.2	33.1	0.30
Condensate pump outlet pressure (bar)	4.48	4.53	1.12
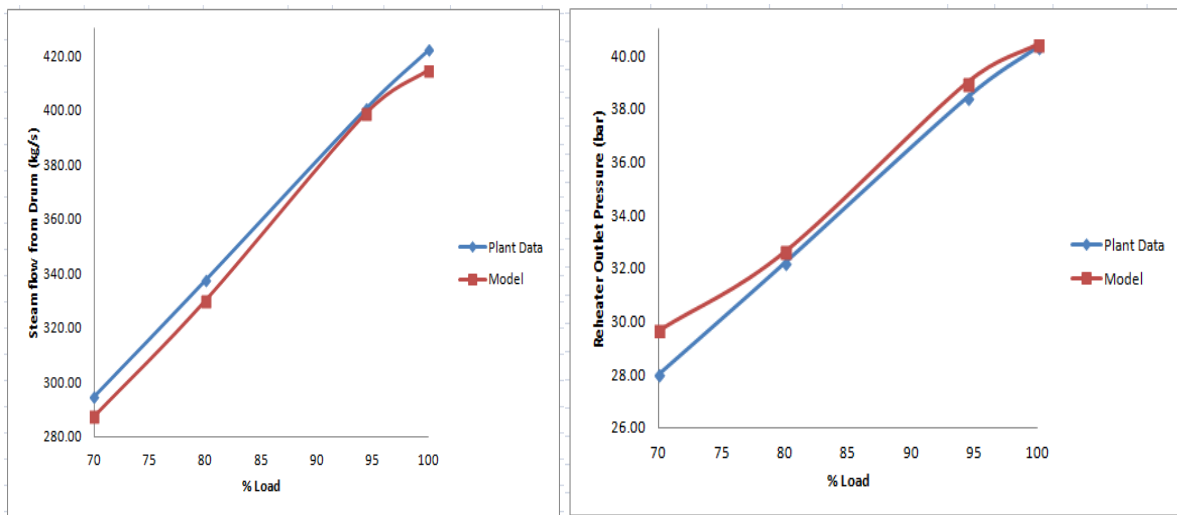
Fig. 3.7 Main steam flowrate and reheater outlet pressure *vs.* Load
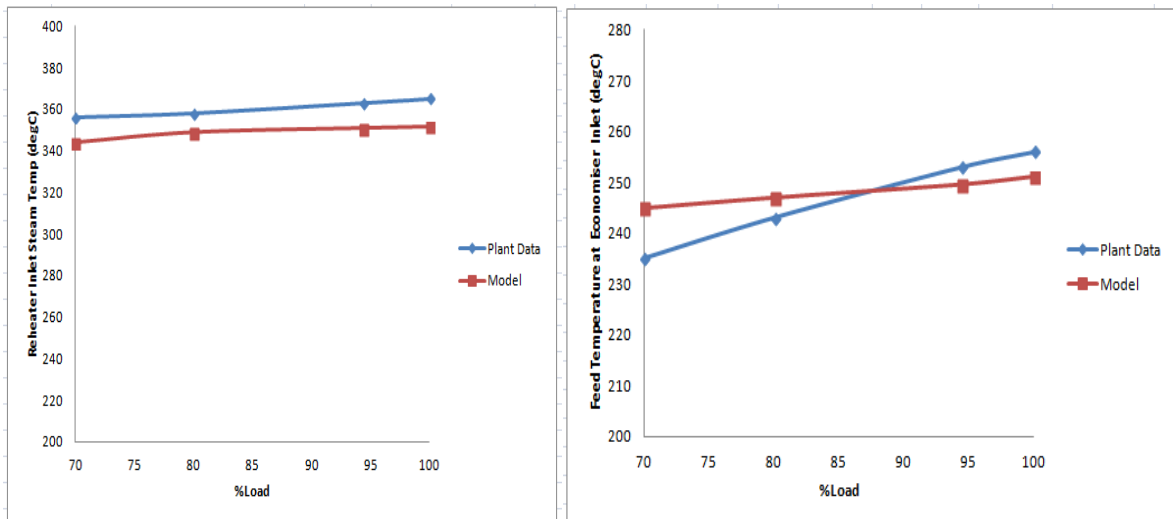
Fig. 3.8 Reheater inlet steam temperature and feedwater temperature at economiser inlet *vs.* Load

3.6 Process analysis

3.6.1 Step change in Load

Step changes in load were implemented to investigate the ability of the process variables to reach the next steady state condition. The total MWe is determined by the power plant power output controllers which manipulate the fuel burn rate and governor valve opening to meet the target power output. During this exercise, the model was simulated at full load (500 MWe) for 200 seconds before it was stepped down to 470 MWe. The plant is maintained at this load level for a further 600 seconds.

As the load is stepped down from 500 to 470 MWe, the fuel burn rate also steps down correspondingly from 52.2 kg/s and steadies at a new value, 49.3 kg/s (Fig.3.9). The fuel burn rate initially drops below this level as the figure reveals before rising to the required level. In addition, drum pressure, drum level, circulation rate in evaporation loop, steam quality at riser outlet, feedwater mass flowrate at drum inlet, furnace pressure and flue gas temperature at economiser exit have been assessed over the course of the change (Fig.3.9).

These variables show relatively fast response and reflect expected trends. For instance, as load decreased the drum pressure decreased. There is a momentary drop in drum level before it begins to rise. This reflects the *swell* phenomenon in the drum. Feedwater mass flowrate initially rises and then dropped as expected before stabilizing. Furnace pressure showed a sharp drop before immediately recovering

and stabilizing. This reflects decrease in air flowrate and it is expected for the circumstance. Flue gas temperature at economiser exit drops sharply and took about 5 mins (300 sec) to reach stable state.

3.6.2 Ramp Change in Load

Here, changes in load (total MW) are implemented by ramping. This is a typical procedure for implementing load change in an actual power plant. This load change approach has been assessed to compare it with step change approach. The total MWe is similarly determined by the power plant power output controllers which manipulate the fuel burn rate and governor valve opening to meet the target power output. The same controllers with the same settings used in Section 3.6.1 were used here.

During the exercise, the power output was maintained at 500 MWe (full load) for 100 seconds. The total MWe is then ramped down to 468.6 MWe over an interval of 700 seconds. It is then maintained at this load level for a further 500 seconds. Response of the fuel burn rate, drum pressure, drum level, circulation rate in evaporation loop, steam quality at riser outlet and feedwater mass flowrate at drum inlet have been assessed over the course of the change (Fig.3.10). The results are agreeable with expected trends in these variables whenever a load change is implemented in real life operation.

In comparison with step changes, ramping is implemented over a time range. The results show that ramp changes induce less fluctuation in the process variables on the steam side than step change during the course of the change. In reality, the strategy for implementing load changes is via ramping and our findings justify the strategy.
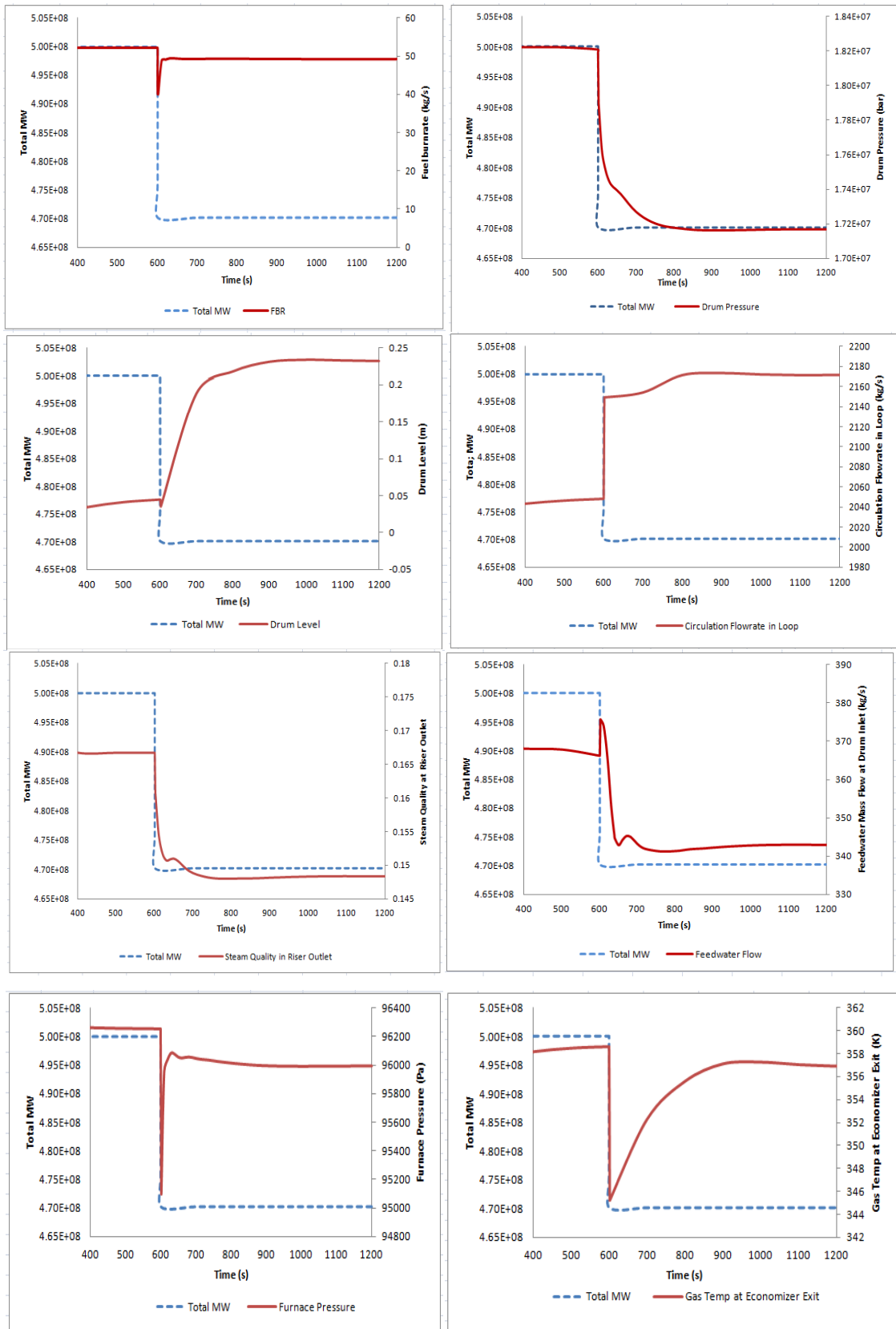
Fig.3.9 Step change in total MWe
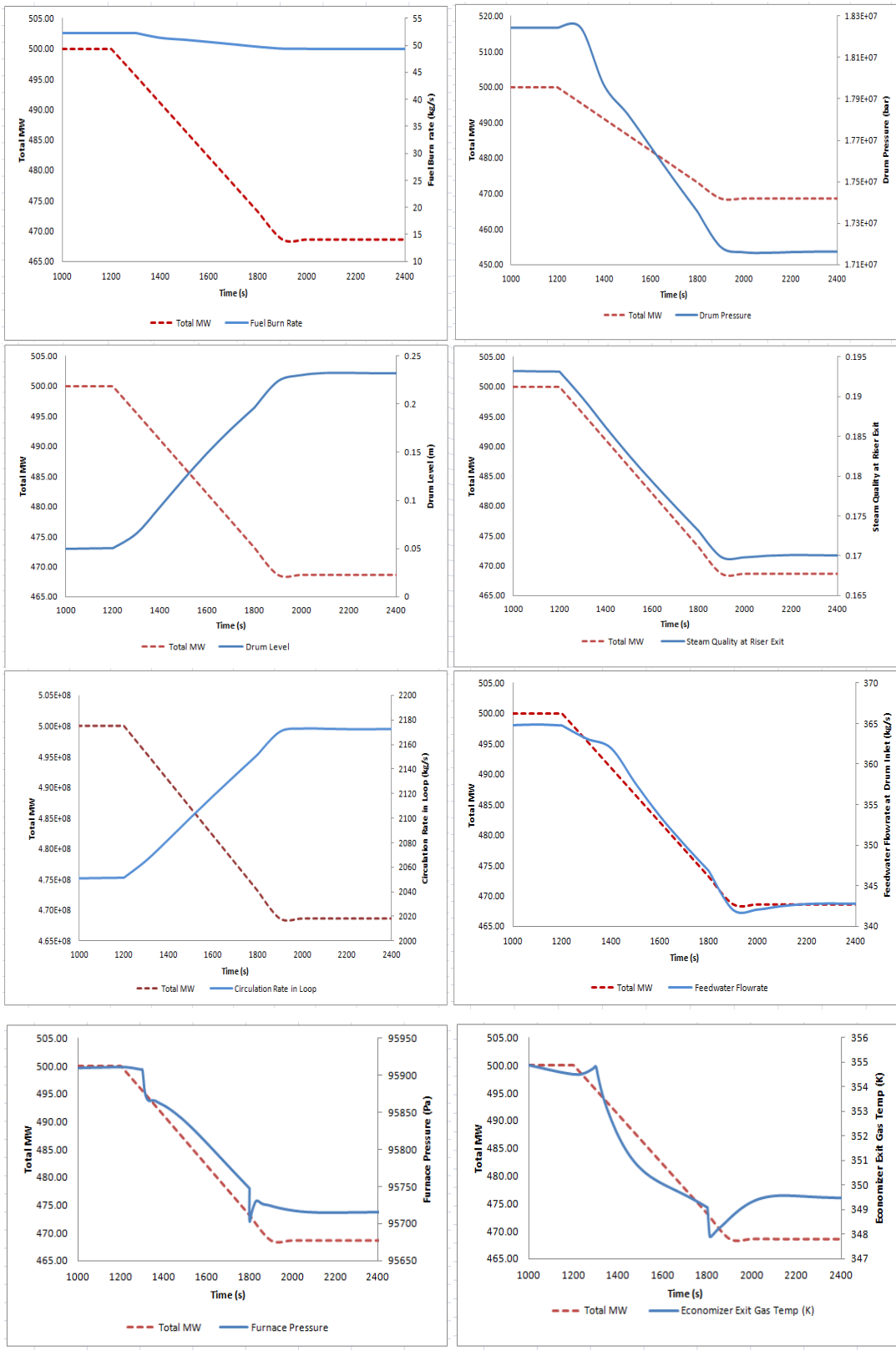
Fig.3.10 Ramp change in total MWe

3.7 Concluding remarks

In this chapter, a dynamic model of a coal-fired subcritical power plant implemented in gPROMS ModelBuilder® was presented. The model comprised of a complete cycle with the feedwater heaters and deaerator. This is often not included in most published models. Also, key dynamics in the boiler such as steam volume below drum level has been included in this model. This is essential for accurate prediction of drum level. This has been modelled in detail in published stand-alone boiler models but hardly in whole plant models.

The model is benchmarked against a unit (500 MWe) of Didcot A coal-fired power station in the UK owned by RWE npower which was closed recently. Most of the model parameters have been obtained from the design/construction data of the benchmark plant. Unavailable parameters were obtained based on operating data. Physical properties were obtained using Peng-Robinson equation of state in Infochem's Multiflash®.

Steady state validations of the model show that the model can predict actual plant data with less than 5% relative error which is reasonable. More interesting point being that the model is able to do that at different load levels in the range of 70-100%. Also, analysis involving step and ramp changes were carried out. The results reflect expected trends in the trajectories of process variables. By comparison, ramp changes tended to induce less process disturbance and this clarifies why in reality load changes are implemented through ramp changes in the industry.

Chapter 4: Simplification of detailed post-combustion CO$_2$ capture plant model

This thesis relies on a detailed rate-based PCC model developed in Lawal *et al.* (2012). The detailed PCC model is very complex and required lengthy time for simulating different case studies and also it is difficult to manage due to numerous external property calls. Using detailed model in the CCS integrated model will involve more difficulty and longer time for simulations due to the complex nature of the CCS network components (*i.e.* CO$_2$ emitter, CO$_2$ capture and transport process). The model of the CCS chain is expected to be used mainly for assessing trajectories of different process variables during operation. As a result, for the model to be very useful, it should be easy to use and require as little time as possible when used for studying different process scenario. As a result, the detailed PCC model was not deemed suitable for use in the CCS integrated model except it is simplified to some extent so long as it retains most of its fidelity.

In order to use the detailed PCC model in the CCS chain model in this thesis, steps presented in this chapter, were therefore taken to simplify the detailed model. The procedure for developing the detailed model in Lawal *et al.* (2010) was described briefly in Section 4.1. The strategy for simplifying the PCC model is presented in Section 4.2. This is followed by some comparison of the predictions from the simplified model and that from the detailed model (Section 4.3). Concluding remarks are given in Section 4.4.

4.1 Detailed rate-based model of the PCC process

The detailed rate-based dynamic model of the PCC process with MEA used as the starting point in this thesis was developed using gPROMS ModelBuilder® (Fig.4.1) as presented in Lawal *et al.*(2010).The main unit operations in the PCC model are the absorber and regenerator units as shown in Fig.4.1. Other unit operations include the reboiler, condenser, holding tank, pump, cooler and cross heat exchangers.

4.1.1 Absorber and regenerator model

Mass transfer process in the absorber and regenerator model are described using two-film theory (rate-based approach). As a result, the vapour-liquid interaction is

viewed as consisting five distinct regions, namely bulk liquid, liquid film, bulk vapour, vapour film and vapour-liquid interface region. One-dimensional distributed energy and mass conservation equations were used to describe the vapour and liquid bulk regions. Energy and mass hold-ups were however neglected in the bulk vapour model. This is because the residence time of the vapour phase in the absorption system is relatively small compared with that of the circulating liquid phase solvent. Also, chemical absorption of CO_2 is assumed to take place only via liquid phase reactions. As a result, the heat of absorption was included only in the liquid bulk energy balance.

The Maxwell–Stefan formulation (Krishna and Wesselingh, 1997) was used to determine the mass fluxes of components in both the vapour and the liquid film. Diffusivity of CO_2 in vapour and liquid phase was determined using the methods of Fuller *et al.* (1966) and Versteeg and Swaaij (1998) respectively. The mass transfer coefficients and the wetted area of packing were obtained using the method of Onda *et al.* (1968). Mass and energy hold-up was neglected in the liquid and vapour film region. The interface model on the other hand is based on equilibrium between liquid and vapour phases. The equilibrium molar compositions of the components in the vapour and liquid phases are estimated based on the vapour and liquid fugacity coefficients.

The CO_2-MEA-H_2O reactions are assumed to reach equilibrium at the interface. With a fast reacting solvent such as MEA, this assumption is reasonable. Other assumptions include plug flow regime, linear pressure drop along the column, and negligible solvent degradation. Heat loss to the surroundings is neglected in the absorber since its operating temperature is only around 40-50°C. However, heat loss to the surroundings is taken into account in the regenerator. This is because the regenerator operates at a much higher temperature (up to 120°C) and as a result has higher potential for heat loss.

4.1.2 Model of other unit operations

The other unit operations, namely pumps, holding tanks and cross heat exchangers were developed based on default models in the Process Model Library in gPROMS ModelBuilder$^{®}$. The condenser and reboiler were developed based on the flash drum

model in the Process Model Library in gPROMS ModelBuilder®. The flash drum is modelled as an equilibrium stage.

Fig.4.1 PCC model flowsheet in gPROMS ModelBuilder® (Lawal *et al.* 2010)

4.1.3 Physical property calculation

Thermodynamic and transport properties calculations in the model were performed using Infochem Multiflash®. The configured Infochem Multiflash® file is imported directly into the gPROMS ModelBuilder® environment. Fugacity coefficients and flash calculations were performed using the ElecNRTL model in Aspen Properties. Aspen Properties is CAPE compliant and therefore accessible via CAPE-OPEN Thermo socket in gPROMS ModelBuilder®.

4.1.4 Model validations

Steady state validation (Lawal *et al.* 2010) and dynamic validation (Biliyok *et al.* 2012) of the model were performed using pilot plant measurements from the Separations Research Programme at the University of Texas at Austin (Dugas, 2006). The results of the validation were acceptable (Lawal *et al.* 2010; Biliyok *et al.* 2012).

In the process flowsheet (Fig.4.1), water wash sections in the absorber and regenerator have been excluded. Also, PI controllers have been used for controlling

amount of water make-up, condenser temperature, reboiler temperature and liquid level.

4.2 Simplification of the rate-based PCC model

As noted earlier, the rate-based PCC model (Lawal *et al.* 2010) described above is very complex and requires lengthy CPU time during simulations. Simpler versions of the PCC model obtained using equilibrium approach do not reflect the true dynamics of the PCC process (Lawal *et al.* 2009a). With reasonable compromise between simplicity and fidelity, simulations using the rate-based model can be done at reduced CPU time (Peng *et al.* 2003). When simplified and integrated with other component models of the CCS chain, meaningful reduction in overall CPU time required for simulating the network model can be achieved.

A typical approach for simplifying rate-based models involves simplifying certain aspects of the model (Peng *et al.*, 2003; Katariya *et al.,* 2006). In Peng *et al.* (2003) and Katariya *et al.* (2006), it was shown that a simpler rate-based model of a packed reactive distillation column for the production of tert-amyl methyl ether (TAME) can be obtained by simplifying the non-linear algebraic equations used for mass transfer calculations. The mass transfer equations are simplified on the basis that they change only a little around steady state condition, in which case they become approximated by a constant value. This assumption eliminates the non-linear algebraic equations for calculating mass transfer parameters and other related equations and effectively reduces the complexity of the model. Peng *et al.* (2003) reported up to two-third reduction in the total model equations in the detailed model of the TAME process. This resulted in nearly 80% reduction in CPU time required to simulate the simplified model for 10 hours period compared to the CPU time used to simulate the detailed model over the same time interval. Interestingly, from comparisons with the detailed model, predictions of the simplified model were only slightly off that of the detailed model.

In this thesis, interest is on rate-based PCC model which have some structural similarity with the rate-based TAME model in Peng *et al.* (2003) notwithstanding that PCC process is fundamentally different from the TAME process. Just like the Peng *et al.* (2003) model, the governing equations of the rate-based PCC model are relatively simple. However, the constitutive equations, mostly algebraic equations for

obtaining heat and mass transfer coefficients, are numerous and numerically unstable. Also, the constitutive equations involve numerous property calls from external physical property applications which in this case are Aspen Properties® and Infochem's Multiflash®. External property calls are inevitable because most equation-base tools like gPROMS ModelBuilder® does not have internal property estimation package. In reducing the model complexity, the constitutive equations are therefore the immediate targets.

Due to the structural similarity of the model rate-based PCC model and the TAME model in Peng *et al.* (2003), the simplification approach in Peng *et al.* (2003) will therefore be used in this thesis. However, the processes (*i.e.* TAME and PCC process), are expected to behave differently since they are fundamentally different. As a result, detailed sensitivity analysis on the mass transfer parameters will be carried out with the detailed PCC model to determine how they vary across the column with respect to changes in temperature, pressure and superficial velocity.

4.2.1 Analysis for model simplification

As noted above, the targets for simplifying the rate-based PCC model are the numerous non-linear algebraic equation and external property references. In the detailed model, the main non-linear algebraic equations are the ones used for mass transfer calculations in the absorber and regenerator. As a result, they are the key algebraic equations considered for simplification. The equations are the Onda *et al.* (1968) correlations given below:

$$k_L \left(\frac{\rho_L}{\mu_L g}\right)^{1/3} = 0.0051 \left(\frac{L_w}{a_w \mu_L}\right)^{2/3} \left(\frac{\mu_L}{\rho_L D_L}\right)^{-1/2} \left(a d_p\right)^{0.4} \tag{4.1}$$

$$\frac{k_G}{a} \frac{RT}{D_v} = 3.6 \left(\frac{V_w}{a \mu_v}\right)^{0.7} \left(\frac{\mu_v}{\rho_v D_v}\right)^{1/3} \left(a d_p\right)^{-2.0} \tag{4.2}$$

$$\frac{a_w}{a} = 1 - exp\left[-1.45 \left(\frac{\sigma_c}{\sigma_L}\right)^{0.75} \left(\frac{L_w}{a \mu_L}\right)^{0.1} \left(\frac{L_w^2 a}{\rho_L^2 g}\right)^{-0.05} \left(\frac{L_w^2}{\rho_L \sigma_L a}\right)^{0.2}\right] \tag{4.3}$$

The equations involves external physical property calls for densities in the liquid and gas phase, viscosities in the liquid and gas phase, surface tension, and parameters for obtaining the vapour diffusivity. In addition, there are other related equations, namely equations for obtaining the diffusivities in the liquid and vapour phase among

others where these coefficients are used directly or indirectly. It must also be noted that the entire model is a distributed model which involves point to point calculations of these coefficients with time. Approximating these coefficients (*i.e. k_L, k_G, and a_w/a*) with a constant value following the method of Peng *et al.* (2003) can therefore be seen to eliminate some of the external property calls and equations (or at least simplify the equations) and consequently reduce the model complexity in terms of number of equations and external property calls. Models of other unit operations in Fig.4.1 are considered simple enough and as a result not considerd for simplfication. In this thesis, the approach of Peng *et al.* (2003) for the TAME process was assessed for the PCC process to determine its suitability considering that the two processes are fundamentally different. As a first step, the sensitivity of the mass transfer parameters across the packed column is accessed for different input conditions. The only inputs expected to vary from time to time are the liquid solvent and flue gas flowrate. We assumed that other inputs, namely temperature, pressure and composition of inlet flue gas and lean MEA solvent are well controlled and do not change significantly. While performing this test, other inputs were therefore kept constant.

The base case which is referred to throughout this chapter as condition B is obtained from Lawal *et al.* (2010). The liquid and gas flowrate at condition B are 0.72 kg/s and 0.12 kg/s respectively (L/G ratio = 6). At this condition, a capture level of about 97% is achieved. At this condition, the coefficients (i.e. k_L, k_G, and a_w/a) across the packed column were determined from the detailed model (Fig.4.2-4.4). For comparison, similar calculations were performed at two other conditions (Condition A: Liquid flowrate = 0.96 kg/s, Gas flowrate = 0.16 kg/s; Condition C: Liquid flowrate = 0.48 kg/s, Gas flowrate = 0.08 kg/s) as shown in Fig.4.2-4.4. This condition sets were selected arbitrarily around the base case condition. The L/G ratio and hence the capture level is the same for the three conditions. Capture level is prefixed by L/G ratio other conditions remaining the same.

The results in Fig.4.2-4.4 show that the coefficients have strong correlation with inlet lean MEA liquid solvent and flue gas flowrate conditions assuming other inlet conditions remain the same. The trends are however similar at different conditions. When actual values of the coefficients are compared relative to the base case conditions in Fig.4.2-4.4, the relative difference is found to be less than 10% with changes in gas flowrate up to $\pm33\%$. The relative difference can be predicted to be

more as the inlet condition (gas and liquid flowrate) moves further away from the base case. When the mass transfer coefficients and wetted ratio are replaced by constant values obtained at specific conditions as in Peng *et al.* (2003), this result shows that the model performance will be best at specific reference conditions. Also at specific conditions, the wetted ratio and the gas phase mass transfer coefficients were observed to vary less visibly compared to the liquid phase mass transfer coefficient across the absorber column. The assessment was also performed for the regenerator column at the base case condition. Similar observations were made except that the gas phase mass transfer coefficient varied more strongly than in the absorber.
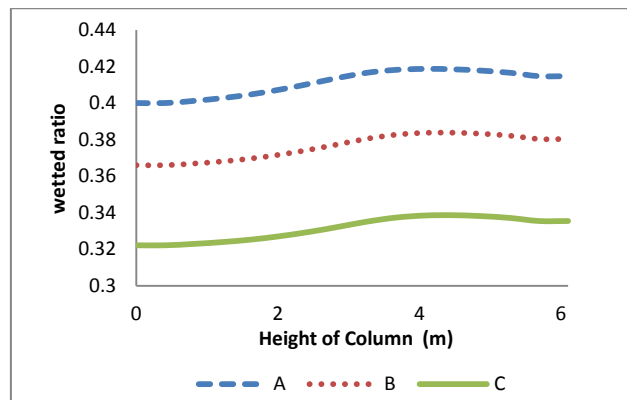
Fig.4.2 Wetted ratio
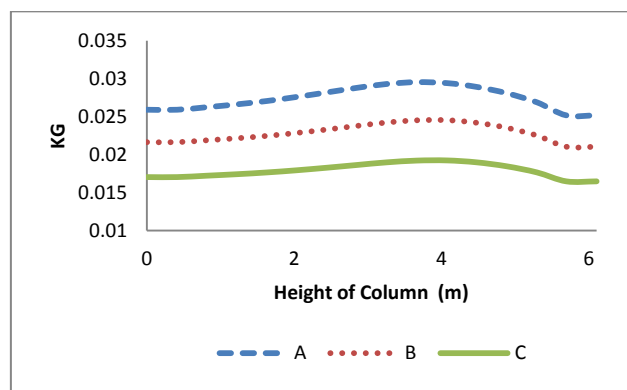
Fig.4.3 Gas phase MTC
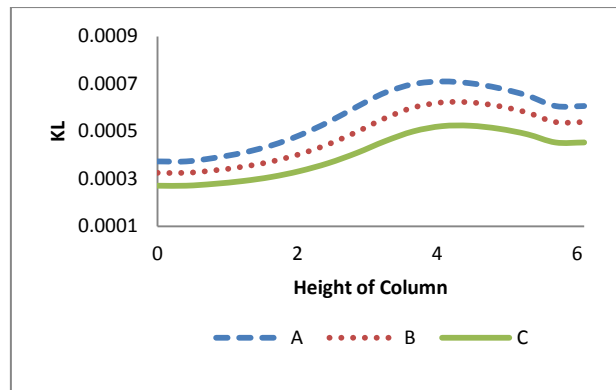
Fig.4.4 Liquid phase MTC

4.2.2 Determination of k_G, k_L and $\frac{a_w}{a}$ for the Simplified Model

The mass transfer coefficients (MTCs) and the wetted ratio (k_G, k_L and $\frac{a_w}{a}$) were estimated based on the base case (Condition B). Average values of these variables across the column were obtained and compared with actual values obtained using the detailed model at the base condition (Fig.4.5-4.7). The relative errors for each of these variables from the comparisons were as follows: wetted ratio $< \pm3\%$, gas phase mass transfer coefficient $< \pm7\%$, liquid phase mass transfer coefficient$< \pm49\%$. The average values of wetted ratio and gas phase mass transfer coefficient is close to the actual value across the column based on this analysis. As a result, the average values will be used for the simplified model. On the other hand, the average of the liquid phase mass transfer coefficient varies widely away from the actual values and cannot be used directly in their place as was for the gas phase mass transfer coefficient and wetted ratio. Rather than the Onda correlation for liquid phase mass transfer coefficient, a linear correlation obtained from correlating k_L against variables such as temperature and superficial liquid phase mass velocity is suggested. This will avoid the need for external property calls, eliminate/simplify related equations and consequently reduce CPU time.
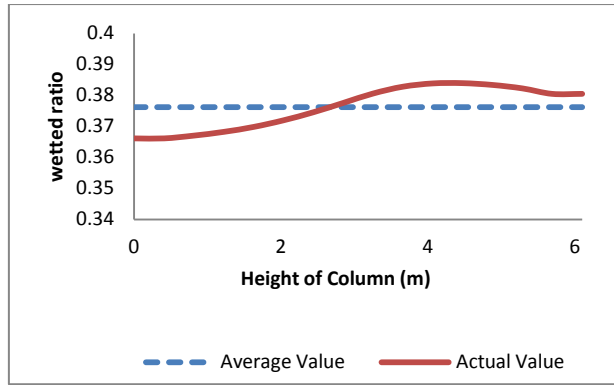
Fig.4.5 Actual vs average wetted ratio across the absorber
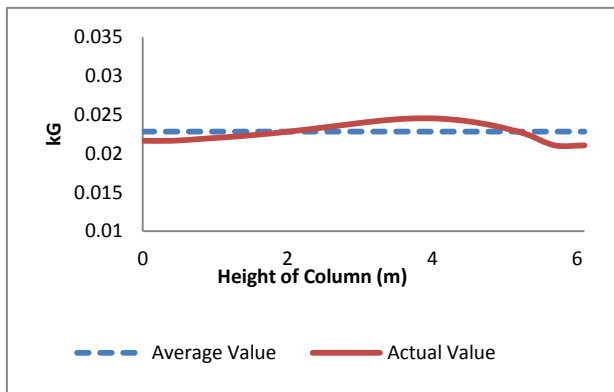
Fig.4.6 Actual vs average gas phase MTC across the absorber
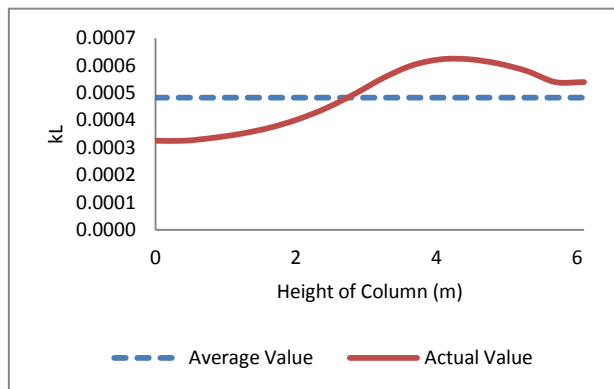
Fig.4.7 Actual vs average liquid phase MTC across the absorber

To develop a linear correlation for determining liquid phase mass transfer coefficient at different points along the column, we first determined how the various variables that change along column, namely temperature, pressure, and superficial mass velocity affect k_L. This will provide basis for accepting or rejecting any of the variable(s) as a component of the correlation.

The liquid phase mass transfer coefficient is plotted against each of these variables as shown in Fig.4.8-4.10. From these results, the liquid mass transfer coefficients

showed stronger sensitivity to superficial mass velocity and temperature and is affected less by pressure as expected. It is considered that the sensitivity to pressure is enough to include pressure in the correlation. Therefore, k_L is correlated against pressure, temperature and superficial mass velocity. A combination of these variables in the correlation is supposed to potentially enhance the prediction accuracy of the correlation.
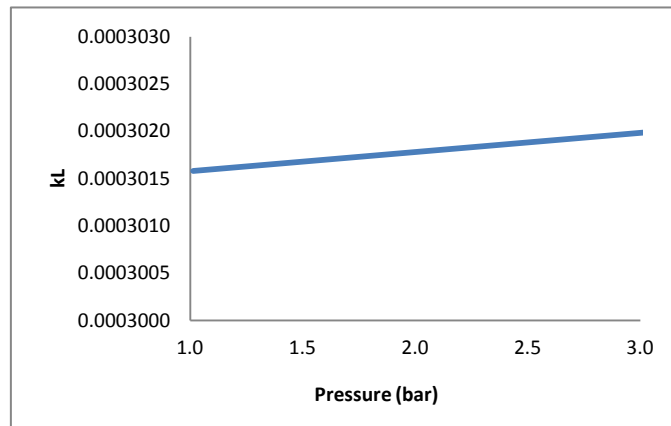
Fig.4.8 Liquid phase MTC vs pressure
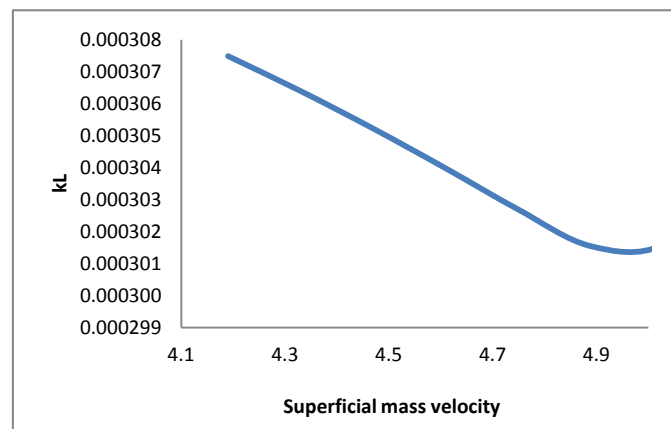
Fig.4.9 Liquid phase MTC vs superficial mass velocity
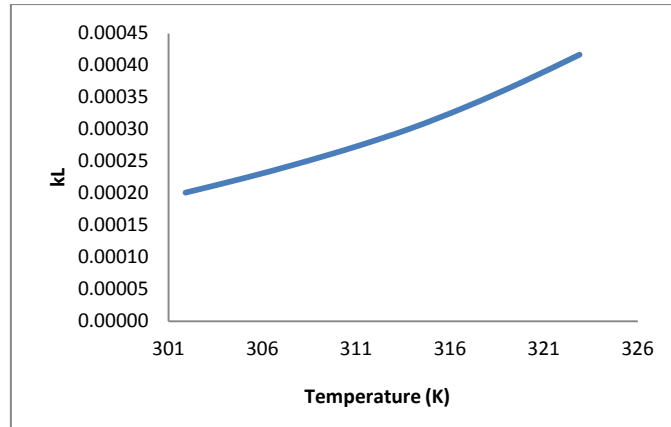
Fig.4.10 Liquid phase MTC vs temperature

The correlation developed is of the form.

$$k_L = k + n_1T + n_2P + n_3L_w \tag{4.4}$$

The values of the constants $k, n_1, n_2 \ and \ n_3$ are obtained through multi-variable linear regression approach in Microsoft-Excel based on temperature, pressure and superficial mass velocity (liquid phase) data obtained using the detailed model under condition B. Validation of this linear correlation has been carried out under condition C and the result is reasonable (Fig.4.11).

The procedure was repeated for the mass transfer coefficients (gas and liquid phase) for the regenerator. Analysis in previous section showed that the mass transfer coefficients (gas and liquid phase) vary considerably across the regenerator. The choice of constant mass transfer coefficients as was the case in Peng *et al.* (2003) will therefore be unsuitable. As a result, similar step taken for the absorber was used to develop a multi-variable linear correlation for predicting the mass transfer coefficients for the regenerator.

4.2.3 Implementation of the simplified model in gPROMS ModelBuilder®

To implement the simplified model in gPROMS ModelBuilder®, the average values of the $k_G \ and \ \frac{a_w}{a}$ and the linear correlation for k_L obtained from the detailed model analysis substitutes Eq.4.1, Eq.4.2 and Eq.4.3 respectively for the absorber. For the regenerator, average value of $\frac{a_w}{a}$ was used alongside multi-variable linear correlations for the mass transfer coefficients. The equations and other related ones are therefore eliminated as discussed earlier. Also, the number of discretisation

intervals for obtaining the solutions of some of the partial differential equations was reduced.
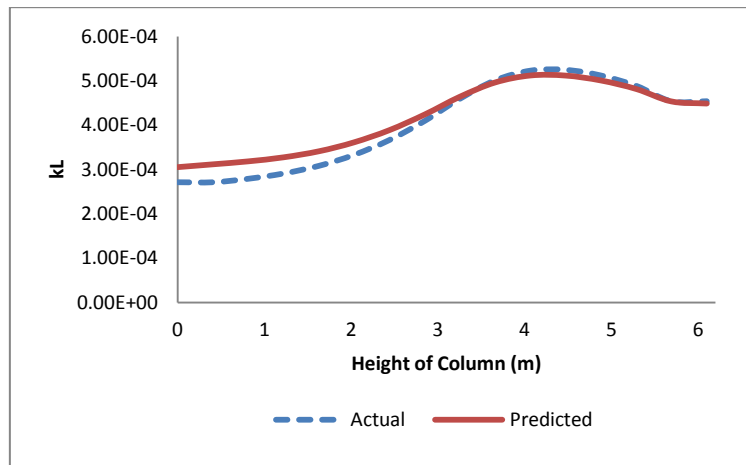
Fig.4.11 Validation of the linear correlation obtained

The simplified model in gPROMS ModelBuilder® was used for simulation study. The simulation results were summarised in **Table 4.1.** The simulations were carried out with an i5-2400 CPU @3.10 GHz processor and 4 GB RAM machine. The results show significant reduction in the model equations and CPU time.

Table 4.1 CPU time of the simplified model

	Detailed Model	Simplified Model
Number of equations	24721	11022
Simulation duration (h)	10	10
Average CPU time (sec)	248	98

4.3 Validation and discussion

Validation tests were performed by comparing the predictions of the detailed model (Lawal *et al.* 2010) and the simplified model at steady state and dynamic conditions. During the validation tests, the lean loading, flue gas flowrate, liquid solvent flowrate and gas inlet composition were kept the same for the detailed and simplified models.

4.3.1 Steady state validation

Steady state tests were carried out by comparing the absorber and stripper temperature profile predictions from the detailed and simplified models (Fig.4.12 and Fig.4.13) across the height of the column. The model predictions are within <5K for

the absorber and stripper. Therefore the simplified model can predict the plant behaviour reasonably well.

4.3.2 Dynamic validation

Dynamic test was carried out by investigating the impact of step and ramp change in flue gas flowrate (Fig.4.14) and reboiler temperature (Fig.4.16) on CO_2 capture level. This is the common change expected when a PCC is coupled to an upstream power generation plant operated in the load following mode. The simplified model should be able to capture this behaviour reasonably to be considered suitable for use in whole chain CCS integration.
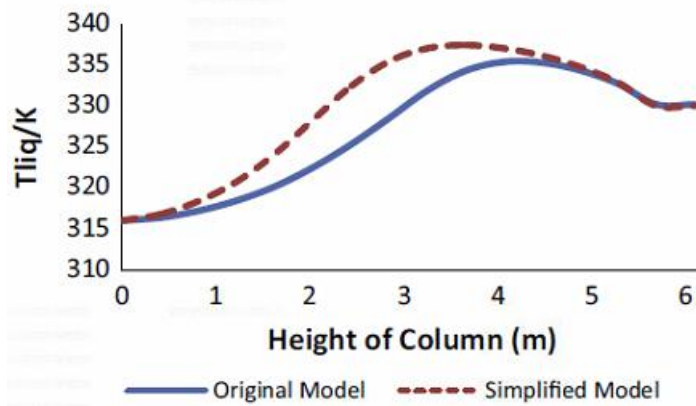
Fig.4.12 Temperature profile for absorber
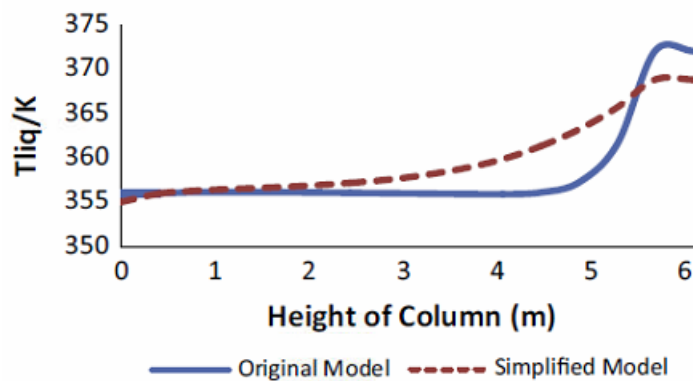
Fig.4.13 Temperature profile for stripper
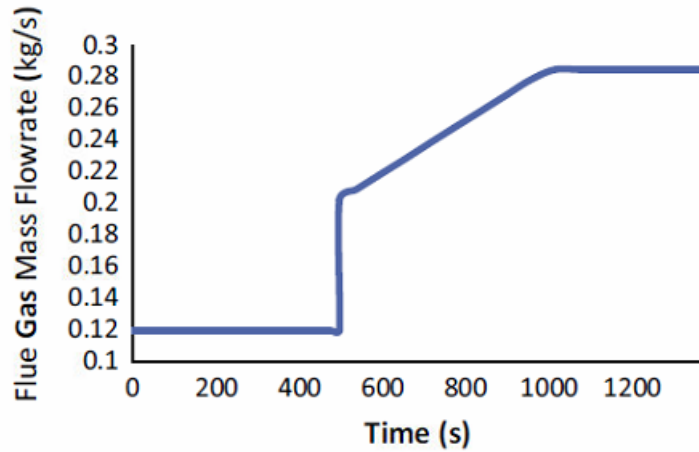
Fig.4.14 Step/ramp change in flue gas flowrate
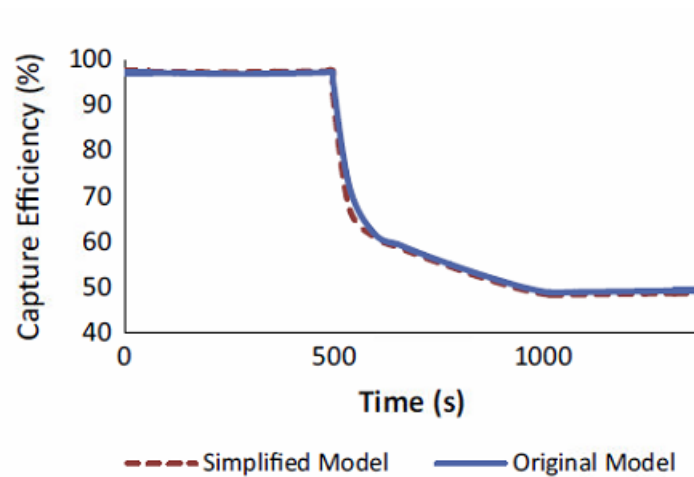
Fig.4.15 Capture level response to step/ramp change in flue gas flowrate

Increase in power plant output over a period of time results in increasing flue gas flowrate. Fig.4.14 shows the response of the CO_2 capture level in detailed rate-based model and the simplified model to a step/ramp change in the flue gas flow rate. The flowrate was maintained at 0.12 kg/s for 500 s (about 8 mins). A step input in the flowrate from 0.12 kg/s to 0.2 kg/s was applied at 500 s. The flowrate was then ramped up by 40% (from 0.2 kg/s to 0.28 kg/s) within 1000s (15 mins). Finally, the condition was maintained for 1500s (25 mins) to achieve steady state. As shown in Fig.4.15, the CO_2 capture level decreased from 97% to about 50% with step/ramp increase in flue gas flowrate from 0.12 kg/s to 0.28 kg/s (the lean solvent flow was kept constant) over a period of 50 mins. This result shows good agreement of the simplified model with the detailed model.

The required heat duty for the reboiler temperature is supplied from the IP/LP steam turbine crossover pipe in the power plant. Hence, an increase in reboiler temperature means a decrease in power generation capacity and vice versa. Fig.4.16 indicates a step/ramp change in the reboiler temperature. The reboiler temperature was maintained at 387 K for 500 s (about 8 mins). A unit step input (from 387K to 388K) in the reboiler temperature was then applied at 500 s before then the absorber temperature was ramped up further to 390K within 1000 s (15 mins). Finally, the reboiler temperature was maintained at 390K for 1500 s (25 mins) to achieve steady state. Fig.4.17 shows the response of the CO_2 capture level in detailed rate-based model and the simplified model to a step/ramp change in the reboiler temperature. The CO_2 capture level increases from approximately 97% to 99% with step/ramp increase in reboiler temperature from 387 K to 390 K over a period of 50 mins. The result shows a good agreement of the simplified model with the detailed model. In addition, this result shows that capture level is very sensitive to changes in reboiler heat duty.
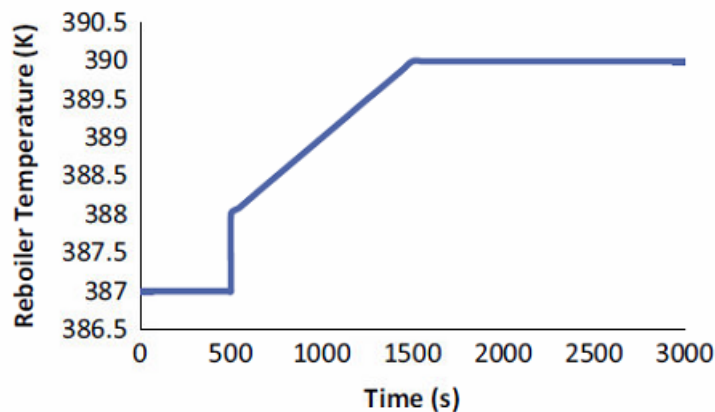
Fig.4.16 Step/ramp change in reboiler temperature
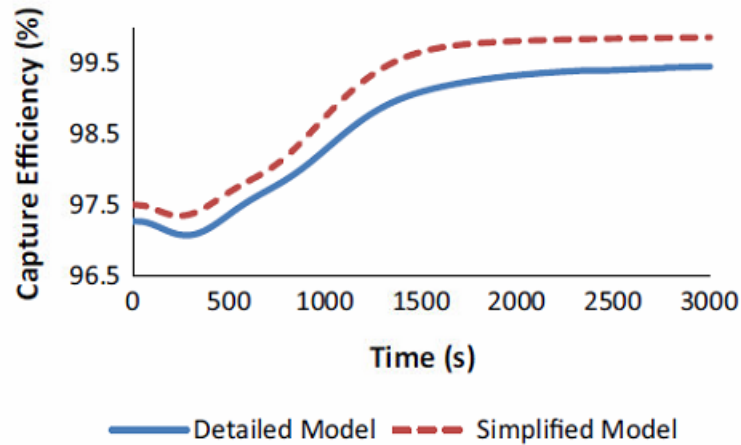
Fig.4.17 Capture level response to step/ramp changes in reboiler temperature

4.4 Concluding remarks

PCC process with MEA solvent can be modelled accurately through rate-based modelling approach (Lawal *et al.*, 2010). Such model is very complex and computationally demanding. As a result, the model should be simplified to reduced the computational requirement when the model is used either as stand-alone or as part of a whole chain CCS model as intended in this thesis. It is however challenging to simplify the model without limiting its performance.

In this thesis, the approach used by Peng *et al.* (2003) for simplifying a rate-based model of a packed reactive distillation column for a TAME process is adopted. The approach was improved in this thesis by the use of multi-variable correlations. The simplification method targeted the non-linear algebraic equations used for determining mass transfer parameters, namely wetted ratio, liquid and gas phase mass transfer coefficients. These equations involve numerous external property calls and are related to a number of other equations including the main governing equations of the model. Simplifying the equations removes the need for most of the property calls, eliminates a good number of other non-linear algebraic equations and simplifies the main governing equations. This simplifies the model drastically and consequently reduces the computational requirement. Steady state and dynamic validation tests performed by comparing the predictions of the detailed and simplified models showed that the simplified model performance was reasonable. An important conclusion here is that the numerous non-linear algebraic equation and external property calls are responsible for the high of CPU time requirements.

70

Chapter 5: Dynamic modelling of CO_2 pipeline transport

In this chapter, CO_2 pipeline transport model comprising of compressors, pipe segments, valves and pump is presented. The chapter begins with a brief review of some key issues considered in CO_2 pipeline transport (Section 5.1). Model equations for CO_2 pipeline transport are described in Section 5.2. Brief description of the Yorkshire and Humber CO_2 pipeline transport case study is given in Section 5.3. In Section 5.4, the case study is analysed using the model to obtain some insight. Finally, concluding remarks are given in Section 5.5.

5.1 CO_2 pipeline transport in CCS applications: Issues

CO_2 pipeline transport in CCS applications differs from CO_2 pipeline transport in EOR applications and hydrocarbon pipelines which has been in existence for decades (IPCC, 2005). The areas of difference between them are already highlighted in Chapter 1. Regardless, experience from CO_2 pipeline transport in EOR applications and hydrocarbon transport will be useful for developing pipeline transport system for CO_2 in CCS applications. CO_2 pipeline transport in CCS presents fresh issues that must be considered in development of CO_2 pipeline transport systems. Some of these issues are discussed below.

5.1.1 Feasible physical state for CO_2 pipeline transport

CO_2 exists in different states, namely solid, liquid, gas and supercritical/dense phase depending on temperature and pressure (Fig.5.1). It is widely recommended that CO_2 should be transported in the supercritical/dense phase in CCS applications (*i.e.* above the critical point where P=73.76 bar and T = 30.97^{o}C) (Lazic *et al.*, 2013). This is due to the following reasons:

- Large volumes of CO_2 are expected to be transported in CCS
- At supercritical condition, it has higher density closer to that of liquid phase CO_2 and lower viscosity close to that of gaseous phase CO_2. As a result, smaller pipeline (because of less pressure drop) will be required to cater for the huge CO_2 volumes expected compared to transport in the gaseous phase. In this phase, cryogenic systems required in liquid CO_2 transport are avoided.

- Possibility of two-phase flow condition is avoided so long as pressure is maintained above critical conditions throughout the pipeline. Two-phase flow causes operational problems, namely slugging, cavitations in pumps/compressors.
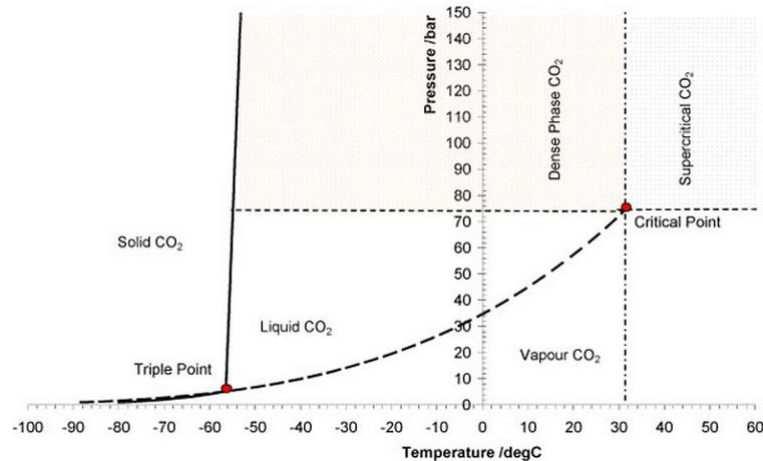
Fig.5.1 Phase diagram for pure CO_2 (IEA GHG, 2010)

It must be noted that CO_2 transport in supercritical/dense phase conditions mean higher operating pressure (>80 bar) and invariably higher CAPEX. Also, at dense phase condition, conventional seals used in valves, pumps and compressors tend to absorb CO_2 and easily become embrittled when depressurized. This is a key concern for adopting existing hydrocarbon pipelines for CO_2 transport. Finally, CO_2 is accompanied by significant cooling when it undergoes rapid and sudden depressurization due to its high Joule-Thompson (J-T) coefficient (Lazic *et al.* 2013). Cooling could be to the extent of formation of a spray of solid CO_2 (dry ice) which has health and safety implications. When CO_2 is transported at dense/supercritical conditions, this type of incidence may arise in the event that leakage occurs. This is another issue that need to be investigated and properly understood.

In circumstances with potentials of CO_2 re-use in the gaseous phase within short distances, CO_2 transport in the gaseous phase can be considered viable (Lazic *et al.*, 2013).

5.1.2 Presence of impurities

CO_2 transported in CCS applications will mostly come from anthropogenic sources (IPCC, 2005). As a result it will inevitably contain some amounts of impurities, such

as H_2, Ar, H_2S, O_2, CH_4 and N_2 among others depending on the type of captured technology used (*i.e.* PCC, pre-combustion or oxy-combustion capture) and the specific source of the CO_2 (e.g. coal-based power plants, natural gas-fired power plants, refineries, cement and steel plants among others). Impurities have been shown to affect CO_2 properties, namely density, viscosity, critical conditions and phase envelope (Li and Yan, 2006). This was further elaborated in Seevam *et al.* (2008) where the temperature and pressure profiles across a pipeline were shown to differ with different CO_2 compositions. This characteristic must be considered when developing CO_2 pipelines for CCS applications.

5.1.3 Compressor type

Compressors are important components of CO_2 pipeline transport systems. Selecting appropriate compressor is therefore essential. Due to the large volumes of CO_2 expected to be transported in CCS, it is suggested that intercooled single shaft multi-stage or multi-shaft integrally geared centrifugal compressors is the most appropriate in CCS applications (Fig.5.2). Multi-shaft integrally geared centrifugal compressors have lower capital cost (due to a lower number and smaller size of impellers). They also have lower OPEX, achieve higher efficiency and are more flexible (Tebodin, 2011). Integrally-geared centrifugal compressors have been selected for some upcoming large scale CCS projects such as the Shell Canada's Quest CCS Project (MDT, 2013). In this thesis, the compressor is modelled as a single shaft multi-stage centrifugal compressor with intercoolers.

5.1.4 Physical property calculation

Accurate physical property calculation is an essential aspect of the model development of any process system, incorrect property calculation could lead to equipment oversizing or undersizing. Decision as to what physical property calculation method to be used is therefore a crucial one. Properties of CO_2 may vary abnormally at supercritical/dense phase conditions making accurate property estimation difficult when they are transported at this condition (Lazic *et al.,* 2013). Property estimation is further complicated by the presence of impurities expected in CCS applications. At the moment there is yet to be a common agreement on the most accurate property method for calculating properties of CO_2 mixtture at

dense/supercritical condition (Luo *et al*. 2014). Different methods have been used in literature. Cubic EOS, namely Soave-Redlich-Kwong (SRK) and Peng-Robinson (PR) have been used widely (Li and Yan, 2009). More complex EOS such as Lee-Kesler, Statistical Associating Fluid Theory (SAFT), GERG and Span and Wagner (SW) has also been reportedly used (Luo *et al*., 2014).

The performance of cubic EOS such as PR is generally poor at dense phase conditions (Moshfeghian, 2012) and the result deteriorates close to critical conditions (E.ON 2010). PR with Boston-Mathias modifications shows some improvements in density and viscosity calculations (Zhang *et al*. 2006). Li *et al*. (2009a and 2009b) and Luo *et al.* (2014) further demonstrated that property calculation of CO_2 mixtures at dense phase condition with PR can be improved by calibrating the binary interaction parameters based on experimental data. On the other hand, SW shows accurate predictions for pure CO_2 (Vandeginste and Piessens, 2008). However, SW cannot be applied to CO_2 mixtures expected in CCS due to its reliance on a large number of parameters (Demetriades *et al*., 2013). Demetriades *et al*. (2013) proposed an EOS that can predict the properties of CO_2 mixtures at dense phase condition with the simplicity of PR and accuracy of SW. Also, SAFT and its variants such as SAFT-VR, PC-SAFT has shown good potential for accurate prediction of properties of CO_2 mixtures (Diamantonis *et al*. 2013). However, there are no reported pipeline modelling studies where the SAFT EOS have been used (Luo *et al*., 2014).
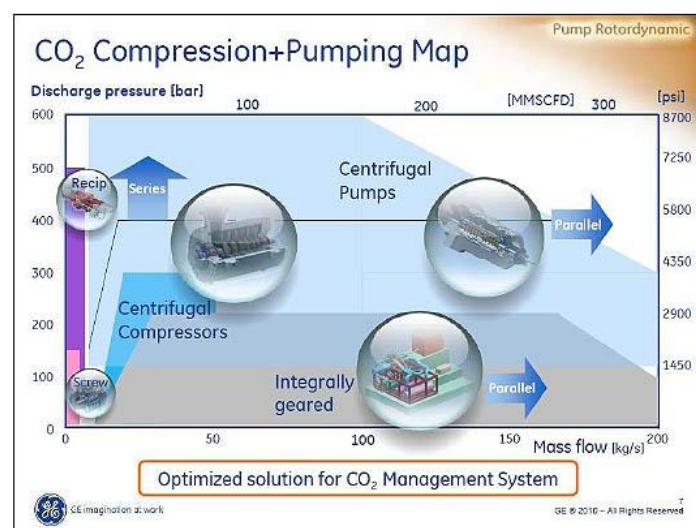
Fig.5.2 CO_2 compressor type selection (Tebodin, 2011)

Finally, GERG-2008 wide range EOS for gas mixtures is an international reference EOS for natural gas (Kunz and Wagner, 2012). GERG-2008 reportedly gives accurate results for gas mixtures from low to high pressures (up to 300 bar). Nimtz *et al.* (2010) and Liljemark *et al.* (2010) among other studies have used GERG-2008 EOS for pipeline modelling study involving CO_2 mixtures at dense phase condition. There is no existing investigation of GERG-2008 performance in CO_2 mixture applications at dense phase conditions. The argument in favour of GERG-2008 for CO_2 mixtures have been based on its success in accurate prediction of the thermophysical properties of natural gas mixtures from low to high pressure. Based on this argument, GERG-2008 from Aspen Properties® was used in this thesis. Aspen Properties® is CAPE compliant and therefore accessible via CAPE-OPEN Thermo socket in gPROMS ModelBuilder®.

5.2 Component models

5.2.1 Compressors

The dynamics of compressors are usually more rapid compared to process plants adjoined to them. As a result, steady state models are usually good enough to represent compressors in overall process simulation (Thomas, 1999, pp.204). On this basis, steady state model will be used for the compressors in this thesis.

The compressor discharge pressure is expected to reach supercritical conditions, up to 130bar. As a result, multi-stage centrifugal compressor with intercoolers is selected. In modelling the multi-stage compressors, polytropic process is assumed to take into account the possibility of non-ideal behaviour. For a polytropic process, the discharge temperature of the compressor is obtained as follows (Moshfeghian, 2011*)*:

$$T_{dis} = T_{suc} \left(\frac{P_{dis}}{P_{suc}} \right)^{\left(\frac{n-1}{n} \right)}$$ (5.1)

The polytropic index (n) is obtained from the following relation:

$$\left(\frac{n-1}{n} \right) = \left(\frac{k-1}{\eta_p k} \right)$$ (5.2)

Polytropic efficiency (η_p) for compressors usually averages between 0.77-0.82 (Ludwig, 2001). In this thesis, the polytropic efficiency of the CO_2 compressor is

assumed to be 0.77. This assumption is necessary because actual CO_2 mixture compressor curve is not available. Average value of the specific heat ratio (k) between suction and discharge has been used to take into account variations in the k value due to changes in temperature and pressure across each compression stage (Honeywell, 2009).

Pressure ratio is calculated as follows based on rated design conditions (*i.e.* design pressure ratio and suction temperature) (Lapina, 1982).

$$r = \left[\frac{T_{rsuc}}{T_{suc}} \left(\left((r_r)^{\frac{(n-1)}{n}} - 1 \right) + 1 \right) \right]^{\frac{n}{(n-1)}} \tag{5.3}$$

Impact of changes in suction temperature on the pressure ratio is captured in Eq.5.3. Fixed pressure ratio has been used in literature in modelling CO_2 compression (Luo *et al.*, 2014). When fixed pressure ratio is used, impact of changes in suction temperature on pressure ratio cannot be captured. It must be noted that the effect of suction pressure which can be quite significant cannot be captured by such model. This is eliminated however in circumstances where compressor curve is used. Rated pressure ratio (r_r) ranges from 1.7-2 (Witkowski *et al.*, 2013). The rated suction temperature (T_{rsuc}) is assumed to be 20°C based on information from the case study (Section 5.3) in this thesis (Luo *et al.*, 2014). Finally, the compressor power requirement GP is computed based on the polytropic head (H_{poly}) (Eq.5.4) using Eq.5.5.

$$H_{poly} = \frac{Z_a R T_{suc}}{MW} \left(\frac{n}{n-1} \right) \left[\left(\frac{P_{dis}}{P_{suc}} \right)^{\left(\frac{n-1}{n} \right)} - 1 \right] \tag{5.4}$$

$$GP = \frac{\dot{m} H_{poly}}{\eta_p} \tag{5.5}$$

Average compressibility (Z_a) takes into account the variations in the actual compressibility values from suction to discharge (Honeywell, 2009). The terms, R and MW are respectively gas constant (=8314.46 J/kmol K) and molecular weight of the CO_2 mixture. The intercoolers were similarly represented with steady state energy and mass conservation equations. The intercooler model is solved by

specifying the intercooler exit temperature. Also, 1% pressure drop across the intercooler is assumed (Witkowski *et al.*, 2013).

5.2.2 Pump and valve

Similar to the compressor, steady state model will be used for the pump in this thesis. The pump and valve model are based on the default models in the Process Model Library in gPROMS ModelBuilder®. The pump is designed to contribute maximum 40 bar pressure to the system with an efficiency of 75%. Temperature rise of 1% is specified to account for imperfections in the pump. The 40 bar pressure rise across the pump had been based on the requirements from the case study which is described in Section 5.3.

5.2.3 Pipe segment

The general conservation equations for a one-dimensional and compressible fluid flow through a pipe are as follows (Thomas, 1999):

Mass conservation equation:

$$A \frac{d\rho}{dt} + \frac{d\dot{m}}{dz} = 0 \qquad (5.6)$$

Momentum conservation equation:

$$\frac{d(\rho v)}{dt} + \frac{d(P + \rho v^2)}{dz} = -\frac{f \rho v |v|}{2D} - \rho g \sin \theta \qquad (5.7)$$

Energy conservation equation:

$$\left(u + \frac{1}{2}v^2 + gz \sin \alpha\right) \frac{d\rho}{dt} + \rho \frac{d}{dt}\left(u + \frac{1}{2}v^2\right) = \frac{q}{A} - \rho v \frac{d}{dz}\left(h + \frac{1}{2}v^2\right) - \left(h + \frac{1}{2}v^2 + \right.$$

$$\left. gz \sin \alpha\right) \frac{d}{dz}(\rho v) - \rho v g \sin \theta \qquad (5.8)$$

In this thesis, these general equations will be rewritten in terms of mass flowrate, temperature and pressure. The variables are easily measurable operating variables. Eq.5.6, Eq.5.7 and Eq.5.8 were rewritten as Eq.5.9, Eq.5.10 and Eq.5.11 respectively. The steps taken to arrive at Eq.5.9, Eq.5.10 and Eq.5.11 are given in Appendix A.

$$\left(\frac{\partial\rho}{\partial P}\right)_T \frac{dP}{dt} + \left(\frac{\partial\rho}{\partial T}\right)_P \frac{dT}{dt} = -\frac{1}{A}\frac{\partial\dot{m}}{\partial z} \tag{5.9}$$

$$\frac{1}{A}\frac{d\dot{m}}{dt} = \left(\frac{\dot{m}^2}{\rho^2 A^2}\left(\frac{\partial\rho}{\partial P}\right)_T - 1\right)\frac{dP}{dz} - \frac{2\dot{m}}{\rho A^2}\frac{d\dot{m}}{dz} + \left(\frac{\dot{m}^2}{\rho^2 A^2}\left(\frac{\partial\rho}{\partial T}\right)_P\right)\frac{dT}{dz} - \frac{f\dot{m}|\dot{m}|}{2\rho A^2 D} - \rho g\sin\alpha \tag{5.10}$$

$$\left(\rho c_p - \left(\frac{\dot{m}}{\rho A}\right)^2\left(\frac{\partial\rho}{\partial T}\right)_P\right)\frac{dT}{dt} + \left(\frac{T}{\rho}\left(\frac{\partial\rho}{\partial T}\right)_P - \left(\frac{\dot{m}}{\rho A}\right)^2\left(\frac{\partial\rho}{\partial P}\right)_T\right)\frac{dP}{dt} + \frac{1}{A^2}\frac{\dot{m}}{\rho}\frac{d\dot{m}}{dt} = \frac{q}{A} - \left(\frac{\dot{m}}{A}c_p - \right.$$

$$\left(\frac{\dot{m}}{\rho A}\right)^3\left(\frac{\partial\rho}{\partial T}\right)_P\right)\frac{dT}{dz} - \left(\frac{\dot{m}}{\rho A}\left[1 + \frac{T}{\rho}\left(\frac{\partial\rho}{\partial T}\right)_P\right] - \left(\frac{\dot{m}}{\rho A}\right)^3\left(\frac{\partial\rho}{\partial P}\right)_T\right)\frac{dP}{dz} - \frac{1}{A^3}\frac{\dot{m}^2}{\rho^2}\frac{d\dot{m}}{dz} - \frac{\dot{m}}{A}g\sin\alpha \tag{5.11}$$

The Darcy friction factor (f) in Eq.5.10 is estimated using the Swamee-Jain (1976) equation (Eq.5.12). Swamee–Jain equation is an approximation of implicit Colebrook–White equation.

$$f = \frac{0.25}{\left[\log\left(\frac{\varepsilon}{3.7D} + \frac{5.74}{Re^{0.9}}\right)\right]^2} \tag{5.12}$$

The density derivatives, $\left(\frac{\partial\rho}{\partial P}\right)_T$ and $\left(\frac{\partial\rho}{\partial T}\right)_P$, are obtained as follows:

$$\left(\frac{\partial\rho}{\partial P}\right)_T = \frac{1}{(v_{son})^2} \tag{5.13}$$

$$\left(\frac{\partial\rho}{\partial T}\right)_P = -\rho\sqrt{\frac{(c_P - c_V)}{T(v_{son})^2}} \tag{5.14}$$

Eq.5.13 and Eq.5.14 are derived from various thermodynamic relations as presented in Appendix B.

Heat transfer between the CO_2 mixture flowing in the pipeline and the surroundings (*i.e.* heat flux per unit length of pipeline) has been approximated by the steady state heat transfer equation (Eq.5.15) (Bai and Bai, 2005) based on internal surface area.

$$q = \pi U_{OHTC} D_i (T_F - T_A) \tag{5.15}$$

In Eq.5.15, the term U_{OHTC} is the overall heat transfer coefficient (W/m K) based on internal surface area, D_i is the pipe internal diameter, T_F and T_A are respectively temperature of fluid flowing inside the pipeline (CO_2 mixture) and the ambient temperature of the pipe surroundings. For the case study (Section 5.3), it is suggested that T_A value ranges from about 5°C during winter to 14°C in summer for the onshore pipeline (ground temperature) and about 16°C for the offshore pipeline

(seawater temperature) (Luo *et al.* 2014). The overall heat transfer coefficient (U_{OHTC}) based on internal surface area is obtained as follows:

$$\frac{1}{U_{OHTC}} = \frac{1}{h_i} + \frac{r_i \ln\left(\frac{r_o}{r_i}\right)}{\kappa_{pipe}} + \frac{r_i}{r_o h_o} \tag{5.16}$$

Insulation layers have not been considered in the U_{OHTC} calculation above for the onshore and offshore pipe section. The internal convective heat transfer coefficient h_i is obtained using dimensionless correlations proposed by Dittus and Boelter (1930). The correlation is given in Appendix C. For the onshore pipeline, it is assumed that the pipelines are fully buried to a depth H_D. On this basis, the external heat transfer coefficient (h_o) for the onshore pipeline is given as follows (Bai and Bai, 2005):

$$h_o = \frac{2\kappa_{soil}}{D_O \ln\left[\frac{2H_D + \sqrt{4H_D^2 - D_O^2}}{D_O}\right]} \tag{5.17}$$

For the offshore pipeline, h_o is calculated using dimensionless correlation proposed by Hilpert (1933). The correlation is given in Appendix C. The offshore pipeline is positioned along the seabed and as a result is assumed to be fully exposed (Bai and Bai, 2005).

5.2.4 Numerical solution

The PDEs are solved by MOLs (Schiesser, 1991). The centered finite difference method (CFDM) is used to discretise the distributed spatial domain using an order of approximation of 2. The resulting set of DAEs is then solved using SRADAU solver in gPROMS ModelBuilder®.

5.3 Case study

5.3.1 Physical description of case study

The planned Yorkshire and Humber CO_2 pipeline network have been selected as case study for testing the model described above. The Y&H CO_2 pipeline network will transport CO_2 mixtures from multiple capture sites, namely Don Valley power plant (Don Valley CCS, South Yorkshire) and Drax power plant (White Rose CCS,

North Yorkshire), to underground storage sites beneath the North Sea off the coast of Bridlington, UK (Luo *et al.*, 2014). Schematic diagram of the case study is shown in Fig.5.3.

In Don Valley CCS project, it is planned that CO_2 will be captured using pre-combustion CO_2 capture technology from a 650 MWe (net) new-build integrated gasification combined cycle (IGCC) power plant (2COEnergy, 2014). Information on 2CO2Energy website shows that five (5) million tonnes of CO_2 per year at about 90% capture level is expected to be captured. However, latest information obtained from National Grid Plc regarding the project showed a different amount of CO_2 captured (Table 5.1). From IPCC (2005), CO_2 captured via pre-combustion from an IGCC plant, include impurities such as H_2S (0.01-0.6 vol %), H_2 (0.8-2.0 vol %), CO (0.03-0.4 vol %), CH_4 (0.01 vol %) and $N_2/Ar/O_2$ (0.03-0.6 vol %).

White Rose CCS project on the other hand is planned to use oxyfuel CO_2 capture from a 450 MWe (gross output) oxy-coal power plant (Capture Power, 2014). It is estimated that two (2) million tonnes of CO_2 per year at about 90% capture level will be captured by the White Rose CCS project according to information on the project website. Again, latest information from National Grid Plc regarding the project showed different amount (Table 5.1). Similarly, from IPCC (2005), CO2 captured through oxyfuel captured with coal as fuel include impurities such as SO_2 (0.5 vol %), NO (0.01 vol %), and $N_2/Ar/O_2$ (3.7 vol %).
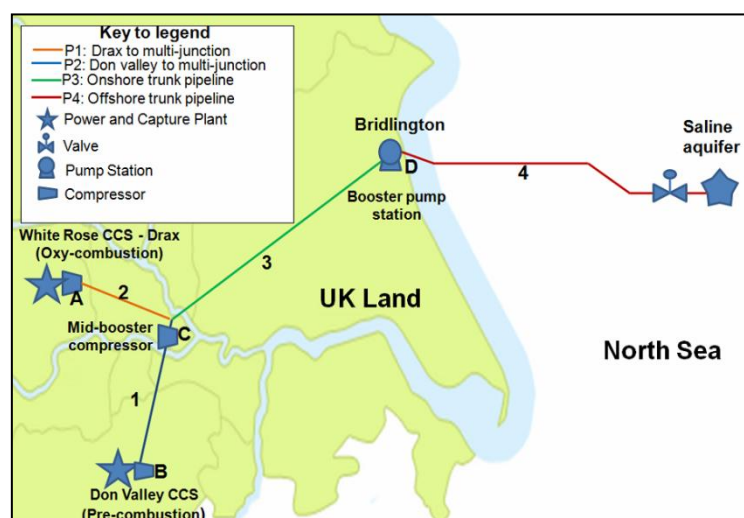
Fig.5.3 Schematic diagram of the case study (Luo *et al.* 2014)

The CO_2 captured from Don Valley site will be transported in gaseous phase at maximum allowable operating pressure (MAOP) of about 35 bar and boosted to an

MAOP of about 120 bar (dense phase condition) after about 15km distance from the Don Valley site (Trunk 1) before entering the common pipeline trunk (Trunk 3). On the other hand, CO_2 captured from the Drax site (White Rose), is compressed to dense phase conditions (about 120 bar) and transported for about 5 km (Trunk 2) before entering Trunk 3. The onshore pipelines are buried at a depth of 1.2 m. A booster pumping station located near the coast at Bridlington will boost the pressure of the CO_2-rich stream before it enters the offshore trunk pipeline (Trunk 4) which channels it to the storage site more than 1 km beneath the bed of the North Sea. The storage site is a saline aquifer formation located approximately 90 km offshore. Summary of pipeline dimensions is shown Table 5.1.

Table 5.1 Parameters of the pipelines

CO_2 Source	Flowrate range (Mt/yr)	Connecting pipeline branch		Onshore trunk pipeline		Offshore trunk pipeline	
		Length (km)	ND* (mm)	Length (km)	ND* (mm)	Length (km)	ND* (mm)
Don Valley	0.91- 6.27	15	750	71	600	91	600
Drax	0.61- 2.65	5	300				

*ND: Nominal dimension

The elevation profile for the various pipeline trunks is given in Fig.5.3. These design information was obtained from an in house design study by National Grid Plc, UK. In this thesis, standard Schedule 40 pipe is selected. Actual sizes of Trunk 2, 3, and 4 were then obtained from Aspen HYSYS® based on nominal sizes closest to the design values in Table 5.1. Actual size of Trunk 1 was obtained from Wenzhou (2014). The selected sizes are as follows:

- Trunk 1 pipeline (*i.e.* from compressor station B to C) : 750 mm nominal diameter (762 mm OD and 738.2 mm ID)

- Trunk 2 pipeline (*i.e.* from compressor station A to C): 304.8 mm nominal diameter (323.8 mm OD and 303.23 mm ID)

- Trunk 3 and 4 pipeline (*i.e.* mid-junction to pump station D (trunk 3) and pump station D to offshore choke manifold (trunk 4) at offshore platform: 609.6 mm nominal diameter (609.6 mm OD and 547.7 mm ID)
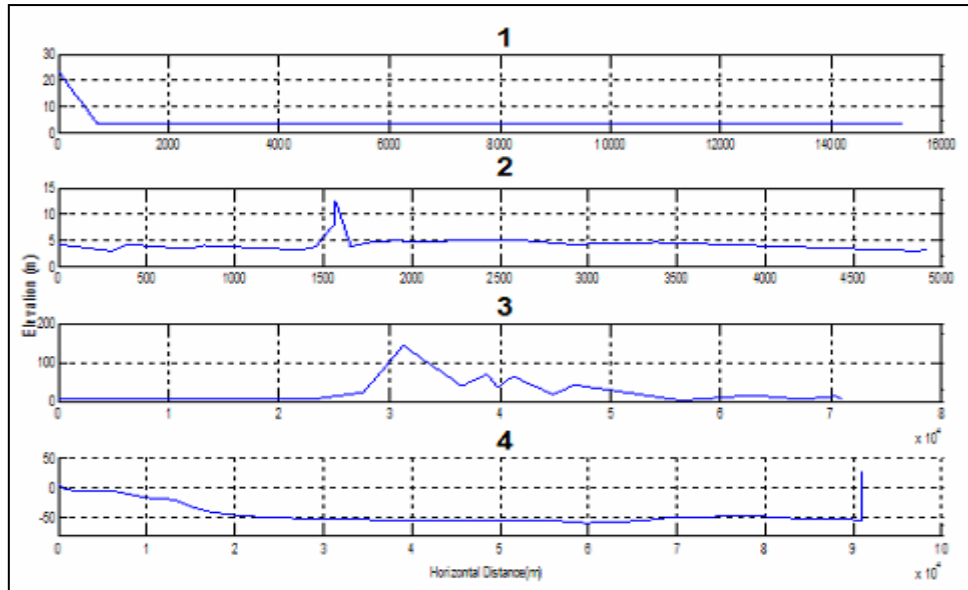
Fig.5.4 Elevation profile of the pipe trunks

5.3.2 Assumptions for case study simulation

For the purposes of simulating the case study, the CO_2-rich stream captured at Don Valley and Drax power plants are assumed to have the following composition:

- Don Valley (Pre-combustion CO_2 capture): 96 mol%CO_2, 2 mol%N_2 and 2 mol%H_2.

- White Rose (Oxy-coal CO_2 capture): 96 mol%CO_2, 2 mol%N_2 and 2 mole%Ar.

These compositions are supposed to have resulted after the original captured CO_2-rich stream had undergone pre-treatment. Also, maximum possible entry flowrate (Table 5.1), 20°C temperature and 1.01 bar pressure are taken as base case inlet condition. Detailed underground storage model is not included in this thesis as mentioned in Chapter 1.

5.3.3 Comparison with Aspen HYSYS model

Model topology of the case study developed with the equations in Section 5.2 using gPROMS ModelBuilder$^{®}$ is given in Fig.5.5. The case study like most large scale CO_2 pipeline transport systems for CCS is still in planning phase. As a result, there are no existing plant data to validate the case study model presented in this thesis. However, some of the steady state predictions of the model were compared with the predictions of a similar model in Aspen HYSYS$^{®}$. Aspen HYSYS$^{®}$ is a commercial simulator used widely in the industry. As a result, comparison with Aspen HYSYS$^{®}$

simulation can demonstrate the reliability of the equations and correlations used in the model in this thesis in the absence of detailed validation.

The same input conditions and parameters are used in the gPROMS ModelBuilder® and Aspen HYSYS® model. Peng Robinson (PR) EOS was however used for the Aspen HYSYS® simulation since GERG-2008 used in the gPROMS ModelBuilder® model is not supported in Aspen HYSYS®. The results of the comparison (Table 5.3) indicate close agreement in terms of the relative differences in their predictions. Note that very detailed momentum conservation equation is used for pressure drop calculation in the gPROMS ModelBuilder® model. In the Aspen HYSYS® model, the semi-empirical Beggs and Brill correlation is used. Also, the high relative difference in the duty prediction of compressor C is because the inlet conditions for the compressors (Trunk 1 exit) in the Aspen HYSYS® and gPROMS ModelBuilder® models differed a bit (See Table 5.2). The result also suggests that the predictions using GERG-2008 in gPROMS ModelBuilder® are not very way off the predictions obtained with PR in Aspen HYSYS®.

Table 5.2 Comparison with similar model in Aspen HYSYS®

Variables	Aspen HYSYS®	gPROMS ModelBuilder®	Rel. Diff. (%)
Compressor A			
Dis. Pressure (kPa)	10080	10101	0.21
Comp Duty (kW)	3.3434×10^4	3.4767×10^4	3.99
Compressor B			
Dis. Pressure (kPa)	3527.4	3527.9	0.014
Comp Duty (kW)	6.269×10^4	6.379×10^4	1.75
Compressor C			
Dis. Pressure (kPa)	10680	10137	-5.08
Comp Duty (kW)	1.7126×10^4	2.0058×10^4	17.12
Trunk 1 Exit			
Temperature (K)	288.39	289.84	0.50
Pressure (kPa)	3136	2970.23	5.29
Trunk 2 Exit			
Temperature (K)	296.21	296.23	0.0069
Pressure (kPa)	11830	11816.5	0.114
Trunk 3 Exit			
Temperature (K)	293.51	295.79	0.78
Pressure (kPa)	10430	10224	1.97
Trunk 4 Exit			
Temperature (K)	288.32	290.79	0.86
Pressure (kPa)	12882.09	12500	-2.97
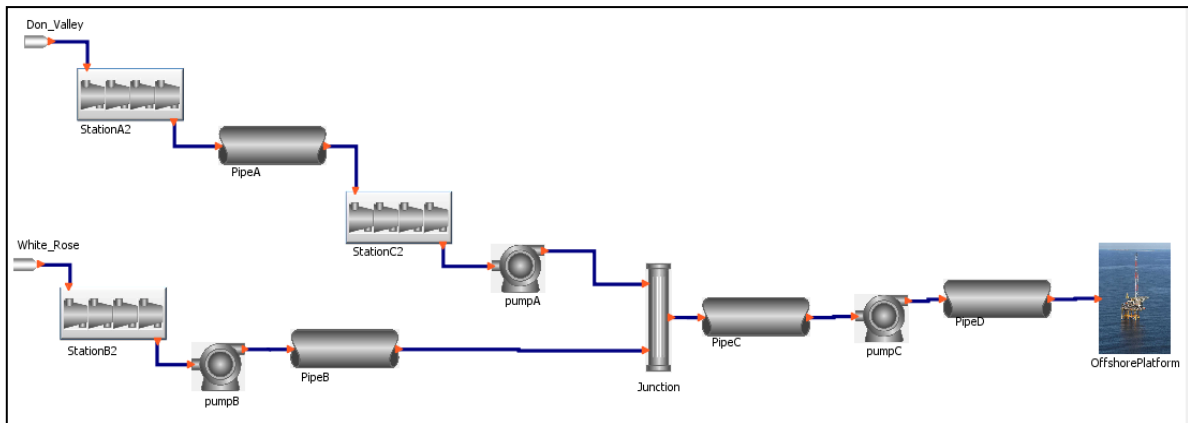
Fig.5.5 Model topology case study in gPROMS ModelBuilder$^{®}$

5.4 Results and discussions

5.4.1 Phase envelope

The phase envelope is important for defining operating boundaries for the CO_2 pipeline transport networks which avoids two-phase flow conditions. Two-phase flow conditions cause operating difficulties such as slugging. The operating boundaries are often defined in terms of temperature and pressure. The case study above involves transport of impure CO_2. Literature findings (Li and Yan, 2006; Seevam *et al.*, 2008) show that impurities alter the phase envelope significantly. For pure CO_2, the phase envelope (Fig. 5.6 A) shows that the two-phase flow region is almost unnoticeable as the liquid and vapour line are superimposed on each other.

The phase envelopes for the CO_2 mixtures from the Don Valley and Drax (White Rose) and the combined mixture from the two capture sites were also developed (Fig. 5.6). Fig 5.6 B and C are respectively the phase envelopes for CO_2 mixture from Don Valley and Drax (White Rose) sites. Fig. 5.6 D on the other hand is the phase diagram for the combined mixture from the two capture sites (trunk 3).

The phase diagram calculations have been performed using GERG-2008 wide ranging EOS in NIST REFPROP (DLL V9.1). The phase diagrams show remarkably higher critical pressure for the CO_2 mixtures (about 82bar) compared to the critical pressure of the pure CO_2 (about 74bar). The critical temperatures of the mixtures were slightly lower (about 302 K) than that of the pure CO_2 (about 304 K). Also, the presence of H_2 impurity tends to widen the two-phase flow envelope at very low temperatures (< 230 K) as can be seen in Fig. 5.6 B and D. The CO_2 mixture without H_2 impurity does not show this behaviour (Fig. 5.6 C).

Key insight from the phase diagram is that if the CO_2 mixture is to be transported at dense phase/supercritical condition, the transport pipeline should be operated at a pressure greater than 82 bar. National Grid PLC suggested a minimum operating pressure of 100 bar for the case study. Their suggestion is agreeable with the insight from the phase diagram. Also, during compression of the CO_2 mixture from the conditions at the capture site (about 1 bar pressure and 293 K temperature) to inlet conditions for pipeline transport, the mixture is expected to be intercooled between compression stages to enhance compression efficiency. The findings in Luo *et al.* (2014) indicate that the lower the intercooled temperature, the more the compression efficiency.

The phase diagram however indicates that intercooling to certain temperature could result to two-phase flow condition at some stage if the intercooler exit temperature falls within the two-phase region. In such circumstance, inter-stage vapour-liquid separator could be installed to remove any resulting liquid flow or a wet gas compressor could be used. Alternatively, the affected compressor stage could be designed to contribute greater pressure rise.

On the hand, higher intercooler exit temperature that avoids the two-phase region eliminates the possibility of two-phase flow condition. In Witkowski *et al.* (2013), intercooler exit temperature for the compressed CO_2 mixture was $38^{o}C$. This eliminates any chance for two-phase flow during compression to dense phase conditions. Obviously, the compressor energy requirement will be higher compared to a scenario involving lower intercooler exit temperature.
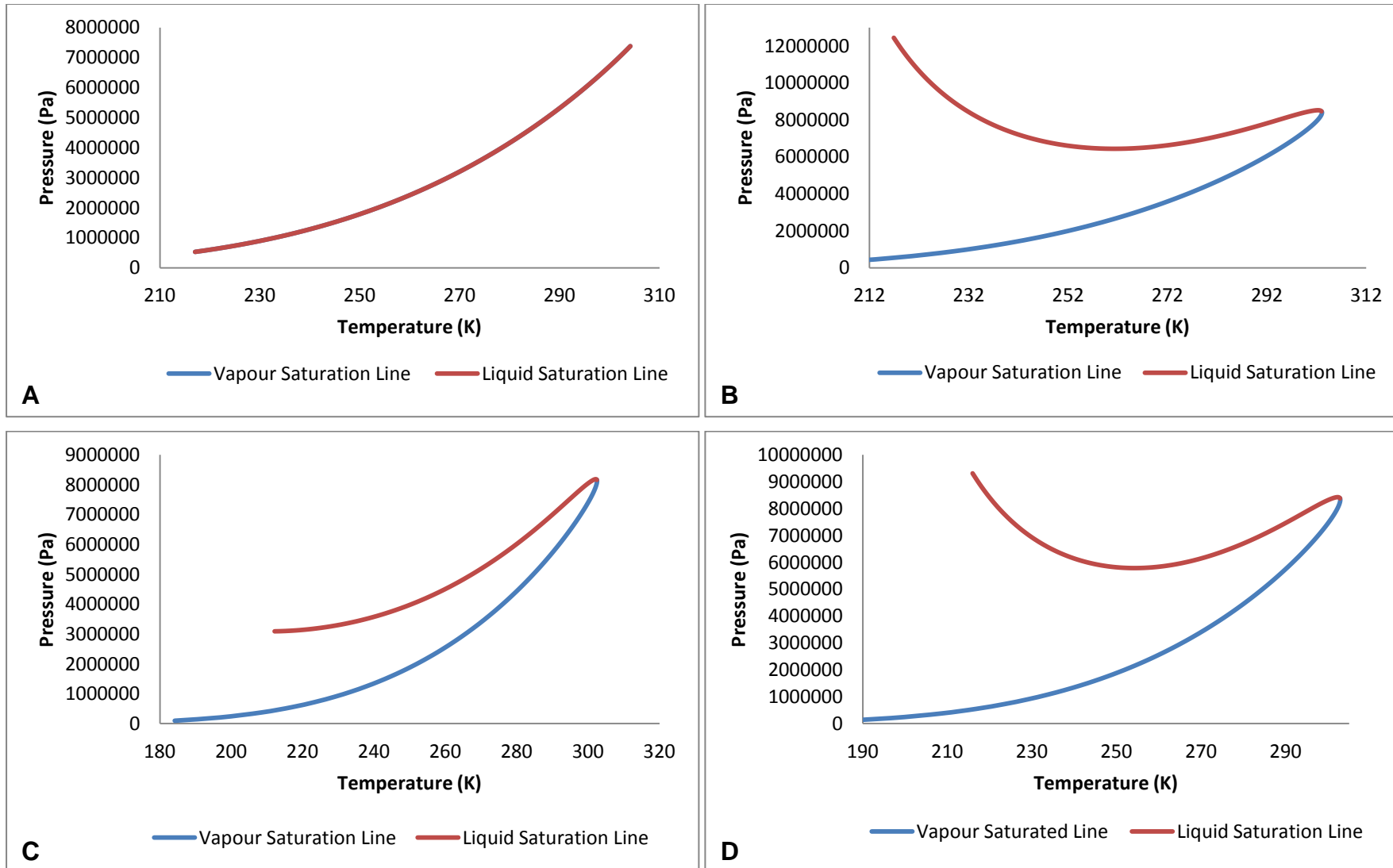
Fig. 5.6 Phase envelope for different CO₂ compositions

5.4.2 Compression

The case study comprise of three compression stations, namely A, B and C (Fig.5.3). Stations A and C comprise of a combination of pump and compressor. The compressor raises the pressure to about 100bar (dense phase) and the pump then raises it further to the final delivery pressure of 120bar (Luo *et al.*, 2014). This configuration results to lower CAPEX and OPEX as illustrated in Luo *et al.* (2014) compared to a scenario where only compressors are used to reach the final delivery pressure. The parameters of the compressors are given in Table 5.3.

On the other hand, station B is modelled to achieve up to 35bar (Luo *et al.*, 2014). In the case study, CO_2 mixture from Don Valley capture site is to be transported in the gaseous phase from B to C (about 15 km distance apart) where it is boosted to dense phase condition. Gaseous phase CO_2 pipelines operate at far less pressure than dense phase CO_2 pipelines (Luo *et al.*, 2014). This arrangement can be justified under any of the following scenario:

i) When the power plant/capture plant operators consider it unsafe for high pressure CO_2 compressors to be located adjacent the power plant/capture plant.

ii) When the power plant is located in a densely populated area and it is considered unsafe to lay high pressure CO_2 pipeline (over 100bar at dense phase condition) across such area.

In A and C, the intercooler exit temperature is $38^{o}C$ (Witkowski *et al.*, 2013). At this intercooler exit condition, the two-phase region and the complications that come with operating in the region is clearly avoided (See phase envelope). The CO_2 mixture is cooled further to $20^{o}C$ after the compressor last stage to meet the entry temperature specification for the Yorkshire & Humber CO_2 pipeline (Luo *et al.*, 2014). In B, the intercooler exit temperature is $20^{o}C$.

5.4.2.1 Temperature profile

The temperature profiles across the compressors *i.e.* A, B and C is given in Fig.5.7. The profiles show that the interstage discharge temperature increases across the compressors. This is a likely scenario because more heat energy is released as density increases during compression. This highlights the need for intercoolers since compression efficiency will inevitably drop without intercooling.

Table 5.3: Compressor parameters

Compressor	Number of Stages	Rated pressure ratio	Rated suction temperature
A	8	1.79	20°C
B	5	2.06	20°C
C	2	1.85	20°C
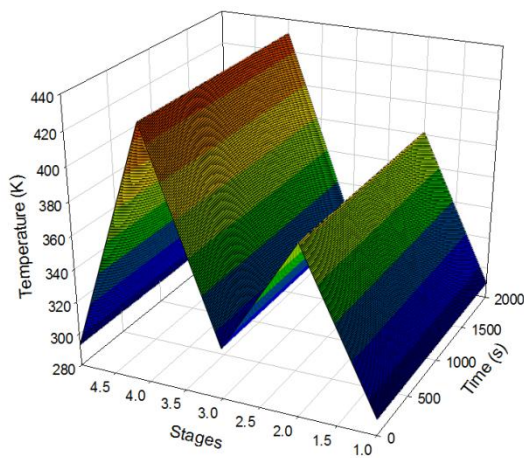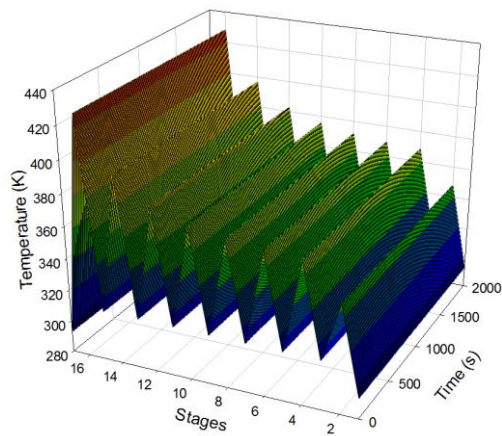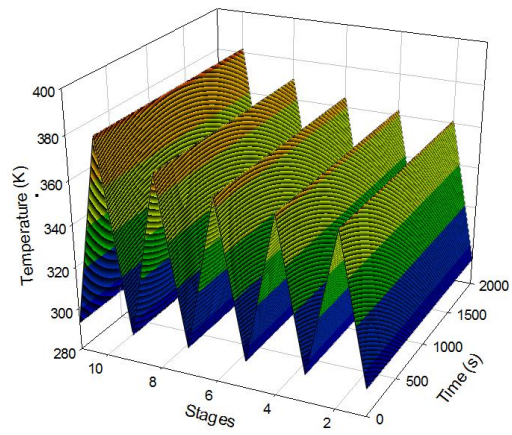
Fig.5.7 Temperature profile for compressor A, B and C

5.4.2.2 Heat integration opportunity

When operating at full load specification (Table 5.1), the total amount of heat energy rejected at the intercoolers for A, B and C is given in Fig.5.8 at an average temperature of about 370 K (Fig.5.7) across the compression stages. This energy can be recovered through heat integration with upstream components of the CCS chain, namely capture plant and power plant to reduce parasitic energy load (difference in net power production before and after CO_2 capture/compression equipment is installed). A model-based technical assessment by Fisher *et al.* (2005) show that heat integration with the capture plant is possible. According to Fisher *et al.* (2005), parasitic energy load could be reduced by 8 – 10 percent through heat integration.

It must be noted however that tight heat integration may sacrifice some of the plant flexibility. Also, for this case study, it is not possible to do heat integration with C considering that it is 15km away from the capture site.
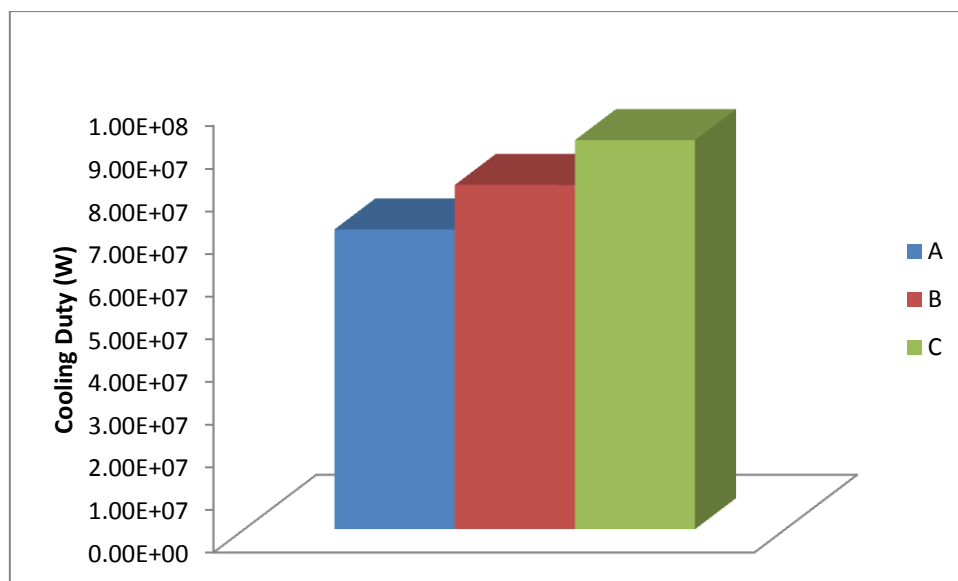
Fig.5.8 Total heat energy rejected at the intercoolers

5.4.2.3 Impact of changes in suction temperature

Impact of changes in suction temperature on discharge pressure was investigated for the three compressor stations *i.e.* A, B and C. Suction temperature conditions can be influenced by conditions at the upstream components of the CCS chain. As a result, it is necessary to understand how such changes will affect compression of the

CO_2 mixture. During this test, every other variable such as number of compression stages, rated pressure ratio and rated suction temperature among others remained unchanged. Only suction temperature was varied. Resulting discharge pressure at different suction temperature for the A, B and C compressors are given in Fig.5.9.
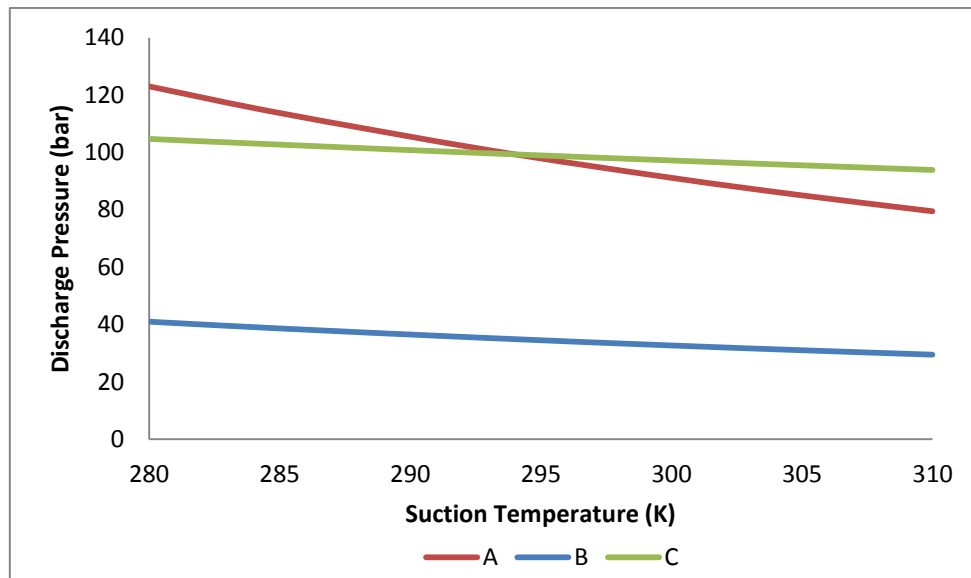
Fig.5.9 Impact of changes in suction temperature

The results show that less discharge pressure will be achieved as suction temperature increases. As a result, more compressor power will be required to maintain the same discharge pressure if suction temperature increases. Also, changes in discharge pressure at different suction temperatures are more significant in A. Compared to B and C, the only distinguishing inlet parameter is the composition of the CO_2 mixture at A. The composition at A includes 2mol% Argon in addition to 96mol% CO_2 and 2mol% N_2. On the other hand, the composition at B and C include 2mol% Hydrogen in addition to 96mol% CO_2 and 2mol% N_2. This is likely the reason for this behaviour in A (Fig.5.9) considering the molecular weight difference between Argon and Hydrogen

5.4.3 Temperature and pressure profile along the pipeline trunks

The temperature and pressure profile along the pipeline trunks is assessed for different scenario, namely:
- Pure CO_2 with elevation changes
- Impure CO_2 without elevation changes

- Base case involving impure CO_2 and pipeline elevation changes

This is important for quantifying the impact of neglecting impurities and pipeline elevation changes commonly assumed in many reported CO_2 pipeline transport models.

The profile obtained at full load for the different pipeline trunks is shown in Fig.5.10-15. For trunk 1 pipeline, the profiles for the conditions are closely matched. This trunk has two pipe segments with one going downwards and the other without elevation change (Fig.5.4). Impact of the elevation change is understandably not very obvious as can be seen from the profile. This indicates that pressure change is largely due to shear stresses (frictional losses) and temperature change is mostly due to heat exchange with the environment.

Pipe trunks 2 and 3 have 19 and 14 pipe segments respectively with different elevation changes. This is evident in the profiles along these trunks (Fig.5.12-15). With several turns (elevation changes) flow is expected to change directions, accelerate, decelerate etc. Pressure change therefore results from a combination of these forces in addition to shear stresses. Influence of fluid compression along the pipeline at some point on temperature is also evident.
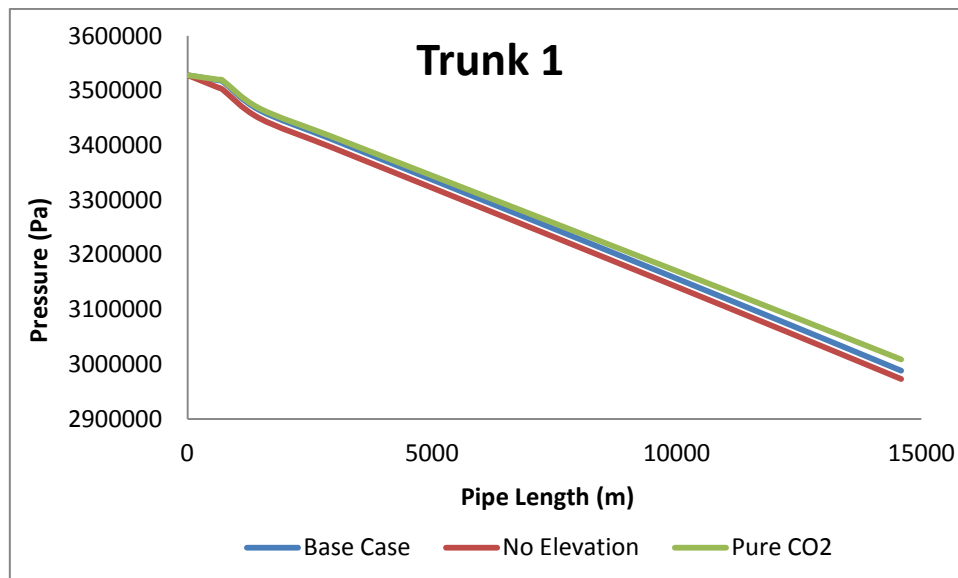
Fig 5.10 Pressure profile
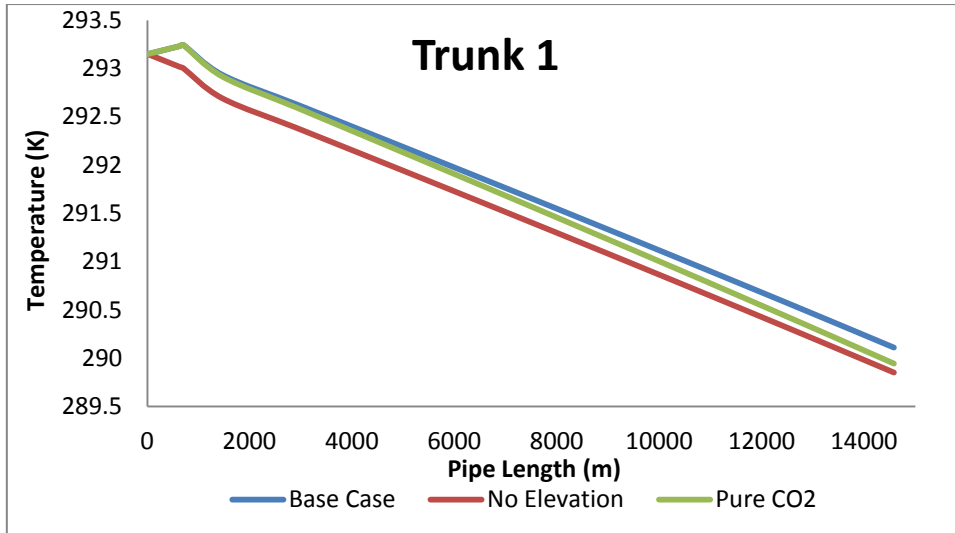
Fig 5.11 Temperature profile
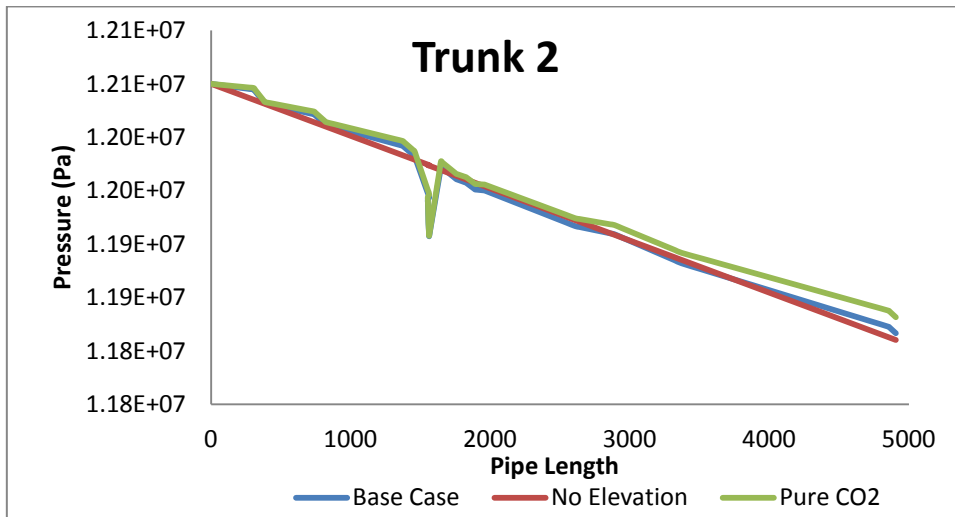
Fig 5.12 Pressure profile
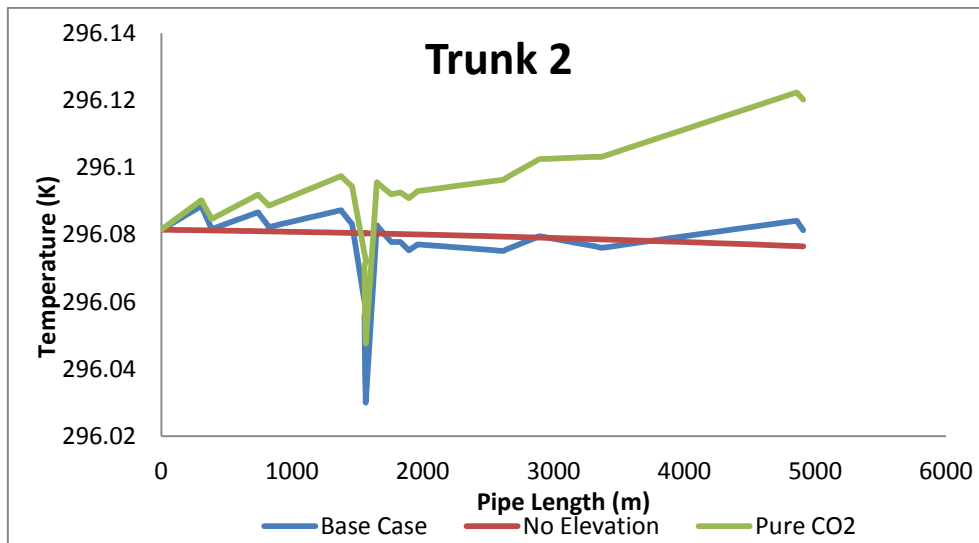
Fig 5.13 Temperature profile
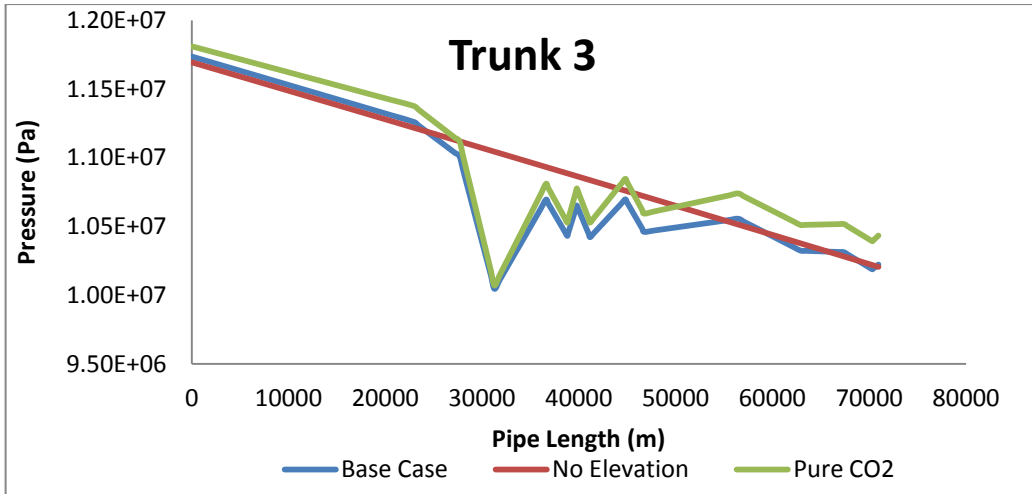
Fig 5.14 Pressure profile
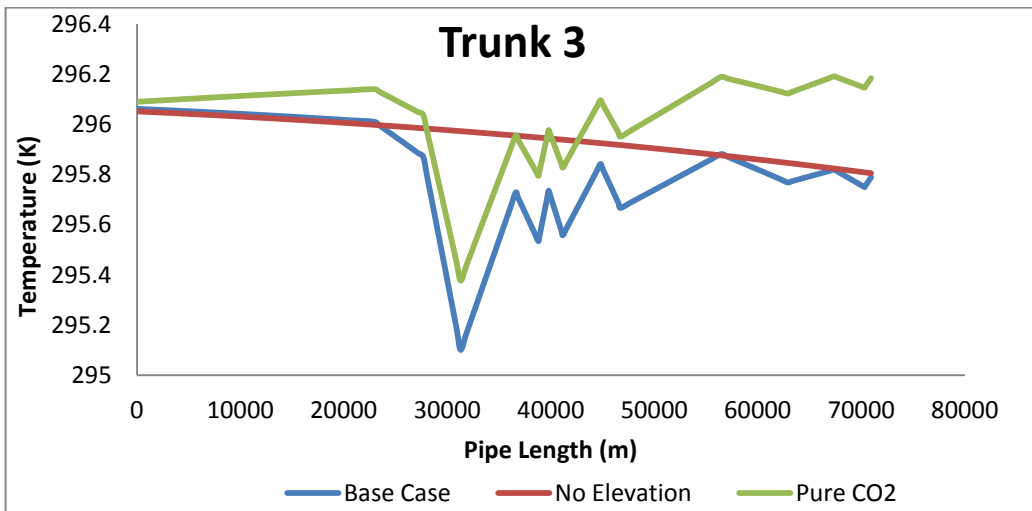
Fig 5.15 Temperature profile
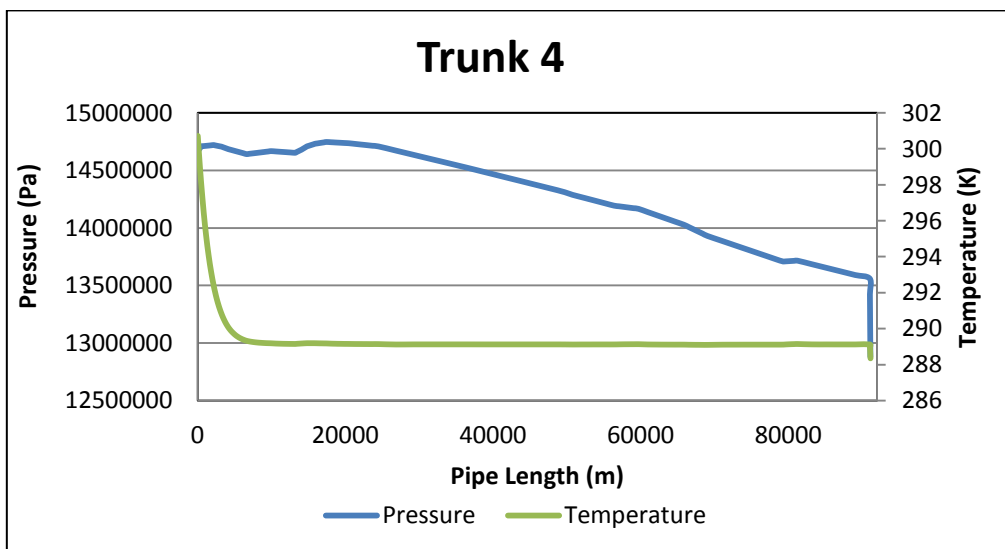
Fig.5.16 Pressure and temperature profile

5.5 Concluding remarks

In this chapter, dynamic modelling of a CO_2 pipeline transport system is presented. Some issues about CO_2 pipeline transport were discussed. The model developed includes dynamic and distributed energy, mass and momentum conservation equations. In addition, pipeline topography and heat transfer with the environment is also taken into account. GERG-2008 wide range equation of state which is rated highly for gas mixture property calculation at high pressures was used for property calculations.

The dynamic model is then used to assess some as aspects of the planned Yorkshire and Humber CO_2 pipeline transport network. Most of the parameters used for the study are initial design data of the Y&H CO_2 pipeline network reported in Luo *et al.* (2014). Assessment of the phase envelope was done alongside impact of common assumptions in literature, namely no elevation changes and impurities. The highlight of this chapter is the presentation of a dynamic model of a CO_2 pipeline system which involves transport of CO_2 mixtures captured from multiple sources with considerations given to pipeline topographical profiles and heat transfer with the environment.

Chapter 6: Dynamic modelling of whole chain CCS network

In this chapter, dynamic model of the whole chain CCS network is presented. Scale-up calculations of the pilot size PCC process presented in Chapter 4 is given in Section 6.1. The structure of the whole chain CCS model is described in Section 6.2. Results and discussion for base case and load change scenario is presented in Section 6.3. The chapter ends with concluding remarks given in Section 6.4.

6.1 PCC scale up calculations

The PCC model presented in Chapter 4 is based on pilot plant size. The first step before integration will then be to scale up the model size to be able to process flue gas flow from the 500 MWe coal-fired subcritical power plant. The amount of flue gas processed by the pilot plant size PCC (0.12 kg/s) is about 5000 times the amount expected to be processed from a 500 MWe coal-fired subcritical power plant (up to 600 kg/s). Considering that PCC process generally involves many interacting variables, accurate scale up of the process is therefore a very complicated exercise.

To avoid the complications, a general procedure for packed column capacity calculation similar to Lawal *et al.* (2012) will be used in this thesis to calculate the packed column sizes (absorber and stripper) required to process the flue gas from 500 MWe coal-fired subcritical power plant. The methodology gives realistic estimate of the PCC capacity and not necessarily the optimal sizes (Lawal et al., 2012). Optimal size of the scaled-up PCC can be obtained through appropriate optimization routines where necessary.

To implement the methodology, the following assumptions were made:

i) Rich and lean solvent loading of 0.48 mol CO_2/mol MEA and 0.28 mol CO_2/mol MEA respectively obtained from the pilot plant is used for the scaled up plant. Therefore, the absorption capacity (*i.e.* difference between rich and lean solvent loading) is 0.2 mol CO_2/mol MEA.

ii) Oxygen is assumed to be inert and other flue gas compositions such SOx and NOx are assumed to have been removed in flue gas treatment units upstream the PCC plant.

iii) Water wash section is excluded.

iv) Controlled water makeup mechanism is used to balance water in the PCC loop.

The steps for the scale up calculations are given in the subsections below:

6.1.1 Estimation of lean solvent flowrate

The solvent flowrate is calculated based on the absorption capacity from the pilot plant (see above), MEA concentration in lean solvent (30.48 wt% MEA) and flue gas flowrate and CO_2 content obtained from simulations of the coal-fired subcritical power plant model at full load (500 MWe). With some allowance maximum flue gas flowrate of 600 kg/s with 20.864 wt%CO_2 was used.

On this basis:

Molar flow of CO_2 entering the absorber $= \frac{600 \times 0.20864}{44} = 2.8451 kmol/s$

Flowrate of lean solvent entering the absorber $= \frac{2.8451 \times 61.08}{0.2 \times 0.3048} \sim 2850\ kg/s$

6.1.2 Estimation of absorber diameter

The absorber column cross-sectional area determines the capacity of the column. It is a critical parameter due to the tight boundaries defined by flooding (upper capacity limit) and minimum liquid load (lower capacity limit) (Lawal *et al.*, 2012) and requirement to ensure good liquid and gas distribution (Sinnot *et al.,* 2005). This must all be considered when estimating the cross-sectional area. The criteria are met by designing the column to operate at the highest economical pressure drop. Sinnot *et al.* (2005) recommended economic pressure drop of 15 to 50 mmH$_2$O per metre of packing for absorbers and strippers.

To estimate the cross-sectional area and consequently the diameter, the generalised pressure drop correlation (GPDC) chart for packing columns (Fig.6.1) is generally used. The pressure drop lines in the chart are in mmH$_2$O per metre of packing. In this thesis, an economic pressure drop of 42 mmH$_2$O per metre of packing is assumed similar to Lawal *et al.* (2012). This is within the recommended interval by Sinnot *et al.* (2005) and it can be read off easily in Fig.6.1.

The term F_{LV} in Fig.6.1 is the flow parameter which represents the ratio of liquid kinetic energy to vapour kinetic energy (Kister *et al.*, 2007). Eq.6.1 is used to calculate F_{LV}.

$$F_{LV} = \frac{L_w^*}{V_w^*} \sqrt{\frac{\rho_V}{\rho_L}} \qquad\qquad (6.1)$$

The $\frac{L_w^*}{V_w^*}$ term is the ratio of liquid to vapour mass flowrate per unit column cross-sectional area. The ratio is similar to L/G ratio (*i.e.* liquid to vapour mass flowrate). The L/G ratio is 4.75 for the absorber in this thesis based on calculations in Section 6.1.1. The liquid and vapour phase densities (*i.e.* ρ_L and ρ_V respectively) were obtained from the pilot scale PCC model simulations in Chapter 4. Based on the information, the absorber F_{LV} is obtained as 0.1658. From Fig.6.1, the capacity parameter (K_4) is approximately 1.2. As a check, the flooding percentage is calculated using Eq.6.2 (Sinnot *et al.*, 2005).

$$\text{Percentage flooding} = \left[\frac{K_4 \text{ at design pressure drop}}{K_4 \text{ at flooding}} \right]^{1/2} \times 100 \qquad (6.2)$$

The K_4 at design pressure drop and at flooding is respectively 1.2 and 2.8 approximately. This gives a percentage flooding of 65.47% which is acceptable (upper limit for flooding percentage is usually about 80% (Sinnot *et al.* (2005)). The cross-sectional area of the column and hence the diameter is then computed in the following steps using the K_4 value.

$$K_4 = \frac{13.1 (V_w^*)^2 F_P \left(\frac{\mu_L}{\rho_L}\right)^{0.1}}{\rho_V (\rho_L - \rho_V)} \qquad\qquad (6.3)$$

Like the densities, the liquid phase viscosity (μ_L) is obtained from the pilot scale PCC model simulations. The packing factor (F_P) depends on selected packing type. 38 mm ceramic Raschig rings used in Lawal *et al.* (2012) are used also in this thesis. Other packing materials such as 38 mm ceramic pall rings (AceChemPack, 2014) among others will also be assessed to determine the impact of different packing materials on the column diameter.

Vapour mass flowrate per unit column cross-sectional area (V_w^*) obtained from Eq.6.3 is 1.158 kg/m^{2}s. The cross-sectional area obtained by dividing the Vapour (flue gas) flowrate with the V_w^* is 518.13 m^2. Diameter obtained from the cross sectional area is 25.68 m. This is about the twice the diameter obtained in Lawal et al. (2012) for the same plant. This was due to an error in the calculation in Lawal *et al.* (2012). In Lawal *et al.* (2012), cross sectional area was expressed as πd^2 instead of $\pi d^2/4$ (d = diameter).
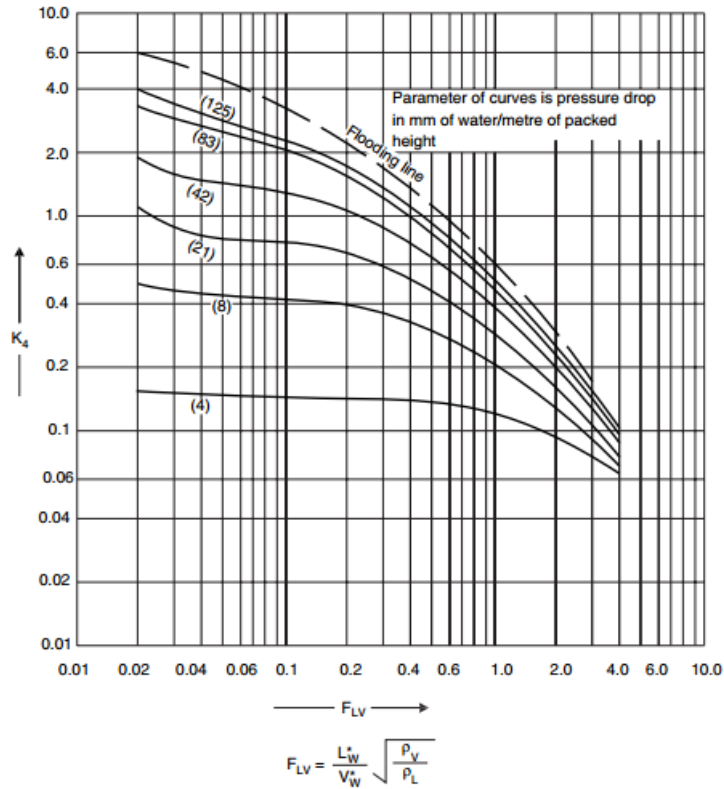
Fig.6.1 Generalised pressure drop correlation (Sinnot *et al*., 2005)

The column diameter was calculated for different packings based on the information above. We found that selected packing type affects column diameter although not very significant for some of them (Fig.6.2). Also, column diameter was computed at different capacity parameters (K_4) (Fig.6.3). The capacity factor depends on the pressure drop assuming the flow parameter (F_{LV}) remain unchanged. On this basis, column diameter can be seen to change in the same way with K_4 and estimated pressure drop. Different K_4 at design condition was obtained from Eq.6.2 by specifying different percentage flooding. K_4 at flooding will be the same since the flow parameter do not change. Fig.6.3 indicates an inverse non-linear relationship between computed column diameter and K_4 (and hence the column pressure drop).
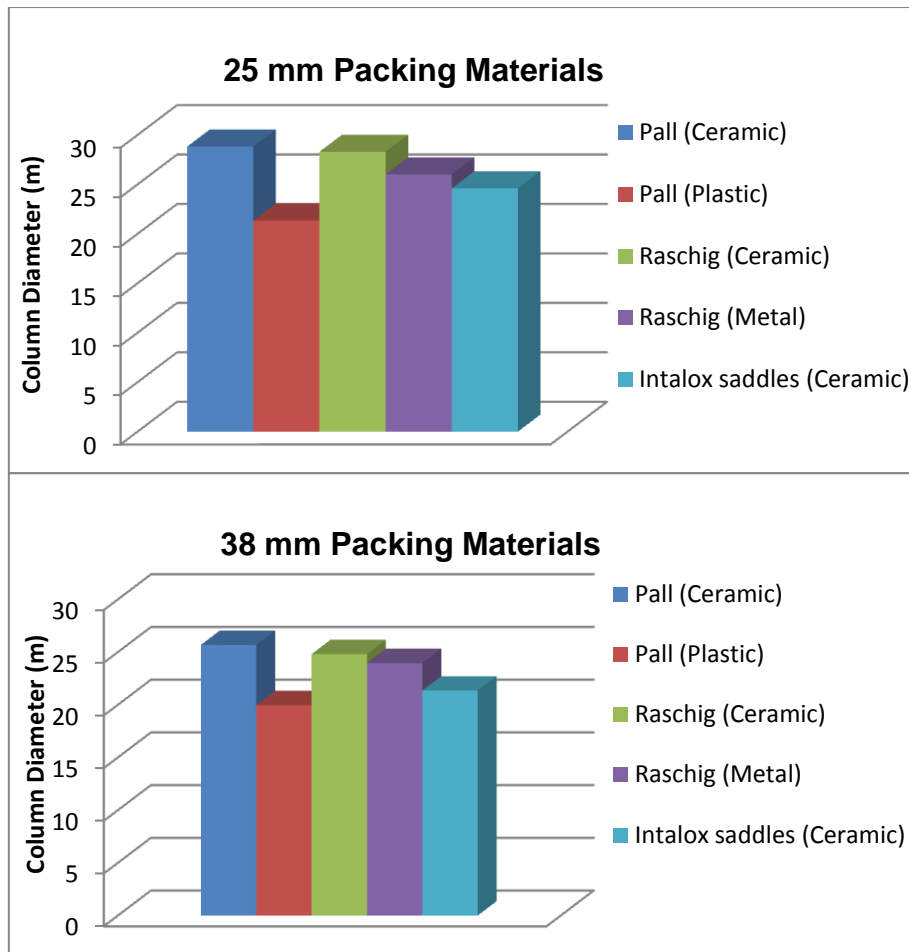
Fig.6.2 Column diameter for different packing materials
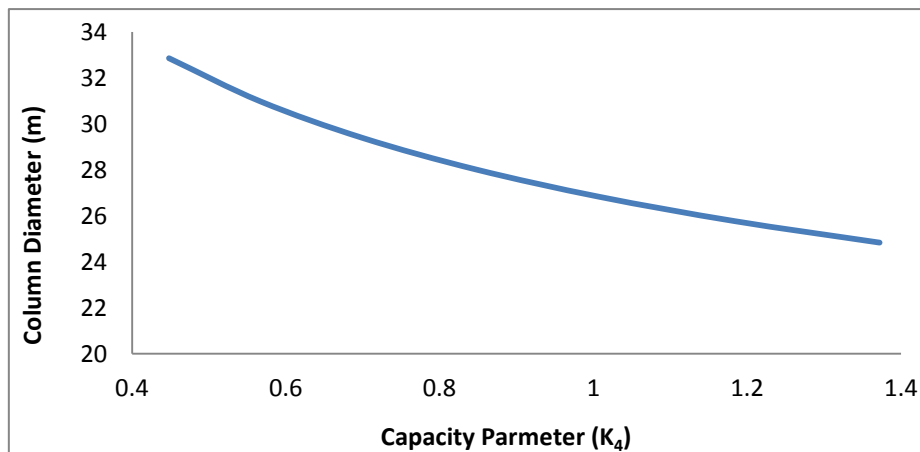
Fig.6.3 Column diameter vs Capacity parameter

Ramezan *et al.* (2007) found that column diameters above 12.2 m (40 ft) is excessive and will suffer more liquid maldistribution leading to lower column efficiency. This may not be the case with better design of column internals in the future. In this thesis, column diameter calculations show huge diameter for the

absorber. Lawal *et al.* (2012) suggested using multiple columns to stay below the 12.2 m diameter limit defined in Ramezan *et al.* (2007). In addition, Lawal *et al.* (2012) argues that using multiple columns increases operational redundancy and turn-down capability of the PCC plant. Going by this, approximately four columns each of about 12.4 m diameter will be needed (Fig.6.4) with 38 mm Raschig ring ceramic packings used in Lawal *et al.* (2012). With other packing materials less number of columns could be required (Fig.6.2). With four columns, the PCC process will remain in operation at very low loads (less than 25%). This will be impossible if a single or two equally-sized columns are used.
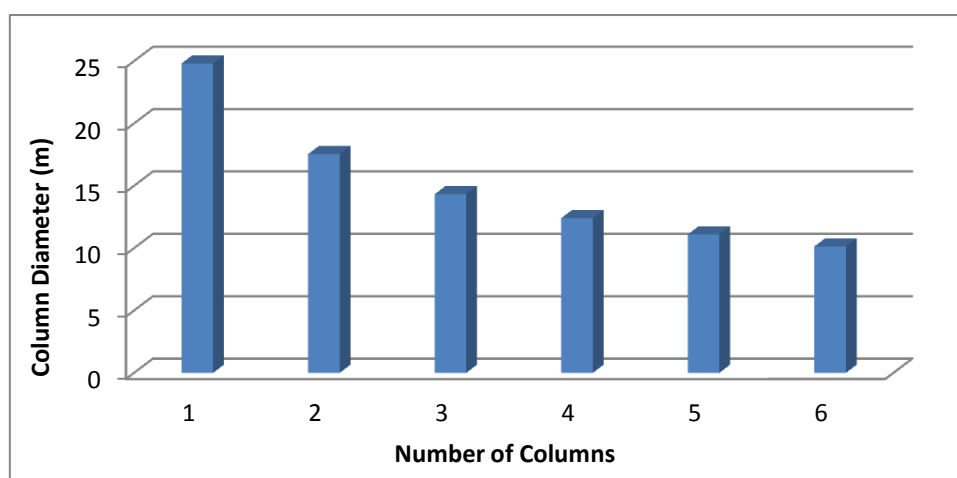
Fig.6.4 Required no of columns and diameters

6.1.3 Estimation of stripper diameter

Using the same procedure as in Section 6.1.2, two stripper columns will be required each of 12.2 m diameter.

6.1.4 Packing height

Rough estimate of the packing height was obtained using a cost-based approach in terms of solvent flowrate and energy used per kg of CO_2 captured. This is the same approach used in Lawal *et al.* (2010) to estimate the packing height. The method involved trialling different packing heights starting with a generic height of 17m reported in Cifre *et al.* (2009). The capture level was maintained at a fixed value for each of the height. As the height increased, solvent flowrate and energy used per kg of CO_2 captured decreased till a certain point where further increments in packing height had little effect on the variables. Using this approach, it is found that a height

of about 27m is ideal for this case (Lawal *et al.*, 2012). Details of this approach can be obtained in Lawal (2010).

6.1.5 Sizing of other unit operations

Apart from the absorber and stripper unit operations, the other key unit operations in the PCC plant (Fig.4.1) include:

- Cross heat exchanger
- Stripper reboiler and condenser
- Lean MEA cooler
- Holding tank for lean MEA
- Pumps

Rough estimates of the sizes of these unit operations were obtained from Lawal (2010).

6.2 Whole chain CCS model

The model is obtained by integrating the 500 MWe coal-fired subcritical power plant in Chapter 3, simplified PCC model scaled up in Section 6.1 and pipeline transport system model in Chapter 5. As noted in Chapter 1, the storage component of the CCS chain is not included in this thesis. In the whole chain model, three links are included between the power plant and the PCC, namely:

- Flue gas stream entering the absorber
- Steam draw-off from the power plant for solvent regeneration in the absorber
- Return of spent steam (condensate) from the PCC back to the power plant.

Details of the integration between the power plant and the PCC plant are already given in Lawal (2010) and not repeated here.

The CO_2 stream leaving the PCC is approximately 95 wt%CO_2 with some H_2O and N_2 impurities. A component splitter is used to isolate the water component since water impurity is unlikely to be allowed in CO_2 pipeline transport system. The resulting stream with 99 wt%CO_2 and N_2 enters the CO_2 pipeline transport system. The pipeline transport system is based on the Yorkshire and Humber case study in Chapter 5. For the purpose of this chapter, it is assumed that the pipeline begins at the multi-junction (Fig.5.3) and going all the way to the offshore platform. Compressor plus pump system is used to raise the pressure to about 120 bar (dense

phase condition) before it enters the onshore pipeline trunk. The pressure is boosted further to 140 bar (dense phase condition) in a pumping station before entering the offshore pipeline trunk. The CO_2 mixture critical pressure is 75.8 bar and the pipelines need to be operated at well above this pressure to ensure dense phase regime throughout the pipeline. Parameters from the Yorkshire and Humber CO_2 pipeline case study in Chapter 5 were used for the pipeline model. These include pipeline elevation, pipe length and diameter and ambient temperatures etc. The compressor and pump energy requirement is assumed to be satisfied from the grid.

6.3 Results and discussions

6.3.1 Base case scenario

The power plant was first simulated at full load to determine base case conditions before the addition of the downstream CCS components. Some important variables under this scenario are shown in Table 6.1. Detailed results from the stand-alone power plant simulations are already given in Chapter 3. Lower flue gas flowrate in the result in Table 6.1 compared to Lawal *et al.* (2012) is because bottom ash formation was included in the mass balance in this thesis. Bottom ash was not included in the mass balance in Lawal *et al.* (2012). The reference coal has about 20 wt% ash (Chapter 3).

<p align="center">Table 6.1 Power plant simulations at full load without CCS</p>

Variables	Value
Net power output (kg/s)	500
Efficiency (%)	37.2
Fuel burn rate (kg/s)	52.2
%wtCO_2 in flue gas	20.86
Flue gas flowrate (kg/s)	541.86

With the addition of the downstream CCS units, there was an accompanying power loss of 26.93% resulting to a reduction of the net power output of the plant to approximately 365 MWe at about 97% capture level. Note that this reduction was due to the stripper reboiler duty only and also at a lower capture level, the energy penalty due to CCS will be less. The energy requirements of the pumps, compressors and other ancillary units in the downstream CCS components are

assumed to come from the grid. When their energy requirements are serviced by the power plant, there will be further reduction in the net power. In literature, it is predicted that power loss due to CCS is within 11-40% or even higher depending on the net efficiency of the power plant (House *et al.*, 2009). Unit #3 of the Boundary Dam Power Station (Canada) which became the only large scale power plant fitted with CCS in the world in Oct., 2014 lost 20% of its power after the addition of CCS (Reuters, 2014). This was only possible after extensive refurbishment of the boilers and steam turbines. The power loss due to CCS can also be reduced through heat integration as discussed in Chapter 5 (Harkin *et al.*, 2009) and intensification of the PCC plant (Wang *et al.*, 2012).

The compressor was an eight-stage compressor with intercoolers. Exit temperature of each intercooler was 38°C except the last stage which was 20°C. At full load, pressure is boosted by approximately 56.83 bar at the entry to the offshore pipeline trunk resulting to a final delivery pressure of 94.6 bar at the offshore platform.

6.3.2 Load change scenario

Ability of downstream CCS units to cope with the inevitable and persistent changes in load in the power plant without an unfavourable influence on the power plants flexible capability is one of the topics that have dominated publications on operability of CCS chain. As a result, in this thesis the impact of load change is studied with the integrated CCS model in this thesis.
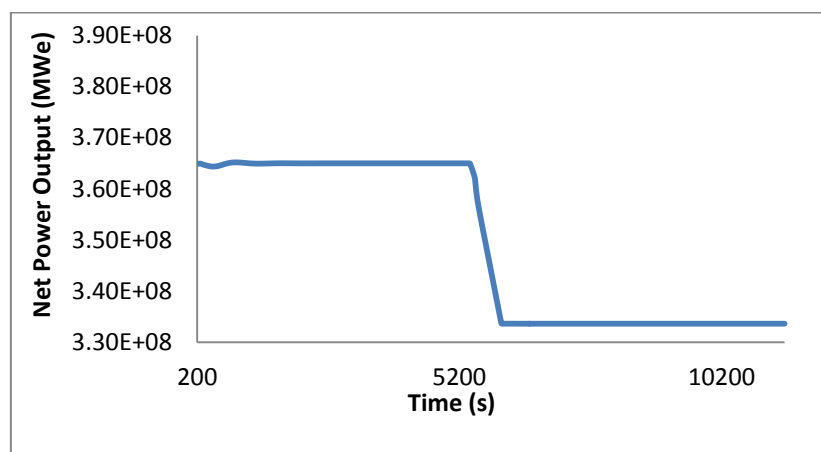
Fig.6.5 Load change scenario

The model is simulated at the maximum load with capture (approximately 365MWe) for about an hour and half before a ramp change was introduced (Fig.6.5). The ramp

was done over a period of 600 seconds (10 mins) before reaching new load level (335MWe) .The behaviour of some variables during the course of these changes were assessed. It must be noted that the power plant controls presented in Chapter 3 was in place during this test. Also, the reboiler temperature was maintained via the reboiler temperature controller. Capture level was not controlled.

The results of the test indicate expected trends (Fig.6.6). First, as the load changed from 365 to 315 MWe, the fuel burn rate decreased correspondingly from 52.2 kg/s to about 49 kg/s as expected with a little fluctuation. The flue gas flowrate changed in like manner. The net efficiency decreased with fluctuations which reflect changes in steam supply to the stripper reboiler. The drum pressure decreased with an initial slight spike. The capture level increased. This is reasonable since the lean solvent loading and flowrate remain the same for the high and lower load. Finally, the CO_2 entering the pipeline transport system decreased by less than 5%. This is the interesting part as it indicates that most of the fluctuations are buffered down in the PCC plant. Experimental investigation conducted by Faber *et al.* (2011) with step changes implemented in a pilot PCC plant showed a similar characteristic. It can be concluded here that small changes in load may not have significant impact on the downstream transport and storage component of the CCS chain.

6.4 Concluding remarks

In this chapter, dynamic model of the CCS chain is presented. The simplified PCC model which was originally based on pilot plant scale was scaled up in capacity to handle flue gas volume from the 500MWe coal-fired subcritical power plant. From the scale-up calculations, it is found that estimated column capacity (*i.e.* cross-section area of column) is affected by selected packing type and maximum allowable pressure drop in the column.

In the whole chain model, load penalty due to the CCS was found to be within common load penalty limits specified in literature. CO_2 from the PCC is initially compressed to 120 bar for onshore pipeline transport (dense phase condition). It is boosted to about 140 bar at the entry to the offshore pipeline and reaches the offshore platform at about 94.6 bar from where it will expectedly be injected underground for storage or EOR. The pipeline model parameters were obtained from the Yorkshire and Humber CO_2 pipeline case study presented in Chapter 5.

Finally, load change scenario was simulated to assess how different variables behave during operation at varying load conditions. It is found that corresponding changes in flowrate of captured CO2 at the entry to the pipeline transport unit is less than 5%. Following this finding, a useful conclusion made is that small changes in load will have minimal impact on the transport and storage units of the CCS chain.
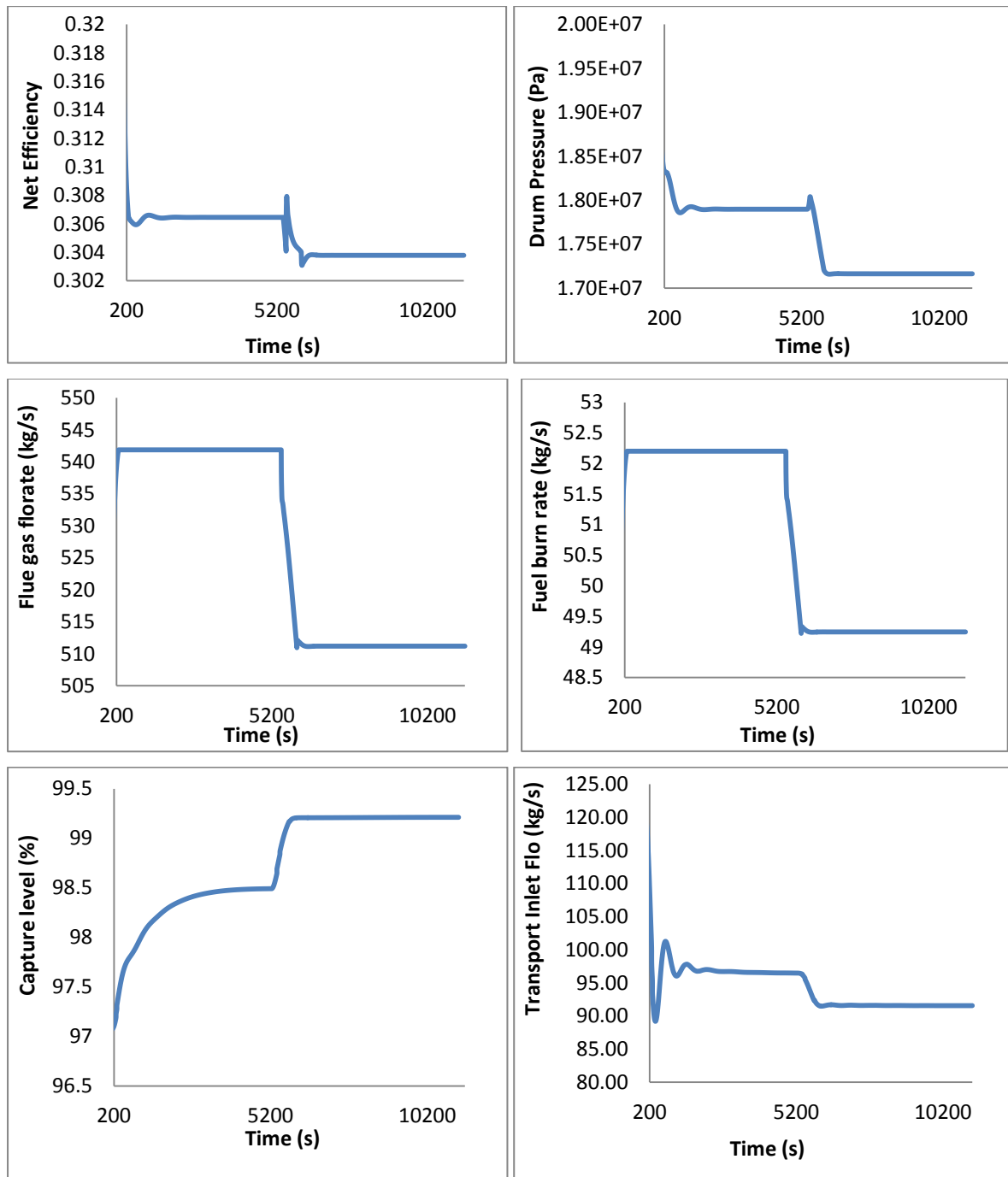
Fig.6.6 Impact of load change scenario

Chapter 7: Neural network approach for predicting drum pressure and level in a coal-fired subcritical power plant

In this chapter, a first order NARX NN model of a drum boiler in a typical coal-fired subcritical power plant capable of predicting the drum-boiler dynamics is presented. The reason for using NARX NN in the model development is given in Section 7.1. General description of NN is summarised in Section 7.2. Data collection procedure is presented in Section 7.3. The NN training is presented in Section 7.4 and results and discussion in 7.5. The chapter ends with concluding remarks given in Section 7.6.

7.1 Introduction

There is increasing need for tighter controls of coal-fired power plants due to more stringent regulations and addition of more renewable sources in the electricity grid. Achieving this requires better process knowledge which can be facilitated through the use of power plant models. Drum-boilers, a key component of coal-fired subcritical power plants, have complicated geometry with complex phase equilibrium and steam bubbles distributed below water level in the drum. Ideally, adequate representation of the dynamic nature of such system will require highly complex routines. Development of such routines is laborious and due to computational requirements they are often unfit for control purposes. Simpler lumped and semi-empirical models have been shown to considerably capture the complex dynamics of drum-boilers [De Mello, 1991; Flynn and Malley, 1999; Åström and Bell, 2000; Oko and Wang, 2014]. However, for control purposes these non-linear models still have to be reduced in model order and then linearized (Chawdhry and Hogg, 1989). The performance of linear models usually deteriorates away from operating point and as a result the model cannot be trusted if big changes in operating conditions are expected.

On the other hand, data-driven (blackbox) approach based on NN incorporates all the complex underlying physics and performs very well so long as it is used within the range of conditions on which it was developed. More importantly, the approach avoids exact determination of model parameters which often vary unpredictably. As a result, this approach is used here to model the drum level and pressure dynamics

in a coal-fired subcritical power plant. First principle model of the drum-boiler is already given in Chapter 3. NN have been used for predicting boiler performance in the past as presented in literature review in Chapter 2.

Most of the studies so far on application of NNs in boiler modelling either as stand-alone or as a component of a thermal power plant have been based on feedforward NNs. In contrast, NARX NN (recurrent NNs) is used in this thesis. Recurrent NNs such as NARX NN have been shown to outperform feedforward NNs in predicting time-series data (Connor *et al.*, 1994) and thus are more suitable for dynamic modelling (Beale *et al.*, 2014). NARX NN modelling have been applied to reactor-exchangers (Chetouani *et al.*, 2007), crude preheater (Ramasamy *et al.*, 2007), hydraulic suspension dampers (Patel and Dunne, 2003), unsteady separation control (Dandois *et al.*, 2013), gas turbines (Asgari *et al.*, 2014; Basso *et al.*, 2005), magnetic levitation (Antić et al., 2013) among others. There is yet to be a case of data-driven drum-boiler models based on NARX NNs as at the time this thesis was prepared. NARX NN is one of the default NN time series tools in MATLAB® which was the platform used for the NARX NN modelling in this thesis. It is easy to use and reportedly gives better results than other NN time series tools in MATLAB® (Beale *et al.*, 2014). This was the basis for using NARX NN in this thesis.

7.2 Neural Networks

Neural Network (NN) is a computational paradigm inspired from the structure of biological neural networks and their way of encoding and solving problems. They are able to identify underlying highly complex relationships based on input-output data only. NN comprises of interconnections of the basic building blocks called neurones (Fig.7.1) organised in layers: the input, hidden and output layers. The inputs to a neurone, $(u_1(t), u_2(t), u_3(t) \dots u_k(t))$, are either the network inputs or outputs of neurones in the previous layer and an externally applied bias (θ).

The bias can either increase or lower the sum of the inputs (φ) depending on its value. Also, the input channels are associated with synaptic weights $(w_1, w_2, w_3 \dots w_k)$ which can have both positive (excitatory) and negative (inhibitory) values. The bias and weights are both adjustable parameters and development (training) of NN is about determining optimal values for the parameters for specific cases. The activation (or transfer) function is typically sigmoid function in the hidden layer and

either linear or sigmoid functions in the output layer. More details on NN can be found in Haykin (1999) among several other books.
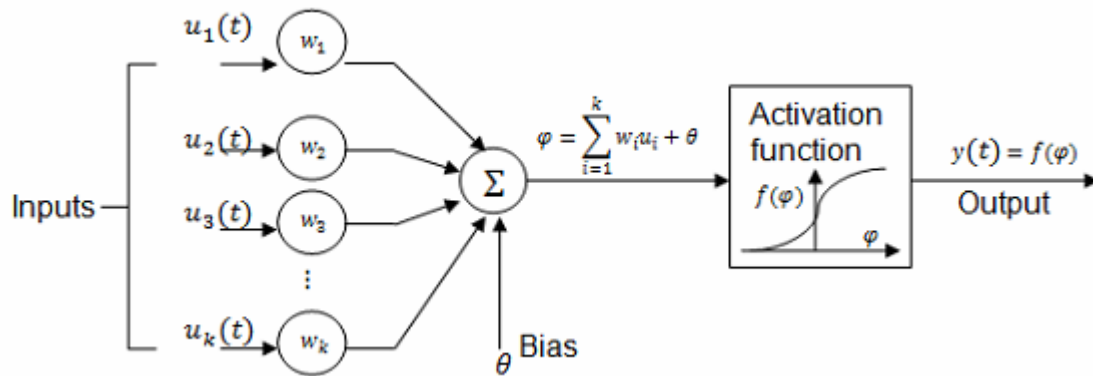
Fig.7.1 Nonlinear model of neurone with sigmoid activation function

Depending on signal flow configuration, NN can be classified into feedforward and recurrent NN. In feedforward NN, the outputs are calculated directly from the inputs through feedforward connections (Beale *et al.*, 2014). Feedforward NN is mostly static networks. Recurrent NN on the other hand are dynamic and have at least one feedback loop. The network outputs are therefore not the result of the external inputs only.

NARX NN belongs to the recurrent NN class. They have a feedback connection enclosing several layers of the network (Fig.7.2). The architecture includes tapped delay lines (TDL) which plays the role of holding past values of the input. This feature makes them more suitable for multi-step-ahead predictions (time-series prediction) than feedforward networks (Beale *et al.*, 2014). It is therefore more appropriate to use them for dynamic modelling. The inputs are normally a sequence of input vectors that occur in a certain time order. A NARX model is generally defined by the equation:

$$y(t) = f\left(y(t-1), y(t-2), \dots, y(t-n_y), u(t-1), u(t-2), \dots, u(t-n_u)\right) \qquad (7.1)$$

In the equation, $y(t)$ is the current value of predicted output signal expressed as a function of the previous values of the output signal $\left(y(t-1), y(t-2), \dots, y(t-n_y)\right)$ and previous values of an independent (exogenous) input signal $\left(u(t-1), u(t-2), \dots, u(t-n_u)\right)$. The terms n_y and n_u are respectively the orders of the output and

exogenous input respectively. The previous values are recorded using TDL and the nonlinear polynomial function (f) approximated using a feedforward NN. Consequently, typical architecture for a first order NARX NN (where n_y and n_u in Eq. 1 are both equal to 1) has the form shown in Fig.7.2.

7.3 Data collection

Collection of data is a crucial step in model development using neural networks. Bear in mind that it is not possible to incorporate a priori knowledge into an NN model, the model is only as good as the data (Beale *et al.*, 2014). Also, NN models do not have the ability to extrapolate accurately beyond the range of the data used in their development, they only generalize well within the data range. As a result, the data must sufficiently cover the input conditions that the NN model is intended to be used.
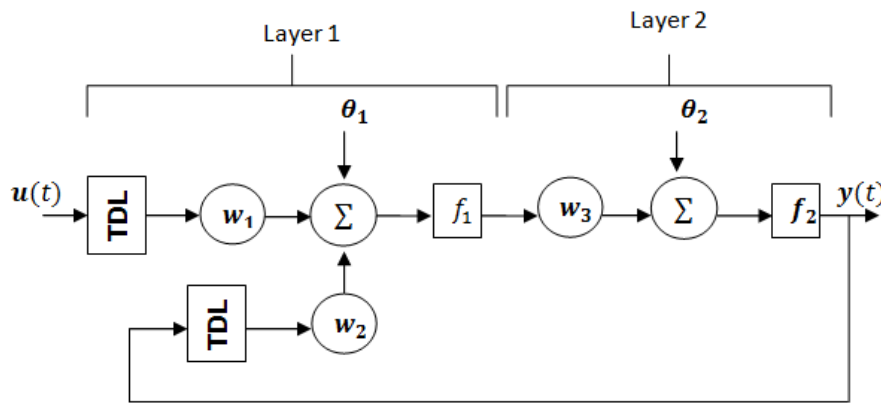
Fig.7.2 Typical NARX neural network architecture

In this study, the data is obtained from simulations of a detailed first principle model of the drum-boiler model same as Åström and Bell (2000). The first principle model is based on a 160 MWe P16-G16 power plant at Öresundsverket in Malmö, Sweden. Complete details of this model can be obtained from Åström and Bell (2000). It is shown in Åström and Bell (2000) that the model captures the drum-boiler dynamics accurately through validations with plant data. In this study, the first principle model was executed using gPROMS ModelBuilder®. Thermodynamic properties of water/steam were obtained using IAPWS-95 formulation in Aspen Properties via COThermo interface. Thermodynamic property derivatives ($\frac{\partial \rho}{\partial P}, \frac{\partial h}{\partial P}$ and $\frac{\partial T_{sat}}{\partial P}$) were

obtained using polynomial approximations of steam table obtained from NIST REFPROP V9.1.

From experience with the first principle model, it is determined that the main inputs to the drum boiler include the heat input, feedwater flowrate and steam flowrate and the outputs are drum level and drum pressure. The heat input is obtained from steady state calculations when the values of the drum pressure, volume of water in the loop and steam flowrate are specified (the values of the drum pressure, volume of water in the loop and steam flowrate used for the steady state calculations were obtained from Åström and Bell (2000). For complete coal-fired subcritical power plant, heat input will be replaced with coal flowrate and steam flowrate could be substituted with governor valve opening. The same input-output set up will be used for the NN model development.

The drum-boiler system is excited by perturbing the inputs in succession with a series of step changes of random heights (Fig.7.3). Perturbation in each input is sustained for an hour resulting to a total test period of 3 hours (10800 seconds). When perturbing one input, the other inputs are maintained at their equilibrium value. Open loop conditions are assumed and control loops were therefore excluded from the model. The data is sampled every second giving a total 10800 data set over the entire test period. The resulting response of the output variables (drum pressure and drum level) during the course of the perturbation is shown in Fig.7-4.

7.4 Training

NN training is the process of obtaining optimal values for the adjustable parameters, weights and biases, necessary to achieve the best fit between input-output data. It is essentially a nonlinear optimization problem and the objective function involves minimization of an error function, typically mean absolute error (MAE), mean squared error (MSE), or sum of squared error (SSE) among others. The training task is accomplished using different optimization algorithm such as gradient descent, Levenberg-Marquardt, Bayesian regularization, scaled conjugate gradient among others. These algorithms are usually executed by performing the calculations backward through the network starting from the output layer. In MATLAB Neural Network Toolbox, the various optimization algorithms are implemented as training

functions, namely *trainlm* function (Levenberg-Marquardt), *trainbr* function (Bayesian regularization), *trainscg* function (scaled conjugate gradient) etc.
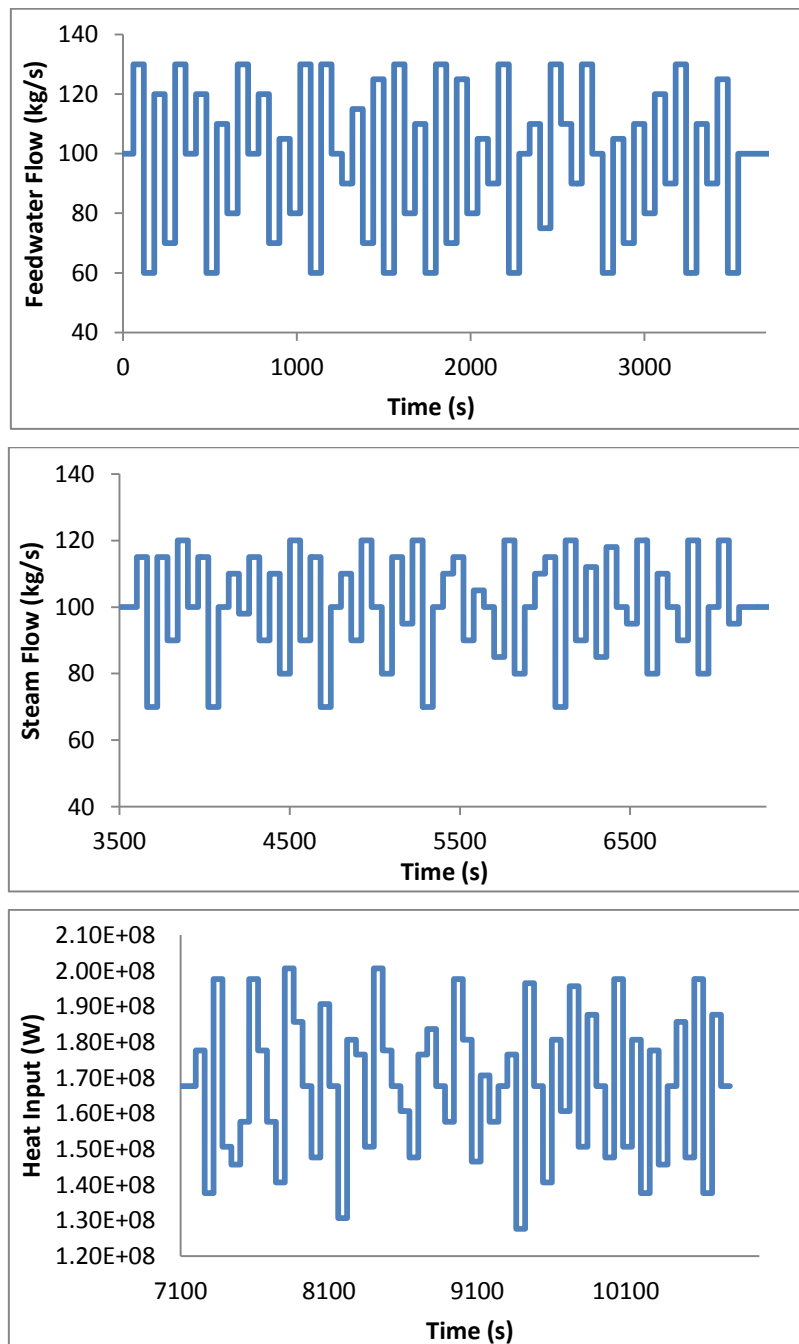
Fig.7.3 Perturbations in model inputs

For dynamic NN with a feedback loop such as NARX NN, training is complicated because some of the inputs (feedback) are also functions of the weights (Fig.7.2). To avoid this complication, NARX NN is trained in open loop (without the feedback loop). This is based on series-parallel architecture where the actual output, rather

than the estimated output fed back to the network, is used as the input. On this basis, the NARX NN is then a purely feedforward network and can be trained as such. Details of this procedure can be found in Beale *et al.* (2014). After training, the *closeloop* function in MATLAB can be used to convert the NN from the series-parallel configuration (open loop) to close loop configuration for multi-step ahead predictions.
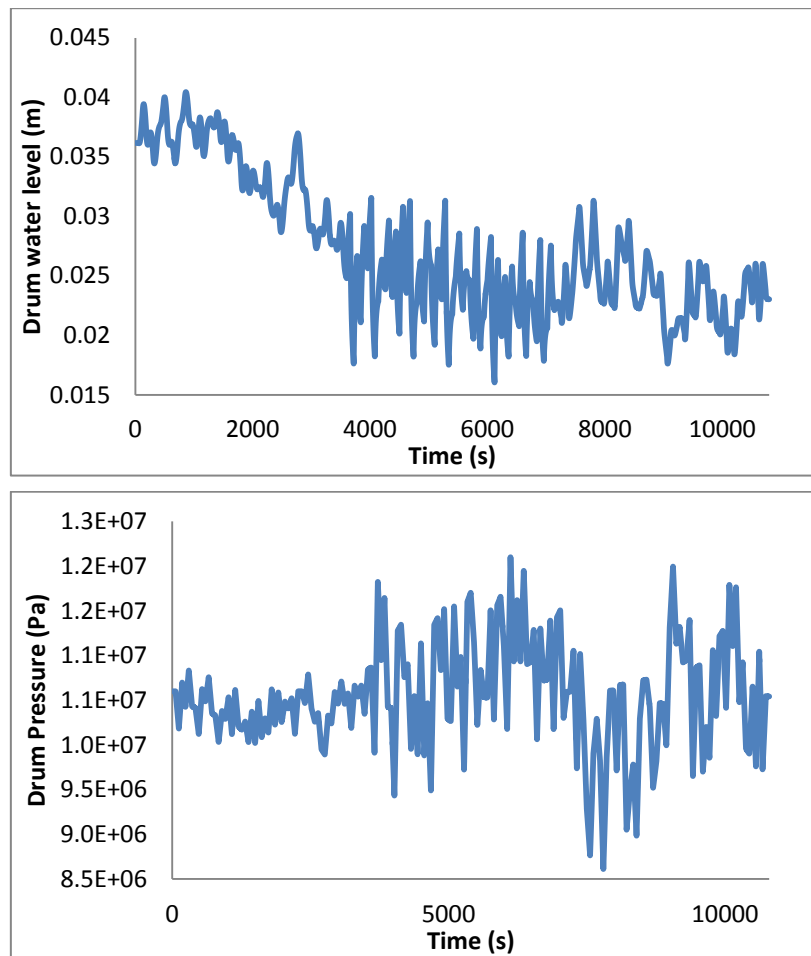
Fig.7.4 Model outputs

Prior to training, the available data (input and target vectors) is pre-processed to transform the data to more suitable form for NN training. This makes the training (or learning) process faster and efficient without the possibility of saturation of the sigmoid transfer function often used in the hidden layers (Beale *et al.*, 2014). Some training algorithm also requires particular pre-processing for optimal performance, e.g. data transformation to a form where their values fall into the interval [−1, 1] for *trainbr* algorithm. When the network is created, the pre-processing function becomes part of the network object, so that whenever the network is used, the data coming

into the network is pre-processed in a similar way. The NN output is similarly post-processed to transform the output to the same form as the actual output. In this study, the *mapminmax* and *removeconstantrows* processing functions in MATLAB have been used. The *mapminmax* function transforms the data so that their values fall into the interval [−1, 1]. On the other hand, *removeconstantrows* functions removes the rows of the data vector that are constant (if any) since they will not provide useful information to the NN. Also, pre-processing for dynamic networks include shifting the data to initialize the TDL. In MATLAB, this is accomplished using *preparets* function. The function uses the network object to initialize the TDL by shifting the data accordingly to create the correct inputs and targets to use in training or simulating the network.

Commonly, overfitting occurs during NN training. This is a situation where the NN memorises the training examples including noise such that it is not able to generalize to new conditions. This can be avoided using either early stopping or regularization techniques. Early stopping technique was used in this thesis following an initial assessment of the two techniques which indicated that regularization technique gave poorer result for the case treated here. In early stopping method the available data is divided into three subsets, namely training, validation and testing sets and training, validation and testing is carried out simultaneously. The error measured for the three data subsets *i.e.* training, validation and testing, will normally be decreasing through different cycles of iterations (Epochs) during the initial phase of the training. Overfitting begins to set in when the validation error begins to increase. The optimal network weights and biases are obtained at the minimum validation set error before overfitting begins to set in.

7.5 Results and discussion

7.5.1 Training results

Based on the discussions above, a two-layer first order NARX NN dynamic model of the drum-boiler with three inputs (*i.e.* feedwater flowrate, steam flowrate and heat input) and two outputs (*i.e.* drum level and drum pressure) was developed in MATLAB using the simulated data (Fig.7.3 and 7.4). There are 100 neurons in the hidden layer each utilizing sigmoid activation function while each of the two outer layer neurones utilize linear activation function. The Levenberg-Marquardt algorithm

(*trainlm* training function in MATLAB) was used to obtain the optimal values of the adjustable parameters, weights and biases. The MSE performance function (Eq.7.2) was used to assess the network performance. In Eq.7.2, z_i = the targets, y_i = network outputs and N = data size.

$$\text{MSE} = \frac{1}{N} \sum_{i=1}^{N} (z_i - y_i)^2 \rightarrow min \tag{7.2}$$

As explained earlier, the early stopping technique used in this thesis involves simultaneous training, validation and testing. The training data comprised of 70% of the entire data while the validation and testing data were 15% each respectively of the entire data. The entire data was for 3 hours period (10800 seconds) and division of the entire data set into the subsets (training, validation and testing sets) was done randomly (*dividerand* function in MATLAB was used for the purpose). Training was stopped at the lowest MSE for the validation set before the MSE started to increase (Fig.7.5). Increase in MSE for the validation set after it reached the minimum value is an indication of onset of overfitting. Network training should be stopped before onset of overfitting. This is the basis of the early stopping technique for network training. Also, there are no significant autocorrelations in the error distribution as can be seen in the error autocorrelation plot for the drum pressure and drum level predictions (Fig.7.6). This suggests reliable estimate of the network parameters, weights and biases.

Fig.7.7 and 7.8 show the response of the network outputs, drum level and drum pressure, as the training progressed. Only the training set is involved in network training, the validation and testing set are not involved in training. The validation set gives an idea of when to stop training while the test set helps to show network performance on a 'foreign' data. The network predicted the drum level and drum pressure correctly based on the test data comparisons with the network data in Fig.7.7 and 7.8.
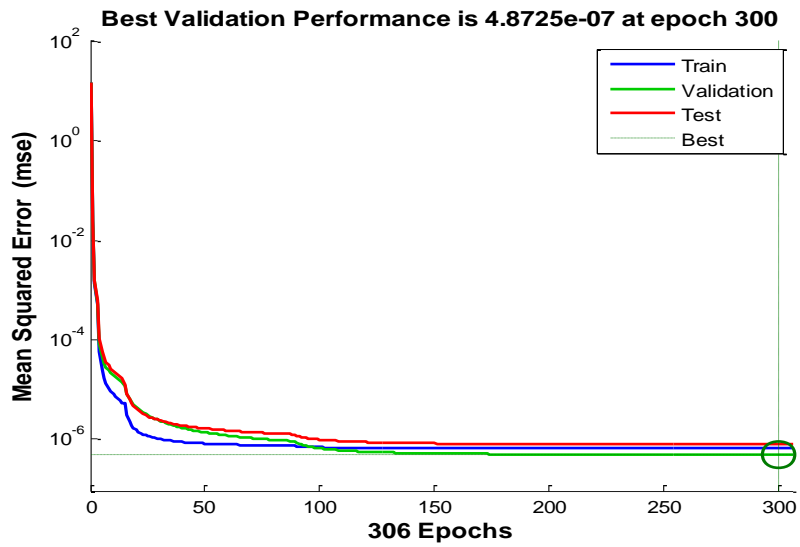
Fig. 7.5 MSE for different training epochs
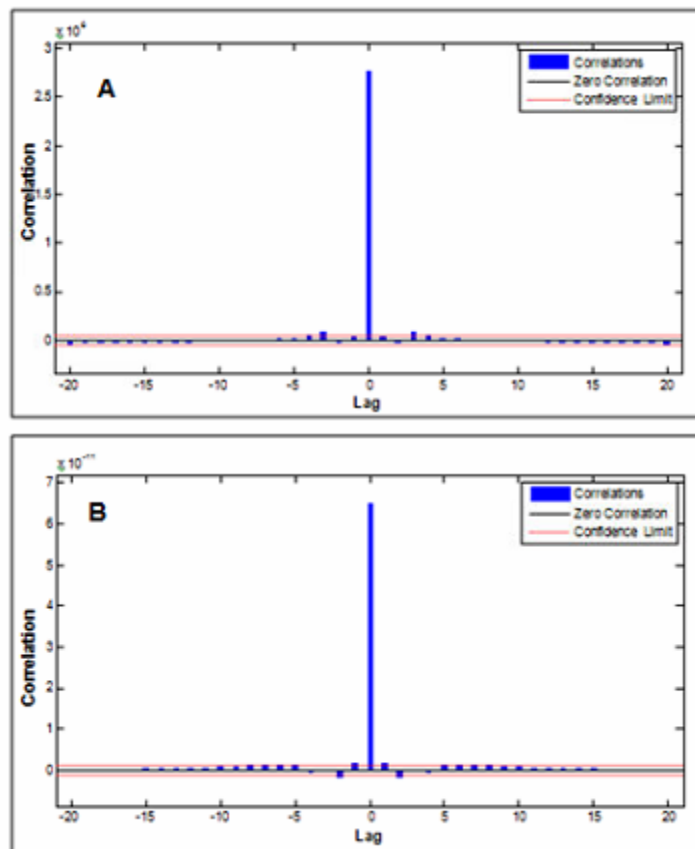
Fig. 7.6 Autocorrelation plot for drum pressure (A) and level (B) prediction error
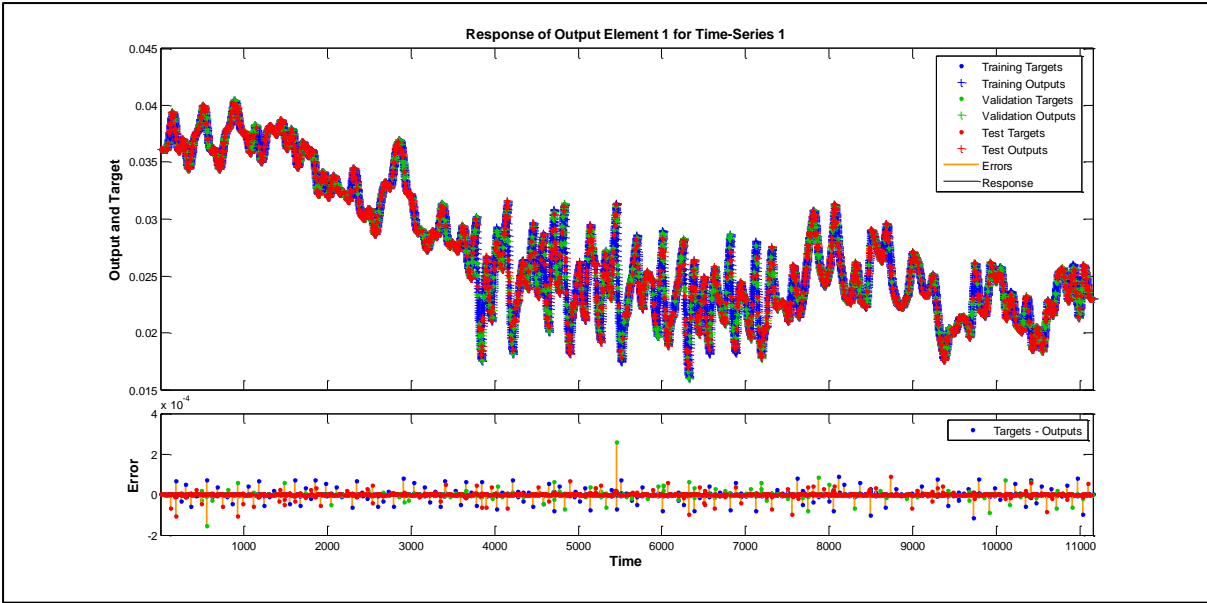
Fig. 7.7 Drum level response
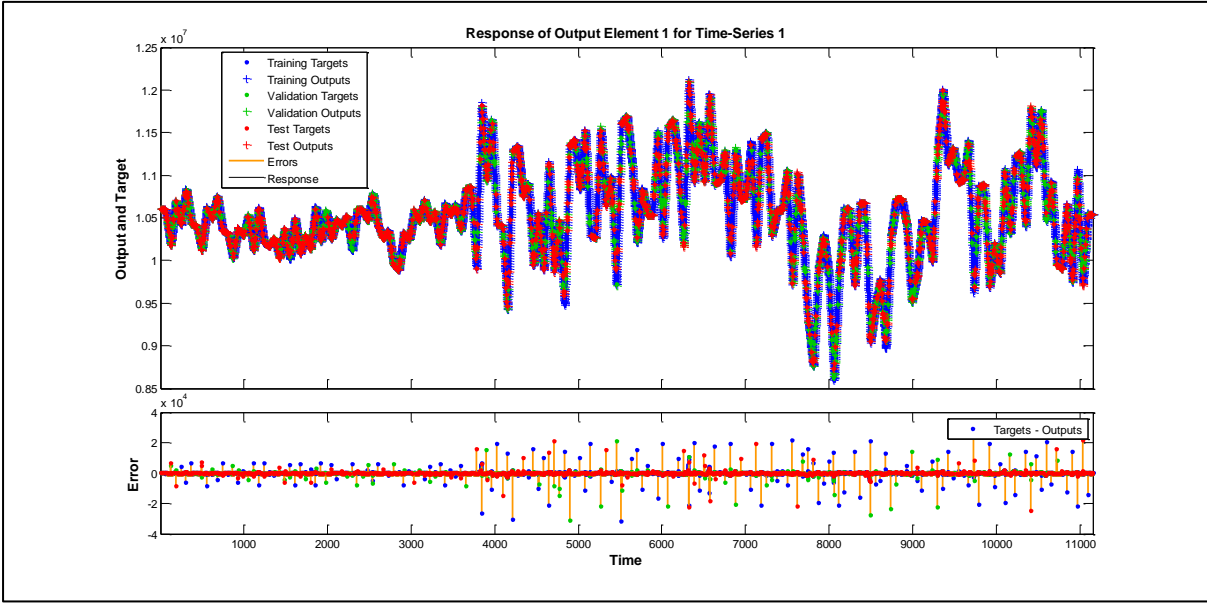
Fig. 7.8 Drum pressure response

7.5.2 Step change test

In this section, step change test on each of the inputs is carried out. The drum pressure and level predictions of the detailed first principle model Åström and Bell (2000) and the NARX NN model are compared. The purpose of the tests is to determine if the NARX NN developed in this study is able to accurately predict the drum pressure and level when changes arise in any of the inputs. Changes in these inputs are expected during operation and the model can only be adjudged

116

satisfactory when it is able to predict the drum level and pressure under these conditions.

During the first test, the feedwater flowrate was maintained at 100 kg/s for 100 seconds before 30 kg/s step. The steam flowrate and the heat input were respectively maintained at 100 kg/s and 167 MWth throughout the test. The drum pressure and level response during this test is shown in Fig.7.9. In the second test, steam flowrate was stepped up by 10 kg/s from 100 kg/s after 100 seconds of steady simulation. The feedwater flowrate and the heat input were respectively maintained at 100 kg/s and 167 MWth throughout the test. The drum pressure and level response during this test is shown in Fig. 7.10. Finally, 10 MWth step change was implemented on the heat input from 167 MWth initial value. The feedwater and steam flowrate was maintained at 100 kg/s. The result of the tests is shown in Fig.7.11. From the test results, it can be seen that the NARX NN model developed in this study predicted the drum pressure and level of the drum-boiler reasonably in the presence of sudden changes in the inputs.
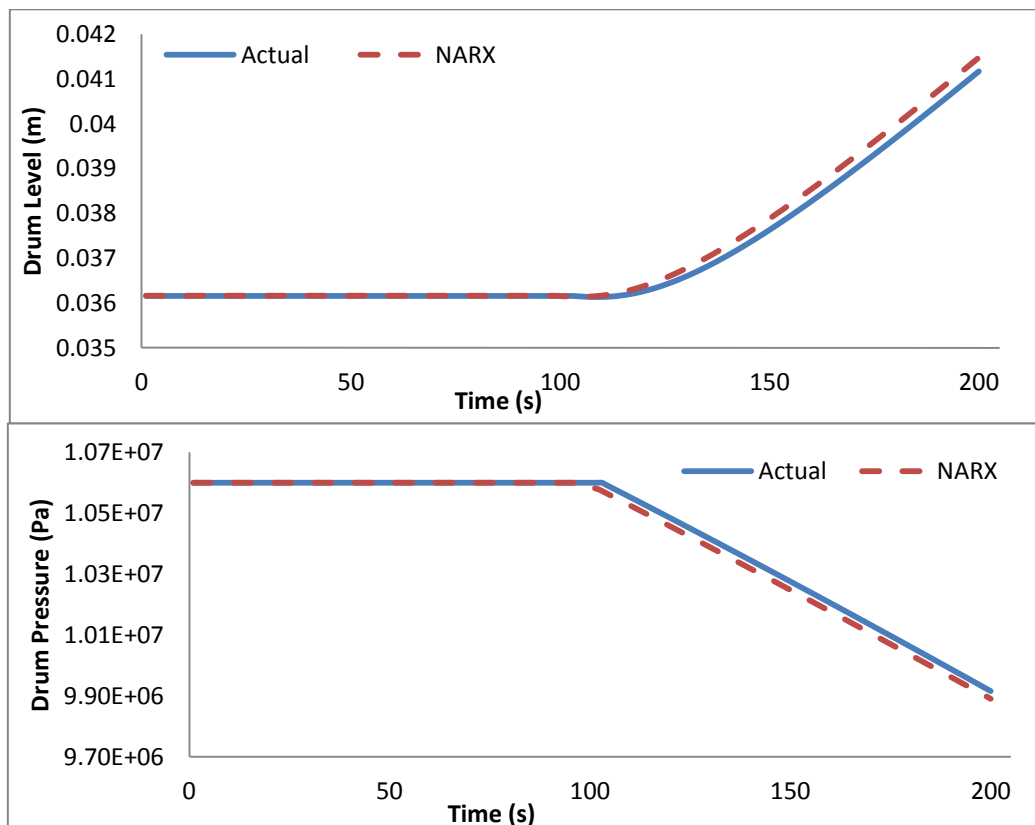
Fig. 7.9 Response to +30 kg/s step change in feedwater flowrate
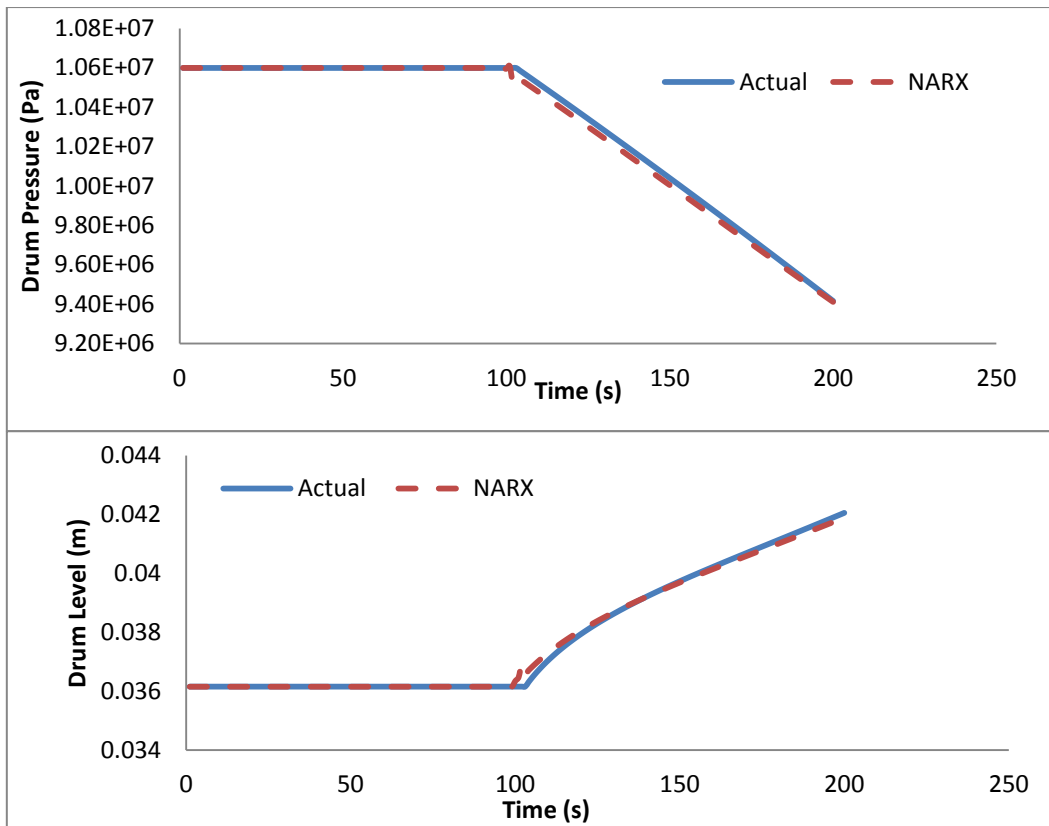
Fig. 7.10 Response to +10 kg/s step change in steam flowrate
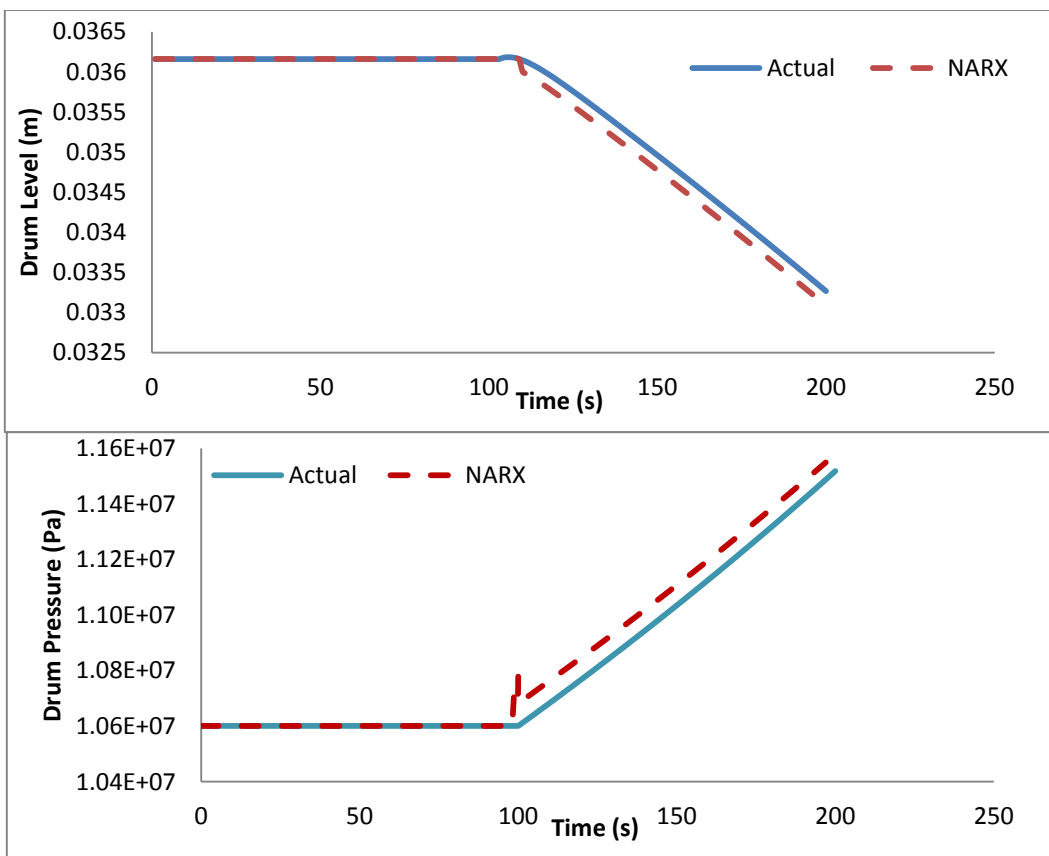
Fig.7.11 Response to +10 MW step change in heat input

118

7.6 Concluding remark

In this chapter, a NARX NN model of a drum boiler is presented. NARX NN is able to capture complex underlying physics which will be difficult to describe in first principle models. The model is simple and easy to develop and can be used for simulated study of the plant and design of controllers. Like other recurrent NN, NARX NN is more suited for dynamic modelling than static feedforward NN commonly used in literature for drum boilers.

The data used to develop the model was obtained through simulation of a reasonably detailed first principle model of a reference drum boiler in a 160 MWe power plant in Sweden (Åström and Bell, 2000). The first principle model of the drum boiler was first developed in gPROMS ModelBuilder®. The test period for data collection was 3 hours and the data was sampled every second giving a total 10800 data.

The results demonstrated reasonable prediction of the drum level and pressure. The highlight of this chapter includes application of the NARX NN for predicting drum-boiler dynamics. In developing the NARX NN model, the ease of development is demonstrated and the model is relatively fast. Complexity of development and simulation speed is common issues with first principle models.

One key issue with blackbox models however is availability of sufficient and good data. In this thesis, we have relied on simulated data and it must be noted that reported results are subject to whatever inherent deficiency that exists in the first principle model used to generate the data. It is recommended that actual plant DATA where available be used for the development of similar model in the future.

Chapter 8: Conclusions and recommendations for future study

8.1 Conclusions

A model-based demonstration of a CCS network comprised of a PCC plant integrated with an upstream 500 MWe coal-fired subcritical power plant (CO_2 emitter) and downstream CO_2 compression and pipeline transport systems has been presented in this thesis. Literature study carried out in Chapter 2 of this thesis indicates that that there has been a lot of study on individual components of the CCS chain. The studies cannot be used for understanding the impacts of integrating the components and operating them as a single unit. Such knowledge will be useful for designing and operating the CCS network. With an integrated model of the CCS network, the impacts of integrating the components and operating them as a single unit can be investigated and understood. To achieve this aim, in addition to extensive literature survey, a dynamic model of a 500 MWe coal-fired subcritical power plant and CO_2 pipeline transport system were developed in this PhD research.

8.1.1 Dynamic modelling of coal-fired subcritical power plant

In Chapter 3, the development of dynamic model of a coal-fired subcritical power plant is presented. The power plant model captures key dynamics of the boiler, namely drum level and pressure, and also included the condensers and feedwater heaters. These features are often not included or very simplified in existing power plant models. Steady state validation of the power plant model was given. From the results, the power plant model predicted the plant conditions with less than 5% relative error between 70-100% load levels. The impact of implementing load changes via step and ramp changes was investigated. From the study, it is seen that ramp changes unsettle the plant to a lesser extent than step changes. This finding corroborates common industrial practice of carrying out load changes through ramping.

8.1.2 PCC model

Rate-based dynamic PCC model developed in Lawal *et al.* (2010) was used as a starting point in this thesis. The rate-based dynamic model is however very complex and computationally intensive. In Chapter 4, the PCC model is simplified through an approach that involved reduction of certain aspects of the model. Sensitivity analysis was used to determine which variable calculations to simplify. Also, correlations were developed and used in the simplified PCC model to reduce the number of external property calls. The simplified model was validated against the predictions from the detailed model. The results showed up to 60% reduction in CPU time and reasonable agreement with the detailed model predictions. The results show that the complexity of the PCC model is mostly due to many non-linear algebraic equations and external property calls.

8.1.3 Model of the CO_2 pipeline transport system

In Chapter 5, the dynamic model developed for CO_2 pipeline transport system includes compressors, pipeline segments, valves and pumps. The compressor and pump models were steady state models. This is justified on the basis that these components have very rapid dynamics compared to other components. Also, the compressors included intercoolers which were understood from literature to reduce compressor energy requirement. The model-based assessment confirmed this finding. The pipeline model comprises of dynamic and distributed conservation equations. Also, GERG-2008 wide ranging EOS was used for estimating thermodynamics and transport properties. GERG-2008 is the international reference EOS for natural gas and has been proven for different gas mixtures from low to high pressure conditions. There is yet to be an agreement on the ideal EOS for CO_2 mixture property estimation. However, GERG-2008 EOS is commonly used.

The model of the CO_2 pipeline transport system was used to study the planned Yorkshire and Humber (Y&H) CO_2 pipeline network in UK. The Y&H CO_2 pipeline is intended to transport CO_2 captured from different sites, *i.e.* Don Valley power plant in South Yorkshire UK and Drax power plant in North Yorkshire UK, to the storage site (saline aquifer) beneath the North Sea off the coast of Bridlington in UK. The highlights of the study carried out with the model are as follows:

- Transport of CO_2 from different sources captured using different technologies *i.e.* pre-combustion for Don Valley capture site and oxy-fuel CCS for Drax

(White Rose) capture site. This therefore gives a picture of CCS cluster systems where CO_2 from different sources are expected to be transported through common pipeline trunk. The study highlighted the impact of impurities and changes in conditions in each of the capture sites on the behaviour of the pipeline system.

- Incorporation of pipeline topographical profile and heat transfer with the environment.

- Off design suction temperature scenario for the compressors.

From the results, we find that the critical pressure of the mixture is about 82 bar as against about 74 bar for pure CO_2. This indicates that the pipeline minimum operating pressure should be greater than 82 bar if the CO_2 mixture is to remain at dense phase regime. Literature studies show that inter-cooling to low temperature (e.g. below 20^oC) reduces compressor energy requirement. However, our findings show that this may be at the risk of reaching the two-phase boundary which result to two-phase flow condition. This condition brings a lot of operating difficulty and is usually avoided. Also, changes in suction temperature are shown to affect the compressor power consumption and final discharge pressure. As a result, upstream cooling system should be controlled to ensure that the temperature at the compressor inlet is within design conditions. Significant amount of heat energy is also seen to be rejected at the intercoolers. Previous studies have suggested that this energy can be recovered through effective heat integration with upstream capture and power plant to reduce the energy penalty due to CCS. While this looks attractive, it must be taken into account that integration will sacrifice some of the plant flexibility and complicate design of the process controllers.

8.1.4 Integrated CCS chain

Integration of the various component models, namely power plant, PCC plant and CO_2 pipeline transport system, to mimic a CCS chain is presented in Chapter 6. The simplified PCC model presented in Chapter 4 was developed based on pilot plant size PCC. As a result, the first task in Chapter 6 was to scale up the PCC model to a capacity that can handle the huge flue gas volumes from the 500 MWe coal-fired subcritical power plant. Scale-up calculations were based on conventional method for packed tower design (Lawal *et al*., 2012). Estimated diameter of the absorber

was about double the size presented in Lawal *et al.* (2012). It is also found that calculated diameter of column is influenced by selected packing material and design pressure drop for the column. From the integrated model, it is found that small changes in load have little impact on the transport and storage components of the CCS chain. This is because the corresponding change in the flowrate entering the pipeline transport unit is very small. In this thesis, the flowrate changed by less than 5% (about 2 kg/s) when about 10% change in load was implemented. This change was also observed to have happened less rapidly indicating that the PCC tended to have buffered down the change in load which happened more rapidly.

8.1.5 Neural network model of the drum-boiler

In addition to the CCS chain, NN model of the drum boiler in a coal-fired subcritical power plant is presented in Chapter 7 of this thesis. The study has been performed as part of an initial study to assess the suitability of NARX NN for modelling the dynamics of a coal-fired subcritical power plant. Literature study showed that NARX NN were yet to be applied to modelling coal-fired subcritical power plant. In this initial study, a first order NARX neural network was used successfully to predict drum level and pressure. The data used for developing the NARX neural network model was obtained from simulation of a detailed first principle model of the drum-boiler similar to Åström and Bell (2000). Comparisons with the first principle model under scenarios of rapid changes in the inputs show that the NARX neural network model has reasonable performance. The model is easier to develop than first principle model. However, the main constraint for developing this type of model is availability of sufficient and good plant operating data.

8.2 Recommendations for future study

The dynamic model of the coal-fired subcritical power plant presented in this thesis was only validated at steady state conditions. Dynamic validations of the model were not carried out due to lack of appropriate plant data in literature. Dynamic validations are important for determining if the model captures actual behaviour of the plant during operation. As a result, it is recommended that detailed dynamic validation of the power plant model should be carried out in the future when appropriate data become available.

The simplified PCC model used in the model of the CCS chain in this thesis was obtained from the detailed rate-based PCC model in Lawal *et al.* (2010). In the rate-based model, CO_2 reaction kinetics was approximated by the assumption that the reactions reach equilibrium. This is not necessarily the case in reality. According to information in literature, actual kinetic model of the CO_2 reactions will give better results. It is therefore recommended that more accurate rate-based dynamic PCC model with actual kinetic model for CO_2 reactions should be derived in the future.

In developing the compressor models, the generic polytropic efficiency value obtained from literature was used alongside arbitrary rated pressure ratio and suction temperature. This is inevitable at the moment since information on CO_2 mixture compressors is hardly available in open literature. The compressor predictions can be improved by using more specific information of the compressor. As a result, it is recommended that actual compressor curve for CO_2 mixtures at high pressure should be used for modelling the compressor as more information becomes available. Also, optimal number of stages and pressure ratio can be obtained through MILP optimization.

Steady state heat exchange with the environment was adopted in the pipeline transport model in this thesis. As a result, temperature transients are not properly captured. Due to health and safety concerns with CO_2 pipeline transport, every detail ought to be studied and understood. Unsteady state heat transfer should therefore be incorporated into the model in the future to get very accurate representation of temperature transients.

In this thesis, control of the system has not been considered in detail. The study by Lawal *et al.* (2012) already indicate that the PCC system is slow and this mean more challenging controller design considering the rapid response capability of the upstream power plant. On the other hand, as we found in this thesis, it is good news for the downstream compression and transport system since the PCC plant will then be buffering fluctuations coming from the power plant. To reduce the expected impact of the sluggishness of the PCC on the power plant's ability to be operated in the load-following mode, it is recommended that the PCC control system be linked to the power plant control system.

Finally, the possibility of using NARX NN for modelling drum-boiler dynamics was demonstrated using simulated data. The model should be retrained and validated with plant data to establish its reliability of this model.

References

2COEnergy, 2014. Don Valley CCS Project, South Yorkshire, UK. Available at: http://www.2coenergy.com/don_valley_power_project.html [Accessed Feb., 2014]

Aboudheir, A., Tontiwachwuthikul, P., Chakma, A. and Idem, R. Kinetics of the reactive absorption of carbon dioxide in high CO_2-loaded, concentrated aqueous monoethanolamine solutions. *Chemical Engineering Science*, Vol. 58 (2003) 5195 – 5210

Abu-Zahra, M. R. M., Schneiders, L. H. J., Niederer, J. P. M., Feron, P. H. M. and Versteeg, G. F. 2007. CO_2 capture from power plants Part I. A parametric study of the technical performance based on monoethanolamine. *International Journal of Greenhouse Gas Control*, Vol. 1, 37–46

AceChemPack, 2014. Ceramic pall rings Available at: http://www.tower-packing.com/ceramic/ceramic_pall_ring_random_packing.htm [Accessed Dec, 2014]

Adam, E.J., and Marchetti, J.L. Dynamic simulation of large boilers with natural recirculation. *Computer and Chemical Engineering*, 23 ((1999), 1031-1040.

Alie, C., Douglas, P. and Croiset, E., 2006. Simulation and optimization of a coal-fired power plant with integrated CO_2 capture using MEA scrubbing. In: *8th International Conference on Greenhouse Gas Control Technologies.* Trondheim, *19-*22 June 2006, IEAGHG.

Antić, D., Milovanović, M., Nikolić, S., Milojković, M. and Perić, S. Simulation model of magnetic levitation based on NARX neural networks. I.J. Intelligent Systems and Applications 2013; 05: 25-32.

Aroonwilas, A. and Veawab, A., 2007. Integration of CO_2 capture unit using single- and blended-amines into supercritical coal-fired power plants: Implications for emission and energy management. *International Journal of Greenhouse Gas Control,* 1(2), pp. 143-150.

Åström, K. J. and Bell, R. D. 2000. Drum-boiler dynamics, *Automatica,* Vol. 36(3), 363-378.

Åström, K.J. and Eklund, K., 1972. A simplified non-linear model of a drum boiler-turbine unit. *International Journal of Control,* 16, 145-169.

Asgari, H., Chen, X., Sainudiin, R., Morini, M., Pinelli, M., Spina, P.R. and Venturini, M. Modelling and simulation of the start-up operation of a heavy-duty gas turbine by using NARX models. ASME Turbo Expo, Düsseldorf, June 16- 20, 2014.

Aursand, P., Hammer, M., Munkejord, Wilhelmsen, Ø, 2013. Pipeline transport of CO_2 mixtures: Models for transient simulation. *International Journal of Greenhouse Gas Control*, Vol. 15, 174-185.

Basso, M., Giarré, L., Groppi, S. and G. Zappa. NARX models of an industrial power plant gas turbine. *IEEE transactions on control systems technology*, Vol. 13, No. 4 (2005), 599-601.

Bai, Y. and Bai, Q. 2005. Subsea pipelines and risers. Elsevier, Britain. ISBN: 0-080-4456-67.

Bar-Meir, Genick, "Basics of Fluid Mechanics", Last modified: Version 0.3.4.0 March 17, 2013, Available at: www.potto.org/downloads.php [Accessed Nov., 2014]

Beale, M. H., Hagan, M. T., and Demuth, H. B. Neural network toolbox™ user's guide (R2014a). The MathWorks, Inc. Massachusetts.

Bell, R. D. and Åström, K. J., 1987. Dynamic models for boiler-turbine-alternator units: Data logs and parameter for a 160MW unit. In: Report TFRT-3192, Lund Institute of Technology, Sweden.

BERR, 2006. Advanced power plant using high efficiency boiler/turbine. ReportBPB010. BERR, Department for Business Enterprise and Regulatory Reform, Available at: www.berr.gov.uk/files/file30703.pdf [Accessed April, 2012]

Bhambare, K.S., Mitra, S.K., Gaitonde, U.N. Modelling of a coal-fired natural circulation boiler. *Journal of Energy Resources Technology*, 129 (2007), 159-167.

Biliyok, C., Lawal, A., Wang, M., Seibert, F. Dynamic modelling, validation and analysis of post-combustion chemical absorption CO_2 capture plant. *International Journal of Greenhouse Gas Control*, Vol. 9 (2012), 428-445.

Bishnoi, S. and Rochelle, G.T. Thermodynamics of Piperazine/Methyldiethanolamine/Water/Carbon Dioxide. *Ind. Eng. Chem.*, 2002, *41* (3), pp 604–612

Blokh, A.G. 1987. Heat transfer in steam boiler furnaces. Hemisphere publishing corporation, London. ISBN 0-89116-626-2

Capture Power, 2014. About the White Rose CCS project. Available at http://www.whiteroseccs.co.uk/about-white-rose [Accessed November, 2014]

Chaczykowski, M. and Osiadacz, A. J. Dynamic simulation of pipelines containing dense phase/supercritical CO_2-rich mixtures for carbon capture and storage. *International Journal of Greenhouse Gas Control*, Vol. 9 (2012), 446-456.

Chaibakhsh, A. and Ghaffari, A., 2008. Steam turbine model. *Simulation Modelling Practice and Theory,* 16 (9), 1145-1162.

Chang, Y., and Yu, J. A long term dynamic simulation method of power system based on variables grouping and seceding grouping strategy. In: *DRPT,* Nanjing, China, 6-9 April, 2008.

Chawdhry, P.K. and Hogg, B.W. Identification of boiler models, IEE Proceedings 1989; 136 (Pt. D, No. 5).

Chetouani, Y. Nonlinear modelling of a reactor-exchanger by using NARX neural networks, Proceedings of European Congress of Chemical Engineering (ECCE-6) Copenhagen, September 16-20, 2007.

Chien, K.L., Ergin, E.I., Ling, C., Lee, A., Calif, A. Dynamic analysis of a boiler. *Transactions of ASME,* Vol.80 (1958), 1890-1819.

Chikukwa, A., Enaasen, N., Kvamsdal, H.M and Hillestad, M. Dynamic modelling of post-combustion CO_2 capture using amines – a review. *Energy Procedia, 23 (2012), 82–91*

Cifre, G.P., Brechtel, K., Hoch, S., García, H., Asprion, N., Hasse, H. and Scheffknecht, G. Integration of a chemical process model in a power plant modelling tool for the simulation of an amine based CO_2 scrubber. *Fuel*, Vol. 88, Issue 12 (2009), 2481-2488.

Clausen, S, Oosterkamp, A. and Strøm, K.L. Depressurization of a 50 km long 24 inches CO_2 pipeline. Energy Procedia 23 (2012) 256 – 265

Clausen, S. and Munkejord, S.T. Depressurization of CO_2 – a numerical benchmark study. Energy Procedia 23 (2012) 266 – 273

CO2CRC, 2011. CO_2 capture/separation technologies. Available at: http://www.co2crc.com.au/aboutccs/cap_absorption.html [Accessed Nov., 2014]

Coelho, P.J. and Carvalho, M.G. 1992. Heat transfer in power station boilers. *ASME Thermodynamics and the design, analysis and improvement of energy systems,* AES-Vol.27/HTD-Vol.228, 365-372.

CO-LaN, 2014. CAPE-OPEN standards and supporting documents. Available at: http://www.colan.org/index-3.html   [Accessed September, 2014]

Colonna, P. and VanPutten, H., 2007. Dynamic modelling of steam cycles. Part II-Simulation of a small simple Rankine cycle system. *Applied Thermal Engineering,* Vol. 27, 2566-2582.

Colburn, A.P. (1939) *Trans. Am. Inst. Chem. Eng.* 35, 211. The simplified calculation of diffusion process

Connor, J.T., Martin, R. D. and Atlas, L. E. Recurrent neural networks and robust time series prediction. *IEEE Transactions on Neural Networks* 1994; 5 (2).

Cooke, D.H., 1983. Modelling of off-design multistage turbine pressures by Stodola's ellipse. In: Energy Incorporated PEPSE® User's Group Meeting, Richmond, Virginia, November 2-3.

Dandois, J., Garnier, E., and Pamart, P.Y. NARX modelling of unsteady separation control. Exp Fluids 2013; 54:1445.

De Mello, F.P. Boiler models for system dynamic performance studies. *IEEE Transactions on Power Systems*, Vol. 6 (1991), 66-74.

De Mello, F.P., Anderson, P., Doudna, J., Fish, J.H., Hamm, P.A.L., Hammons, T.J., Hurley, J.D., Kundur, P., Schulz, R., Tandy, G., Taylor, C.W and Younkins, K. 1991. Dynamic models for fossil fueled steam units in power system studies. *IEEE Transactions on Power Systems*, Vol. 6, No. 2.

De, S., Kaiadi, M., Fast, M. and Assadi, M. Development of an artificial neural network model for the steam process of a coal biomass co-fired combined heat and power (CHP) plant in Sweden, Energy 2007; 32: 2099–2109.

Demetriades TA, Drage TC and Graham RS. Developing a new equation of state for carbon capture and storage pipeline transport. Proc IMechE Part E: J Process Mechanical Engineering 2013; 227: 117–124.

Diaz, S. P. 2001, Modelling and simulation of an industrial steam boiler with EcosimPRO. *1st Meeting of EcosimPRO Users,* May 3-4, Madrid, UNED, pp. 5-1.

Diamantonis, N.I., Boulougouris, G.C., Mansoor, E., Tsangaris, D.M., Economou, I.G., 2013. Evaluation of Cubic, SAFT, and PC-SAFT Equations of State for the

Vapor–Liquid Equilibrium Modeling of CO_2 Mixtures with Other Gases. *Industrial & Engineering Chemistry Research*, Vol. *52* (10), 3933–3942.

Dittus, F. W., and Boelter, L. M. K., (1930), University of California, Berkeley, Publications on Engineering, Vol. 2, p.443.

DtEC, 2009. Pall rings. Available at: http://www.traysrus.co.uk/pall-rings-saddles.php [Accessed Dec, 2014]

Dugas, E. R. (2006), *Pilot plant study of carbon dioxide capture by aqueous monoethanolamine,* M.S.E thesis, University of Texas at Austin, USA.

E.ON. 6.23 Equation of state prediction of carbon dioxide properties.
Kingsnorth Carbon Capture & Storage Project; 2010.
Available from: http://webarchive.nationalarchives.gov.uk/20111209170139/
https:/www.decc.gov.uk/en/content/cms/emissions/ccs/demo_prog/feed/
e_on_feed_/transport/transport.aspx [Accessed Feb., 2014].

Edali, M., Aboudheir, A. and Idem, R. Kinetics of carbon dioxide absorption into mixed aqueous solutions of MDEA and MEA using a laminar jet apparatus and a numerically solved 2D absorption rate/kinetics model. *International Journal of Greenhouse Gas Control*, Vol.3 (2009) 550–560

Eklund, K., 1968. Linear mathematical models of the drum-downcomer-riser loop of a drum boiler. In: Report 6808, Division of automatic control, Lund Institute of Technology, Sweden.

Eswaran, S., Wu, S. and Nicolo, R., 2010. Advanced amine-based CO_2 capture for coal-fired power plants. In: *Coal-Gen 2010*, Pittsburgh, Pennsylvania, Aug. 10-12.

Faber, R., Kopcke, M., Biede, O., Knudsen, J.N. and Andersen, J. Open-loop step responses for the MEA post-combustion capture process: Experimental results from the Esbjerg pilot plant. *Energy Procedia.* 2011, 4, 1427-34.

Finkenrath, M., Smith, J., and Volk, D. 2012. CCS retrofit analysis of the globally installed coal-fired power plant fleet. Sustainable Energy Policy and Technology Directorate, International Energy Agency (IEA). Available at:
http://www.iea.org/publications/freepublications/publication/CCS_Retrofit.pdf
[Accessed Sept., 2013]

Fisher, K S., Beitler, Rueter, C., Searcy, K., Rochelle, G., Jassim, M. and Figueroa, J.D. Integrating MEA regeneration with CO_2 compression to reduce CO_2 capture costs. Fourth annual conference on carbon capture and sequestration DOE/NETL May 2-5, 2005

Flynn, M.E. and Malley, M.J.O. A drum boiler model for long term power system dynamic simulations. *IEEE Transactions on Power Systems,* Vol. 14(1999), 209-217.

Flynn, M.E.1999. Generator resources and the scheduling problem. PhD Thesis, University College Dublin

Fuller, E.N., Schettler, P.D., Giddings, J.C. New method for prediction of binary gas-phase diffusion coefficients. *Ind. Eng. Chem.* 1966, 58(5), 18-27.

Gáspár, J. and Cormoş, A. Dynamic modelling and validation of absorber and desorber columns for post-combustion CO_2 capture. Computers & Chemical Engineering, Vol. 35 Issue 10 (2011), 2044-2052

Genick, B. 2013. Basics of fluid mechanics. Available at: http://www.potto.org/FM/fluidMechanics.pdf [Accessed October, 2014]

Goff, G. S. and Rochelle, G. T. Monoethanolamine degradation: O_2 mass transfer effects under CO_2 capture conditions. *Ind. Eng. Chem. Res.* 2004, 43, 6400-6408

Habbi, H., Zelmat, M. and Bouamama, B.O., 2003. A dynamic fuzzy model for a drum-boiler-turbine system, Automatica, 39 (7) 1213-1219.

Harkin, T., Hoadley, A. and Hooper, B. Optimization of power stations with carbon capture plants – the trade-off between costs and net power. *Journal of Cleaner Production,* 2012, 1-12.

Harkin, T., Hoadley, A. and Hooper, B., 2010. Reducing the energy penalty of CO_2 capture and compression using pinch analysis. *Journal of Cleaner Production,* 18(9), 857-866.

Harkin, T., Hoadley, A., and Hooper, B., 2009. Process integration analysis of a brown coal-fired power station with CO_2 capture and storage and lignite drying. *Energy Procedia,* 1, 3817-3825.

Harun, N., Douglas, P.L., Ricardez-Sandoval, L. and Croiset, E. 2011. Dynamic simulation of MEA absorption processes for CO_2 capture from fossil fuel power plant. *Energy Procedia*, Vol. 4, 1478–1485

Haykin, S. Neural Networks: A comprehensive foundation. Pearson Education Inc. Delhi, 1999.

Hilpert, R., (1933), Warmeabgabe von geheizen Drahten und Rohren, Forsch. Gebiete Ingenieurw., Vol. 4, p.220.

Ho, M.T., Allinsona, G.W., Wiley, D.E., 2009. Factors affecting the cost of capture for Australian lignite coal fired power plants. *Energy Procedia,* 1, 763–770.

Honeywell, J. 2009. John M. Campbell Tip of the month (May, 2009): The sensitivity of k-values on compressor performance. Available at: http://www.jmcampbell.com/tip-of-the-month/2009/05/the-sensitivity-of-k-values-on-ompressocr-performance/ [Accessed November, 2014]

House, K.Z., Harvey, C.F., Aziz, M.J. and Schrag, D.P. The energy penalty of post-combustion CO_2 capture & storage and its implications for retrofitting the U.S. installed base. *Energy Environ. Sci.*, Vol.2 (2009) 193-205

IEA, 2010. Energy technology perspectives: Scenarios and strategy to 2050. Available at: http://www.iea.org/techno/etp/etp10/English.pdf [Accessed Sept., 2014]

IEA, 2011. CO_2 emission from fuel combustion highlights. Available at: http://www.iea.org/co2highlights/co2highlights.pdf [Accessed Dec., 2011]

IEA, 2014. Medium-term renewable energy market report 2014 – Market analysis and forecast to 2020. ISBN 978-92-64-21821-5

IEA GHG 2002. Pipeline transmission of CO_2 and energy: Woodhill Engineering Consults. Report number: PH 4/6.

IEA GHG, 2006. CO_2 capture as a factor in power station investment decisions. Available at: http://www.ieaghg.org/docs/overviews/2006-8.pdf [Accessed Nov., 2014]

IEA GHG, 2010. CO_2 pipeline infrastructure: An analysis of global challenges and opportunities. Available at: http://decarboni.se/sites/default/files/publications/99971/development-global-co2-pipeline-infrastructure.pdf [Accessed Jan., 2015]

Idem, R., Wilson, M., Tontiwachwuthikul, P., Chakma, A., Veawab, A., Aroonwilas, A. and Gelowitz, D. Pilot Plant Studies of the CO_2 Capture Performance of Aqueous MEA and Mixed MEA/MDEA Solvents at the University of Regina CO_2 Capture Technology Development Plant and the Boundary Dam CO_2 Capture Demonstration Plant. *Ind. Eng. Chem. Res.*, 2006, *45* (8), 2414–2420

IEEE Committee Report. Dynamic models for steam and hydro turbines in power systems studies. Task Force on Overall Plant Response, *IEEE Transactions on Power Apparatus and Systems*, Vol.92 (1973), 1904-1915.

Infochem, 2012. User guide for models and physical properties, Version 4.1. Infochem Computer Services Ltd

Inoue, S., Itakura, T., Nakagaki, T., Furukawa, Y., Sato, H. and Yamanaka, Y. Experimental study on CO_2 solubility in aqueous piperazine/alkanolamines solutions at stripper conditions. Energy Procedia, Vol. 37 (2013), 1751-1759

IPCC, 2005: IPCC Special Report on Carbon Dioxide Capture and Storage. Prepared by Working Group III of the Intergovernmental Panel on Climate Change [Metz, B., O. Davidson, H. C. de Coninck, M. Loos, and L. A. Meyer (eds.)]. Cambridge University Press, Cambridge, United Kingdom and New York, NY, USA, 442 pp.

IPCC, 2014a. Final Draft of Working Group III Assessment Report 5-Mitigation of Climate Change. Available at: http://report.mitigation2014.org/drafts/final-draft-postplenary/ipcc_wg3_ar5_final-draft_postplenary_full.pdf [Accessed Sept., 2014]

IPCC, 2014b. Climate change 2014: Synthesis Report. Available at: http://www.ipcc.ch/pdf/assessment-report/ar5/syr/SYR_AR5_LONGERREPORT_Corr2.pdf [Accessed Jan., 2014]

Irwin, G., Brown, M., Hogg, B. and E. Swidenbank, E. Neural network modelling of a 200MW boiler system. IEE Proc.-Control *Theory Appl., 1995;* 142(6).

Jinxing, L. and Jiong, S. 2011. Non-linear modelling of drum-boiler-turbine unit using an evolving Takagi-Sugeno fuzzy model. *Int. J. Modelling, Identification and Control*, *Vol.* 12, Nos. 1/2.

Katariya, A.M., Kamath R.S., Mahajani, S.M., Moudgalya, K.M. Study of non-linear dynamics in reactive distillation for TAME synthesis using equilibrium and non-equilibrium models. *Comp. Aided Chem. Eng.* Vol. 21 (2006), 469-474.

Kenig, E.Y., Schneider, R. and Górak, A. Reactive absorption: optimal process design via optimal modelling. *Chem. Eng. Technol.*, 56 (2001), 343–350

Khan, F.M., Krishnamoorthi, V. And Mahmud, T. Modelling reactive absorption of CO_2 in packed columns for post-combustion carbon capture applications. *Chemical Engineering Research and Design,* Vol. 89, Issue 9 (2011), 1600-1608.

Khalilpour, R. and Abbas, A., 2011. HEN optimization for efficient retrofitting of coal-fired power plants with post-combustion carbon capture. *International Journal of Greenhouse Gas Control*, 5, 189–199

Kim, H., and Choi, S. A model on water level dynamics in natural circulation drum-type boilers. *International Communications in Heat and Mass Transfer*, vol. 32 (2005), 786 – 796

Kister, H.Z., Scherffius, J., Afshar, K. And Abkar, E. 2007. Realistically predict capacity and pressure drop for packed columns. AiChE Spring Meeting, Houston Texas.

Knudsen, J.N., Jensen, J.N., Vilhelmsen, P. and Biede, O. Experience with CO_2 capture from coal flue gas in pilot-scale: testing of different amine solvents. *Energy Procedia*, 1 (1) (2009), 783–790

Krishna, R., and Wesselingh, J.A. The Maxwell-Stefan approach to mass transfer. *Chem. Eng. Sci.* 1997, 52(6), 861-911.

Kucka, L., Müller, I., Kenig, E. Y. and Górak, A., 2003. On the modelling and simulation of sour gas absorption by aqueous amine solutions. *Chemical Engineering Science,* 58 (16), pp. 3571-3578.

Kunz, O and Wagner, W. 2012.The GERG-2008 wide-range equation of state for natural gases and other mixtures: An expansion of GERG-2004, J. Chem. Eng. Data, Vol. 57, 3032−3091

Kvamsdal, H.M. and Rochelle, G.T. Effects of the temperature bulge in CO_2 absorption from flue gas by aqueous monoethanolamine. *Ind. Eng. Chem. Res.*, 2008, *47* (3), 867–875

Kvamsdal, H.M., Jakobsen, J.P. and Hoff, K.A. Dynamic modelling and simulation of a CO_2 absorber column for post-combustion CO_2 capture. *Chemical Engineering and Processing: Process Intensification*, Vol. 48 Issue 1 (2009), 135-144

Kwan, H.W., Anderson, J.H., 1970. A mathematical model of a 200MW boiler. *International Journal of Control*, 12(6), 977-998.

Lapina, R. P. (1982). Estimating centrifugal compressor performance. Houston, Tex., Gulf Publ.

Lawal, A., Wang, M., Stephenson, P., Yeung, H. Dynamic modelling of co_2 absorption for post combustion capture in coal-fired power plants, *Fuel* 2009a, 88(12), 2455-2462.

Lawal, A., Wang, M., Stephenson, P., Yeung, H. Dynamic modelling and simulation of CO_2 chemical absorption process for coal-fired power plants. *Comp. Aided Chem. Eng.* 2009b, 27, 1725-1730.

Lawal, A., Wang, M., Stephenson, P., Koumpouras, G. and Yeung, H. Dynamic modelling and analysis of post-combustion CO_2 chemical absorption process for coal-fired power plants. *Fuel*, Vol. 10, Issue 10 (2010), 2791-2801

Lawal, A., Wang, M., Stephenson, P. and Obi, O. Demonstrating full-scale post-combustion CO_2 capture for coal-fired power plants through dynamic modelling and simulation. *Fuel,* Vol. 101 (2012), 115-128.

Lawal, A. 2010. Study of post-combustion Carbon Dioxide capture for coal-fired plant through modelling and simulation. PhD Thesis, Cranfield University.

Lazic, T., Oko, E. and Wang, M. Case study on CO_2 transport pipeline network design for Humber region in the UK. *Proc IMechE Part E: J Process Mechanical Engineering* 2014, Vol. 228(3) 210–225.

Lee, A.L. 1967. Heat capacity of coal. Canadian Coal Conferences, March 30, Ottawa, Canada.

Leng, W., Abbas, A., and Khalilpour, R., 2010. Pinch analysis for integration of coal-fired power plants with carbon capture", Pierucci, S., and Ferraris, G.P. (ed.), In: *European Symposium on Computer Aided Process Engineering - ESCAPE20,* Naples, Italy, June 6-9, 2010.

Leva, A., Maffezzoni, C. and Banelli, G. 1999. Validation of drum boiler models through complete dynamic tests. *Control Engineering Practice*, Vol. 7 (1999), 11-26

Li, H. and Yan, J. Impacts of impurities in CO_2 fluids on CO_2 transport process. In: ASME 51st turbo expo, Barcelona, 6–11 May 2006, vol. 4, 8–11.

Li, H. and Yan, J. Evaluating cubic equations of state for calculation of vapour–liquid equilibrium of CO_2 and CO_2-mixtures for CO_2 capture and storage processes. Appl Energy 2009a; 86 (6):826–36.

Li, H. and Yan, J. Impacts of equations of state (EOS) and impurities on the volume calculation of CO_2 mixtures in the applications of CO_2 capture and storage (CCS) processes. *Applied Energy*, 2009b; 86 (12):2760–70.

Li, B., Chen, T. and Yang, D., 2005. DBSSP–A computer program for simulation of controlled circulation boiler and natural circulation boiler start up behavior. *Energy Conversion and Management,* 46(4), pp. 533-549.

Liebenthal, U., Linnenberg, S., Oexmann, J. and Kather, A. Derivation of correlations to evaluate the impact of retrofitted post-combustion CO_2 capture process on steam power plant performance. *International Journal of Greenhouse Gas Control*, Vol. 5 (2011) 1232-1239.

Liljemark, S., Arvidsson, K., McCann, M.T.P., Tummescheit, H., Velut, S., 2011. Dynamic simulation of a carbon dioxide transfer pipeline for analysis of normal operation and failure modes. *Energy Procedia,* Vol. 4, 3040-3047.

Lin, G. and Yiping, D. 2011. A new linear model of fossil fired steam unit for power system dynamic analysis. *IEEE Transactions on power systems*, Vol. 26, No. 4.

Lin, J., and Shen, J., 2011. Nonlinear modelling of drum-boiler-turbine unit using an evolving Takagi-Sugeno fuzzy model. *International Journal of Modelling, Identification and Control,* 12(1/2), 56-65.

Lin, Y-J., Wong, D.S-H., Jang, S-S., and Ou, J-J., 2012. Control strategies for flexible operation of power plant with CO_2 capture. *AICHE Journal*, vol. 58 (9), 2697-2704.

Lin, Y-J., Pan, T-H., Wong, D.S-H., Jang, S-S., Chi, Y-W., Yeh, C-H., 2011. Plant-wide control of CO_2 capture by absorption and stripping using monoethanolamine solution. *Ind. Eng. Chem. Res.*, vol. 50, p.1338-1345.

Liu, C., Liu, J., Niu, Y., and Liang, W. 2001.Nonlinear boiler model of 300MW power unit for system dynamic performance studies. ISIE, Pusan, KOREA.

Liu, C., Liu, J., Niu, Y., and Jin, X., 2004. Nonlinear modelling and simulation for large scale coal-fired power unit. In: *30th Annual Conference of the IEEE Industrial Electronics Society,* Busan, Korea, Nov. 2-6, 2004.

Liu, X.J., Kong, X.B., Hou, G.L. and Wang, J.H. Modelling of a 1000 MW power plant ultra-super-critical boiler system using fuzzy-neural network methods. *Energy Conversion and Management* Vol. 65 (2013), 518–527.

Lo, K.L. and Song, Z.M. Development of a static-state estimator for a power station boiler, Part I: Mathematical Model. *Electrical Power Systems Research,* Vol. 18 (1990), 175-189.

Lu, S. 1999. Dynamic modelling and simulation of power plant systems. *Proc Instn Mech Engrs, Part A, Journal of Power and Energy,* Vol. 213, 7-22.

Lu, S. and Hogg, B.W. 2000. Dynamic nonlinear modelling of power plant by physical principles and neural networks. *Electrical Power and Energy Systems*, Vol, 22, 67-78.

Lucquiaud, M. and Gibbins, J., 2011a. Effective retrofitting of post-combustion CO_2 capture to coal-fired power plants and insensitivity of CO_2 abatement costs to base plant efficiency. *International Journal of Greenhouse Gas Control,* 5(3), pp. 427-438.

Lucquiaud, M. and Gibbins, J., 2011b. Steam cycle options for the retrofit of coal and gas power plants with post combustion capture, *Energy Procedia,* 4, 1812-1819.

Ludwig, E. E. 2001. Applied process design for chemical and petrochemical plants, Vol. 3, Third Ed. Gulf Professional Publishing, Oxford.

Luo, X., Wang, M., Oko, E. and Okezue, C. Simulation-based techno-economic evaluation for optimal design of CO_2 transport pipeline network. *Applied Energy*, Vol. 132 (2014), 610–620.

MacDowell, N. Samsatli, N.J. and Shah, N. Dynamic modelling and analysis of an amine-based post-combustion CO_2 capture absorption column. *International Journal of Greenhouse Gas Control*, Vol.12 (2013), 247-258

MacDowell, N. and Shah, N. Dynamic modelling and analysis of a coal-fired power plant integrated with a novel split-flow configuration post-combustion CO_2 capture process. *International Journal of Greenhouse Gas Control*, Vol. 27 (2014) 103-119.

Maffezzoni, C. 1992. Issues in modelling and simulation of power plants. In Proceedings of IFAC symposium on control of power plants and power systems, Vol. 1, pp 19-27, Munchen, Germany.

Mangalapally, H.P. and Hasse, H. 2011a. Pilot plant study of post-combustion carbon dioxide capture by reactive absorption: Methodology, comparison of different structured packings, and comprehensive results for monoethanolamine. *Chemical Engineering Research and Design,* Vol. 89, 1216-1228.

Mangalapally, H.P. and Hasse, H. 2011b. Pilot plant experiments for post combustion carbon dioxide capture by reactive absorption with novel solvents. *Energy Procedia*, Vol. 4, 1–8

Masada, G.Y. 1979. Modelling and control of power plant boiler-turbine—generator systems, Sc. D Thesis, Department of Mechanical Engineering, MIT.

McCoy, S. and Rubin, E. An engineering-economic model of pipeline transport of CO_2 with application to carbon capture and storage. *International Journal of Greenhouse Gas Control*, 2 (2) (2008), 219–229

MDT, 2013. Shell captures CO_2 with MAN integrally-geared centrifugal compressor. Available at: http://www.corporate.man.eu/en/responsibility/news-and-reports/press-releases/Shell-captures-CO2-with-MAN-integrally-geared-centrifugal-compressor-46468.html [Accessed Nov., 2014]

MIT, 2014a. https://sequestration.mit.edu/tools/projects/index.html [Accessed November, 2014]

MIT, 2014b. AEP Mountaineer Factsheet: Carbon dioxide capture and storage project. Available at: https://sequestration.mit.edu/tools/projects/aep_alstom_mountaineer.html [Accessed Nov., 2014]

MIT, 2014c. Boundary Dam Fact Sheet: Carbon dioxide capture and storage project. Available at: https://sequestration.mit.edu/tools/projects/boundary_dam.html [Accessed March, 2014]

Moser, P., Schmidt, S., Sieder, G., Garcia, H., Stoffregen, T. and Stematov, V. 2011. The post-combustion capture pilot plant Niederaussem – Results of the first half of the testing programme. *Energy Procedia*, Vol. 4, 1310–1316

Moshfeghian, M. Compressor calculations: rigorous using equation of state vs shortcut method. Tip of the Month, November 2011. Available at: http://www.jmcampbell.com/tip-of-the-month/2011/11/compressor-calculations-rigorous-using-equation-of-state-vs-shortcut-method/ [Accessed Nov., 2014]

Moshfeghian M. Transportation of CO_2 in dense phase. Tip of the Month, January 2012. Available at: http://www.jmcampbell.com/tip-of-the-month/2012/01/transportation-ofco2-in-dense-phase/ [Accessed Jan., 2013]

NERC, 2014. Storing carbon dioxide beneath the Moray Firth explored. Available at: http://www.bgs.ac.uk/research/highlights/2010/scottishCCS.html [Accessed August, 2014]

Nimtz, M., Klatt, M., Wiese, B., Kühn, M., Joachim K.H. Modelling of the CO_2 Process and transport chain in CCS systems—examination of transport and storage processes. Chem Erde 2010; 70:185–92.

Notz, R., Asprion, N., Clausen, I. and Hasse, H. 2007. Selection and pilot plant tests of new absorbents for post-combustion carbon dioxide capture. *Chemical engineering research and design, Vol. 85, Issue 4, 510-515.*

Ofgem e-serve, 2013. The final report of the carbon emissions reduction target (CERT) 2008-2012. Available at: https://www.ofgem.gov.uk/ofgem-publications/58425/certfinalreport2013300413.pdf [Accessed Nov., 2014]

Oko, E. and Wang, M. Dynamic modelling, validation and analysis of coal-fired subcritical power plant, *Fuel* Vol. 135 (2014), 292–300

Oke, O. O., 2008. Dynamic modelling of subcritical coal-fired power plant. MSc Thesis, Cranfield University.

Ordys, A. W., Pike, A.W., Johnson, M. A., Katebi, R. M., and Grimble, M. J., 1994. *Modelling and simulation of power generation plants.* Springer Verlag. (Advances in Industrial Control), ISBN 9783540199076, London.

Panahi, M., Karimi, M., Skogestad, S., Hillestad, M and Svendsen, H.F. 2010. Self-optimizing and control structure design for a CO_2 capturing plant. Proceedings of the 2nd Annual Gas Processing Symposium, January 10-14, Qatar.

Panahi, M. and Skogestad, S. 2011. Economically efficient operation of CO2 capturing process part I: Self-optimizing procedure for selecting the best controlled variables. *Chemical Engineering and Processing: Process Intensification*, Vol.50, Issue 3, 247-253.

Panahi, M. and Skogestad, S. 2012. Economically efficient operation of CO_2 capturing process. Part II. Design of control layer. *Chemical Engineering and Processing: Process Intensification,* Vol. 52, 112–124.

Park, S-E., Min, B-M., Lee, J-S., and Eum, H-M., 2004. A study about CO_2 absorption process design for thermal power plant flue gas. *Studies in surface science and catalysis*, 153, pp. 539-542.

Parkinson, G., 2012. Could solar thermal technology make CCS cost competitive? Available at: http://reneweconomy.com.au/2012/could-solar-thermal-technology-make-ccs-cost-competitive-97883 [Accessed: August, 2012].

Patel, A. and Dunne, J.F. NARX neural network modelling of hydraulic suspension dampers for steady-state and variable temperature operation. Vehicle System Dynamics: International Journal of Vehicle Mechanics and Mobility 2003; 40(5): 285-328.

Paul S, Shepherd R, Bahrami A, et al. Material selection for supercritical CO_2 transport. In: First international forum on the transportation of CO_2 by pipeline, Hilton Newcastle-Gateshead Hotel, Gateshead, UK, 1–2 July 2010.

Peng, J., Edgar, T.F., Eldridge, R.B. Dynamic rate-based and equilibrium models for a packed reactive distillation column. *Chem. Eng. Sci.* 2003, 58, 2671 – 2680.

Peng, J., Lextrait, S., Edgar, T.F. and Eldridge, R.B. A comparison of steady-state equilibrium and rate-based models for packed reactive distillation columns. *Ind. Eng. Chem. Res.*, 2002, *41* (11), 2735–2744.

Posch, S. and Haider, M. Dynamic modelling of CO_2 absorption from coal-fired power plants into an aqueous monoethanolamine solution. *Chemical Engineering Research and Design*, Vol. 91, Issue 6, (2013), 977–987

PSE, 2014a. The ETI CCS System Modelling Tool-kit project. Available at: http://www.psenterprise.com/power/ccs/eti_smtk_project.html [Accessed August, 2014]

PSE, 2014b. gPROMS ModelBuilder[®] at-a-glance. Available at: http://www.psenterprise.com/modelbuilder/overview.html [Accessed Sept., 2014]

Raimondi, L CO_2 transportation with pipelines – model analysis for steady, dynamic and relief simulation. *Chemical Engineering Transactions*, Vol. 36 (2014) 619-624

Ramasamy, M., Zabiri, H., Thanh Ha, N.T. and Ramli, N.M. Heat exchanger performance prediction modelling using NARX-type neural networks.

Proceedings of the WSEAS Int. Conf. on Waste Management, Water Pollution, Air Pollution, Indoor Climate, Arcachon, France, October 14-16, 2007.

Ramezan, M., Skone, T.J., Nsakala, N., 2007. Carbon dioxide capture from existing coal-fired power plants. In: DOE/NETL-401/110907.

Rao, A.B., Rubin, E.S., Berkenpas, M.B., 2004. An integrated modelling framework for carbon management technologies. In: U.S. Department of Energy (DE-FC26-00NT40935)

Ray, A. Dynamic modelling of once-through subcritical steam generator for solar applications. *Appl. Math. Modelling*, vol.4 (1980), 417-423.

Reuters, 7th Oct., 2014. Carbon capture's energy penalty problem: Kemp. Available at: http://www.dailymail.co.uk/wires/reuters/article-2783304/Carbon-captures-energy-penalty-problem-Kemp.html [Accessed Dec., 2014]

Richardson, M. J. 1993. The specific heats of coals, cokes and their ashes. *Fuel,* Vol. 72(7), pp. 1047-1053.

Romeo, L.M. and Gareta, R. Neural network for evaluating boiler behaviour. *Applied Thermal Engineering* Vol. 26 (2006), 1530–1536.

Roytelman, I., and Shahidehpour, S.M. A comprehensive long term dynamic simulation for power system recovery. *IEEE Transactions on Power Systems,* Vol. 9 (1994), 1427-1433.

Rusinowski, H. and Stanek, W. Neural modelling of steam boilers. *Energy Conversion and Management*, Vol.48 (2007), 2802–2809.

Rusinowski, H. and Stanek, W. Hybrid model of steam boiler. *Energy*, Vol. 35 (2010), 1107-1113.

Sanpasertparnich, T., Idem, R., Bolea, I., DeMontigny, D., Tontiwachwuthikul, P., 2010. Integration of post-combustion capture and storage into a pulverized coal-fired power plant. *International Journal of Greenhouse Gas Control*, Vol. 4, pp. 499–510

Schiesser, W. E. 1991. The numerical method of lines: Integration of partial differential equations 1st Ed. ISBN-13:978-0126241303. Academic Press Inc., Boston.

Schlumberger, 2014. ECLIPSE: Industry reference reservoir simulator. Available at: http://www.software.slb.com/products/foundation/Pages/eclipse.aspx [Accessed Dec, 2014]

Seevam, P.N., Race, J.M., Downie, M., J., Hopkins P. Transporting the next generation of CO_2 for carbon, capture and storage: the impact of impurities on supercritical CO_2 pipelines. In: 2008 7th International Pipeline Conference; Calgary, Alberta, Canada: International Petroleum Technology Institute and the Pipeline Division; 2008.

Sinnot, R.K. 2005. Chemical Engineering Design. In: J. M. Coulson and J. F. Richardson. Eds. Chemical Engineering, Vol. 6, 4th Edition. Oxford: Elsevier Butterworth-Heinemann

Smrekar, J., Assadi, M., Fast, M., Kuštrin, I. and De, S. Development of artificial neural network model for a coal-fired boiler using real plant data. *Energy*, Vol. 34 (2009), 144–152.

Sobanska, P. and Szczepaniak, P., 2006. Neural modelling of steam turbines. In: *Proceedings of the International Multiconference on Computer Science and Information Technology,* Wisla, Poland, Nov. 6-10, Polish Information Processing Society.

Spirax Sarco, 2015. Water-tube boilers. Available at: http://www.spiraxsarco.com/Resources/Pages/Steam-Engineering-Tutorials/the-boiler-house/water-tube-boilers.aspx [Accessed Jan., 2015]

Svensson, R., Odenberger, M., Johnsson, F. and Strömberg, L. Transportation systems for CO_2—application to carbon capture and storage. Energy Conversion Management, Vol.45, No 15–16 (2004), 2343–2353

Swamee, P.K., Jain, A.K., 1976. Explicit equation for pipe flow problems, *Journal of Hydraulic Division, ASCE,* Vol. 102, No. 5, 657-664.

TBWES, 2014. Radiant boiler. Available at: http://www.tbwes.com/products/subcritical-boilers/ [Accessed Oct., 2014]

TCE, 2013. DoE pledges funds to design modular nuclear reactors, *Issue 862, April 2013, pp. 12.*

Tebodin, 2011. Knowledge sharing report – CO_2 liquid logistics shipping concept (LLSC): overall supply chain optimization. Available at: http://decarboni.se/sites/default/files/publications/19011/co2-liquid-logistics-shipping-concept-llsc-overall-supply-chain-optimization.pdf   [Accessed Oct., 2014]

Thomas, P.J. 1999. Simulation of industrial processes for control engineers. Elsevier Science and Technology Books. ISBN: 0750641614

Thompson, F. T. A dynamic model of a drum-type boiler system. *IEEE Transactions on Power Apparatus and Systems,* PAS-86, Vol. 5 (1967), 625-635.

Tobiesen, F.A., Svenden, H.F. and Juliussen, O. Experimental validation of a rigorous absorber model for CO_2 post-combustion capture AIChE J., 53 (2007), 846–865

TSA, 2014. Burner isolation valves. Available at: http://www.tsasales.com/case-studies/energy-case-studies/coal-fired-power-plant-burner-isolation-valve/ [Accessed Sept., 2014]

Tyssø, A. Modelling and parameter estimation of a ship boiler. *Automatica,* Vol. 17 (1981), 157-166.

Uilenreef, J., and Kombrink, M. Flow Assurance and Control Philosophy: Rotterdam Opslag en Afvang Demonstratie (ROAD) Project. Special Report for the Global Carbon Capture and Storage Institute. *Global CCS Inst. Ltd.*, Melbourne, 2013.

Versteeg, G.F., and Van Swaaij, W.P.M. Solubility and Diffusivity of Acid Gases (CO_2, N_2O) in Aqueous Alkanolammine Solutions. *J. Chem. Eng. Data*, Vol. 33 Issue 1 (1998), 29-34.

Vandeginste, V. And Piessens, K. Pipeline design for a least-cost router application for CO_2 transport in the CO_2 sequestration cycle. *International Journal of Greenhouse Gas Control*, Vol.2 Issue 4 (2008), 571-581.

Onda, K., Takeuchi, H., Okumoto, Y. Mass Transfer Coefficients between Gas and Liquid Phases in Packed Columns. *J. Chem. Eng. Japan*, Vol.1 Issue 1 (1968), 56-62.

Wang, M., Lawal, A., Stephenson, P., Sidders, J. and Ramshaw, C. Post-combustion CO_2 capture with chemical absorption: A state-of-the-art review. *Chemical Engineering Research and Design*, Vol. 89, Issue 9 (2011), 1609-1624

Wenzhou, 2014. Pipe dimension. Available at: http://www.nan-long.com/Metal%20Steel%20Technology%20Summary/Pipe%20Dimension-NPS%20DN%20NB-5.htm [Accessed Dec, 2014]

Werner, M., Sutter, D., Krättli, A., Lafci, Ö. Mutschler, R., Oehler, P., Winkler, J. and Mazzotti, M. A physical model for geological CO_2 storage–Replacing misconceptions by visual explanation. *International Journal of Greenhouse Gas Control*, Vol. 25 (2014), 42-53.

Witkowski, A., Rusin, A., Majkut, M., Rulik, S., Stolecka, K. Comprehensive analysis of pipeline transportation systems for CO_2 sequestration: Thermodynamics and safety problems. *Energy Conversion and Management*, Vol. 76 (2013), 665-673.

World Metrological Organisation (WMO) Global Atmosphere Watch (GAW). Greenhouse Gas Bulletin, 9th Sept., 2014. Available at: https://drive.google.com/file/d/0BwdvoC9AeWjUT0FTYVQzS19MRkE/edit [Accessed Jan., 2015]

Xu, G., Jin, H., Yang, Y., Xu, Y., Lin, H., and Duan, L., 2010. A comprehensive techno-economic analysis method for power generation systems with CO_2 capture. *International Journal of Energy Research*, 34 (4), pp. 321-332.

Yang, Y. and Zhai, R. 2010. MEA-based CO_2 capture technology and its application in power plants, paths to sustainable energy, Artie, Ng (Ed.), ISBN: 978-953-307-401-6, InTech, Available from: http://www.intechopen.com/books/paths-to-sustainable-energy/mea-based-co2-capture-technology-and-itsapplication-in-power-plants

Yun-tao, C., Chun, L., Qiang, C., Huai-chun, Z. Distributed parameter modelling and simulation for the evaporation system of a controlled circulation boiler based on 3-D combustion. *Applied Thermal Engineering*, Vol. 28 (2008), 164-177.

Zaii, S., Rochelle, G.T. and Edgar, T.F. Dynamic modelling to minimize energy use for CO_2 capture in power plants aqueous monoethanolamine. *Ind. Eng. Chem. Res.* Vol. 48 (2009), 6105-6111.

Zhang, Z.X., Wang, G.X., Massarotto, P., Rudolph, V. Optimization of pipeline transport for CO_2 sequestration. *Energy Convers. Manage.* 2006;47(6):702–15.

Zhang, Y., Chen, H., Chen, C., Plaza, J.M., Dugas, R., Rochelle, G.T. Rate-based process modelling study of CO_2 capture with aqueous Monoethanolamine solution. *Ind. Eng. Chem. Res.,* Vol. 48 (2009), 9233-9246.

Zhang, D., Liu, P., Logan, W., Li, Z., and Ni, W., 2011.Reducing initial barriers for CCS deployment on pulverized coal-fired power plants in China by optimizing the capture ratio of carbon dioxide. In: *Proceedings of the International Conference on Materials for Renewable Energy and Environment (ICMREE 2011)*, May 20-22, 2011, Shanghai, China

Zhu, Y. 2001. Multivariable system identification for process control. Elsevier Science & Technology Books; ISBN: 0080439853.

Zimmer, G. Modelling and simulation of steam turbine processes: individual models for individual tasks. *Mathematical and Computer Modelling of Dynamic Systems: Method, Tools and Applications in Engineering and Related Sciences*, Vol. 14 Issue 6 (2008), 469-493.

Appendix A: Main governing equations for the pipeline segment model

The main governing equations for the pipeline segment in Chapter 5 (*i.e.* mass, energy and momentum conservation equations) and the steps taken to rewrite them in terms of mass flowrate, temperature and pressure are presented here.

Mass conservation equation

$$A\frac{d\rho}{dt} + \frac{d\dot{m}}{dz} = 0 \tag{A.1}$$

To rewrite the mass conservation equation (A.1) in terms of mass flowrate, pressure and temperature, the $d\rho$ term is replaced from A.2 to obtain the final equation (A.3).

$$d\rho = \left(\frac{\partial\rho}{\partial P}\right)_T dP + \left(\frac{\partial\rho}{\partial T}\right)_P dT \tag{A.2}$$

$$\left(\frac{\partial\rho}{\partial P}\right)_T \frac{dP}{dt} + \left(\frac{\partial\rho}{\partial T}\right)_P \frac{dT}{dt} = -\frac{1}{A}\frac{d\dot{m}}{dz} \tag{A.3}$$

Momentum conservation equation

$$\frac{d(\rho v)}{dt} + \frac{d(P+\rho v^2)}{dz} = -\frac{f\rho v|v|}{2D} - \rho g \sin\alpha \tag{A.4}$$

To rewrite the momentum conservation equation (A.4), the fluid velocity (v) is first replaced from A.5 to obtain A.6.

$$v = \frac{\dot{m}}{\rho A} \tag{A.5}$$

$$\frac{1}{A}\frac{d\dot{m}}{dt} = -\frac{dP}{dz} - \frac{d}{dz}\left(\frac{\dot{m}^2}{\rho A^2}\right) - \frac{f\dot{m}|\dot{m}|}{2\rho A^2 D} - \rho g \sin\alpha \tag{A.6}$$

The term $\frac{d}{dz}\left(\frac{\dot{m}^2}{\rho A^2}\right)$ is expanded thus:

$$\frac{d}{dz}\left(\frac{\dot{m}^2}{\rho A^2}\right) = \frac{2\dot{m}}{\rho A^2}\frac{d\dot{m}}{dz} - \frac{\dot{m}^2}{\rho^2 A^2}\frac{d\rho}{dz} \tag{A.7}$$

The terms $d\rho$ and $\frac{d}{dz}\left(\frac{\dot{m}^2}{\rho A^2}\right)$ in A.6 is then replaced from A.2 and A.7 respectively and the resulting equation rearranged to obtain the final equation (A.8).

$$\frac{1}{A}\frac{d\dot{m}}{dt} = \left(\frac{\dot{m}^2}{\rho^2 A^2}\left(\frac{\partial\rho}{\partial P}\right)_T - 1\right)\frac{dP}{dz} - \frac{2\dot{m}}{\rho A^2}\frac{d\dot{m}}{dz} + \left(\frac{\dot{m}^2}{\rho^2 A^2}\left(\frac{\partial\rho}{\partial T}\right)_P\right)\frac{dT}{dz} - \frac{f\dot{m}|\dot{m}|}{2\rho A^2 D} - \rho g \sin\alpha \tag{A.8}$$

Energy conservation equation

$$\left(u + \tfrac{1}{2}v^2 + gz\sin\alpha\right)\frac{d\rho}{dt} + \rho\frac{d}{dt}\left(u + \tfrac{1}{2}v^2\right) = \frac{q}{A} - \rho v\frac{d}{dz}\left(h + \tfrac{1}{2}v^2\right) - \left(h + \tfrac{1}{2}v^2 + \right.$$

$$\left. gz\sin\alpha\right)\frac{d}{dz}(\rho v) - \rho vg\sin\alpha \tag{A.9}$$

To rewrite the energy conservation equation (A.9), the internal energy u and $\frac{d}{dz}(\rho v)$ term is replaced from A.10 and A.11 (from mass conservation equation) and rearranged to obtain A.12.

$$u = h - \frac{P}{\rho} \tag{A.10}$$

$$\frac{d}{dz}(\rho v) = -\frac{d\rho}{dt} \tag{A.11}$$

$$-\frac{P}{\rho}\frac{d\rho}{dt} + \rho\frac{d}{dt}h - \rho\frac{d}{dt}\frac{P}{\rho} + \frac{\rho}{2}\frac{d}{dt}v^2 = \frac{q}{A} - \rho v\frac{d}{dz}h - \frac{\rho v}{2}\frac{d}{dz}v^2 - \rho vg\sin\alpha \tag{A.12}$$

The term $\frac{d}{dt}\frac{P}{\rho}$ is expanded:

$$\frac{d}{dt}\frac{P}{\rho} = \frac{1}{\rho}\frac{dP}{dt} - \frac{P}{\rho^2}\frac{d\rho}{dt} \tag{A.13}$$

The fluid velocity v and the term $\frac{d}{dt}\frac{P}{\rho}$ in A.12 are replaced from A.5 and A.13 and rearranged to obtain:

$$\rho\frac{d}{dt}h - \frac{dP}{dt} + \frac{\rho}{2}\frac{d}{dt}\left(\frac{\dot{m}}{\rho A}\right)^2 = \frac{q}{A} - \frac{\dot{m}}{A}\frac{d}{dz}h - \frac{1}{2}\frac{\dot{m}}{A}\frac{d}{dz}\left(\frac{\dot{m}}{\rho A}\right)^2 - \frac{\dot{m}}{A}g\sin\alpha \tag{A.14}$$

The terms $\frac{d}{dt}\left(\frac{\dot{m}}{\rho A}\right)^2$ and $\frac{d}{dz}\left(\frac{\dot{m}}{\rho A}\right)^2$ are expanded:

$$\frac{d}{dt}\left(\frac{\dot{m}}{\rho A}\right)^2 = \frac{2\dot{m}}{\rho^2 A^2}\frac{d\dot{m}}{dt} - \frac{2\dot{m}^2}{A^2\rho^3}\frac{d\rho}{dt} \tag{A.15}$$

$$\frac{d}{dz}\left(\frac{\dot{m}}{\rho A}\right)^2 = \frac{2\dot{m}}{A^2\rho^2}\frac{d\dot{m}}{dz} - \frac{2\dot{m}^2}{A^2\rho^3}\frac{d\rho}{dz} \tag{A.16}$$

The terms $\frac{d}{dt}\left(\frac{\dot{m}}{\rho A}\right)^2$ and $\frac{d}{dz}\left(\frac{\dot{m}}{\rho A}\right)^2$ are then substituted in A.14 from A.15 and A.16 and rearranged to obtain:

$$\rho \frac{d}{dt} h - \frac{dP}{dt} + \frac{1}{A^2} \frac{\dot{m}}{\rho} \frac{d\dot{m}}{dt} - \frac{1}{A^2} \frac{\dot{m}^2}{\rho^2} \frac{d\rho}{dt} = \frac{q}{A} - \frac{\dot{m}}{A} \frac{d}{dz} h - \frac{1}{A^3} \frac{\dot{m}^2}{\rho^2} \frac{d\dot{m}}{dz} + \frac{1}{A^3} \frac{\dot{m}^3}{\rho^3} \frac{d\rho}{dz} - \frac{\dot{m}}{A} g \sin \alpha \qquad (A.17)$$

Finally, dh and $d\rho$ is replaced in A.17 from A.18 and A.2 respectively and then re-arranged to obtain the final equation (A.19).

$$dh = c_{\mathrm{p}} dT + \left[1 + \frac{T}{\rho} \left(\frac{\partial \rho}{\partial T} \right)_P \right] \frac{dP}{\rho} \qquad (A.18)$$

$$\left(\rho c_p - \left(\frac{\dot{m}}{\rho A} \right)^2 \left(\frac{d\rho}{dT} \right)_P \right) \frac{dT}{dt} + \left(\frac{T}{\rho} \left(\frac{\partial \rho}{\partial T} \right)_P - \left(\frac{\dot{m}}{\rho A} \right)^2 \left(\frac{d\rho}{dP} \right)_T \right) \frac{dP}{dt} + \frac{1}{A^2} \frac{\dot{m}}{\rho} \frac{d\dot{m}}{dt} = \frac{q}{A} - \left(\frac{\dot{m}}{A} c_p - \right.$$

$$\left(\frac{\dot{m}}{\rho A} \right)^3 \left(\frac{d\rho}{dT} \right)_P \right) \frac{\partial T}{\partial z} - \left(\frac{\dot{m}}{\rho A} \left[1 + \frac{T}{\rho} \left(\frac{\partial \rho}{\partial T} \right)_P \right] - \left(\frac{\dot{m}}{\rho A} \right)^3 \left(\frac{d\rho}{dP} \right)_T \right) \frac{\partial P}{\partial z} - \frac{1}{A^3} \frac{\dot{m}^2}{\rho^2} \frac{\partial \dot{m}}{\partial z} - \frac{\dot{m}}{A} g \sin \alpha \qquad (A.19)$$

Appendix B: Relations for calculating density derivatives

Derivation of the relations for calculating density derivatives (*i.e.* $\left(\frac{\partial \rho}{\partial T}\right)_P$ and $\left(\frac{\partial \rho}{\partial P}\right)_T$) in the pipeline transport model in Chapter 5 is presented here. This derivation was done because external call of density and other property derivatives is presently not possible in gPROMS ModelBuilder®.

Derivation of the relation for calculating $\left(\frac{\partial \rho}{\partial P}\right)_T$

The relation for $\left(\frac{\partial \rho}{\partial P}\right)_T$ is obtained as follows based on isothermal compressibility (β) (Bar-Meir, 2013, p.24):

$$\beta = \frac{1}{\rho}\left(\frac{\partial \rho}{\partial P}\right)_T \tag{B.1}$$

Isothermal compressibility is related to the speed of sound in the fluid (v_{son}) in the relation (Thomas, 1999, p.240):

$$v_{son} = \sqrt{\frac{1}{\rho\beta}} \tag{B.2}$$

By combining B.1 and B.2, the relation below results:

$$\left(\frac{\partial \rho}{\partial P}\right)_T = \frac{1}{(v_{son})^2} \tag{B.3}$$

Derivation of the relation for calculating $\left(\frac{\partial \rho}{\partial T}\right)_P$

The relation for $\left(\frac{\partial \rho}{\partial T}\right)_P$ is obtained based on thermal expansion coefficient, second law of thermodynamics and Maxwell relations.

To begin with, thermal expansion coefficient (γ) is given by (Bar-Meir, 2013, p.25):

$$\gamma = -\frac{1}{\rho}\left(\frac{\partial \rho}{\partial T}\right)_P \tag{B.4}$$

From 2nd law of thermodynamics:

$$dq = Tds \tag{B.5}$$

Also,

$$ds = \left(\frac{\partial s}{\partial T}\right)_P dT + \left(\frac{\partial s}{\partial P}\right)_T dP \tag{B.6}$$

$$dP = \left(\frac{\partial P}{\partial T}\right)_v dT + \left(\frac{\partial P}{\partial v}\right)_T dv \tag{E.7}$$

Combine B.5, B.6 and B.7:

$$dq = T\left[\left(\frac{\partial s}{\partial T}\right)_P dT + \left(\frac{\partial s}{\partial P}\right)_T \left(\left(\frac{\partial P}{\partial T}\right)_v dT + \left(\frac{\partial P}{\partial v}\right)_T dv\right)\right] \tag{B.8}$$

If specific volume v is constant (*i.e.* $dv = 0$) then:

$$\left(\frac{dq}{dT}\right)_v = T\left(\frac{\partial s}{\partial T}\right)_P + T\left(\frac{\partial s}{\partial P}\right)_T \left(\frac{\partial P}{\partial T}\right)_v \tag{B.9}$$

The term on the left side of the equation is C_V (*i.e.* specific heat capacity at constant volume) and the first term on the right hand side is C_P (*i.e.* specific heat capacity at constant pressure).

From Maxwell relations:

$$\left(\frac{\partial s}{\partial P}\right)_T = \left(\frac{\partial v}{\partial T}\right)_P \tag{B.10}$$

Substitute C_V, C_P and B.10 in B.9:

$$C_P - C_V = T\left(\frac{\partial v}{\partial T}\right)_p \left(\frac{\partial P}{\partial T}\right)_v \tag{B.11}$$

From thermodynamic relations:

$$\left(\frac{\partial v}{\partial T}\right)_p = \gamma v \tag{B.12}$$

Substitute $\left(\frac{\partial v}{\partial T}\right)_p$ in B.11 from B.12:

$$c_P - c_V = T\gamma v\left(\frac{\partial P}{\partial T}\right)_v \tag{B.13}$$

But:

144

$$dv = \left(\frac{\partial v}{\partial T}\right)_P dT + \left(\frac{\partial v}{\partial P}\right)_T dP \qquad (\text{B.}14)$$

Again specific volume v is constant (*i.e.* $dv = 0$) then B.14 reduces to:

$$\left(\frac{\partial P}{\partial T}\right)_v = -\left(\frac{\partial v}{\partial T}\right)_P \Big/ \left(\frac{\partial v}{\partial P}\right)_T \qquad (\text{B.}15)$$

Again, from thermodynamic relations:

$$\left(\frac{\partial v}{\partial P}\right)_T = -\beta v \qquad (\text{B.}16)$$

The final relation is then obtained by combining B.12, B.13, B.15 and B.16:

$$c_P - c_V = \frac{T\gamma^2}{\rho\beta} \qquad (\text{B.}17)$$

The relation for calculating $\left(\frac{\partial \rho}{\partial T}\right)_P$ is then by obtained combining B.2, B.4 and B.17:

$$\left(\frac{\partial \rho}{\partial T}\right)_P = -\rho\sqrt{\frac{(c_P - c_V)}{T(\mathrm{v}_{son})^2}} \qquad (\text{B.}18)$$

Appendix C: Correlations for calculating heat transfer coefficients

The correlations for calculating the pipe inside convective heat transfer coefficient (h_i) and outside convective heat transfer coefficients (h_o) (offshore pipeline) in Chapter 5 are presented here.

Dittus and Boelter (1930) correlation

Dittus and Boelter (1930) correlation (C.1) is a dimensionless correlation for calculating the internal convective heat transfer coefficient (h_i)

$$Nu_i = 0.0255 Re_i^{0.8} Pr_i^n \qquad (C.1)$$

Hilpert (1933) correlation

Hilpert (1933) correlation (C.2) is similarly a dimensionless correlation for calculating the external convective heat transfer coefficient (h_o)

$$Nu_o = C Re_o^m Pr_o^{1/3} \qquad (C.2)$$

In C.1 and C.2, Nu, Re and Pr are the Nusselt number, Reynolds number and Prandtl number respectively. The relations for the dimensionless numbers are as follows:

$$Nu = \frac{\Phi D}{\kappa} \qquad (C.3)$$

$$Re = \frac{\rho v D}{\mu} \qquad (C.4)$$

$$Pr = \frac{c_P \mu}{\kappa} \qquad (C.5)$$

The parameter n in C.1 is equal to 0.3 (Bai and Bai, 2005). Similarly, the value of parameters C and m in C.2 is 0.027 and 0.805 respectively (Bai and Bai, 2005). The term Φ in C.3 is the heat transfer coefficient (*i.e.* h_i or h_o)

Appendix D: Peer-reviewed publications

Peer-reviewed journal papers

Oko, E. and Wang, M. 2014. Dynamic modelling, validation and analysis of coal-fired subcritical power plant, *Fuel*, Vol. 135, 292-300.

Oko, E., Wang, M. and Olaleye, A.K. 2015. Simplification of detailed rate-based model of post-combustion CO_2 capture for full chain CCS integration studies. *Fuel*, Vol. 142, 87–93.

Oko, E., Wang, M. and Zhang, J. Neural network approach for predicting drum pressure and level in coal-fired subcritical power plant. *Fuel* (In Press).

Lazic, T., **Oko, E.** and Wang, M. 2014. Case study on CO_2 transport pipeline network design for Humber region in the UK, *Proc IMechE Part E: J Process Mechanical Engineering*, Vol. 228(3), 210–225.

Luo, X., Wang, M., **Oko, E.** and Okezue, C. 2014. Simulation-based techno-economic evaluation for optimal design of CO_2 transport pipeline network, *Applied Energy*, Vol. 132, 610-620.

Joel, A.S., Wang, M., Ramshaw, C. And **Oko, E.** Process analysis of intensified absorber for post-combustion CO_2 capture through modelling and simulation, *International Journal of Greenhouse Gas Control*, Vol. 21, 91-100.

Peer-reviewed conference papers

Luo, X., Mistry, K., Okezue, C., Wang, M., Cooper, R., **Oko, E.** and Field, J. 2014. Process simulation and analysis for CO_2 transport pipeline design and operation – case study for the Humber region in the UK, *Proceedings of the 24th European Symposium on Computer Aided Process Engineering – ESCAPE*, 24 June 15-18, Budapest, Hungary.

Oko, E. and Wang, M. 2014. Neural network model predictive controller for drum level control in Coal-fired subcritical power plants. *Proceedings of the 10th European Conference on Industrial Furnaces and Boilers* – INFUB 10, 7-10 April, Gaia (Porto), Portugal.

Conference presentations

Oko, E. and Wang, M. 2012. Dynamic modelling and validation of coal-fired subcritical power plant, *9th European conference on coal research and its applications – ECCRIA*, 10-12 September, University of Nottingham, UK (Poster).

Li, F., Zhang, J., Wang, M. and **Oko, E.** (2014). Modelling and Optimisation of a Post-combustion CO_2 Capture Process Using Neural Networks, *10th European conference on coal research and its applications – ECCRIA*, 15-17 September, University of Hull, UK (Oral).

Oko, E. and Wang, M. (2014). Neural network approach for predicting drum pressure and level in a coal-fired subcritical power plant, *10th European conference on coal research and its applications – ECCRIA*, 15-17 September, University of Hull, UK (Oral).